AD-A168 083 ELECTROMAGNETIC FIELD-TO-WIRE COUPLING IN THE SHF/EHF FREQUENCY RANGE(U) SYRACUSE UNIV NY A T ADAMS ET AL. MAR 86 RADC-TR-86-28 F30602-81-C-0169 1/1

UNCLASSIFIED F/G 20/14 NL

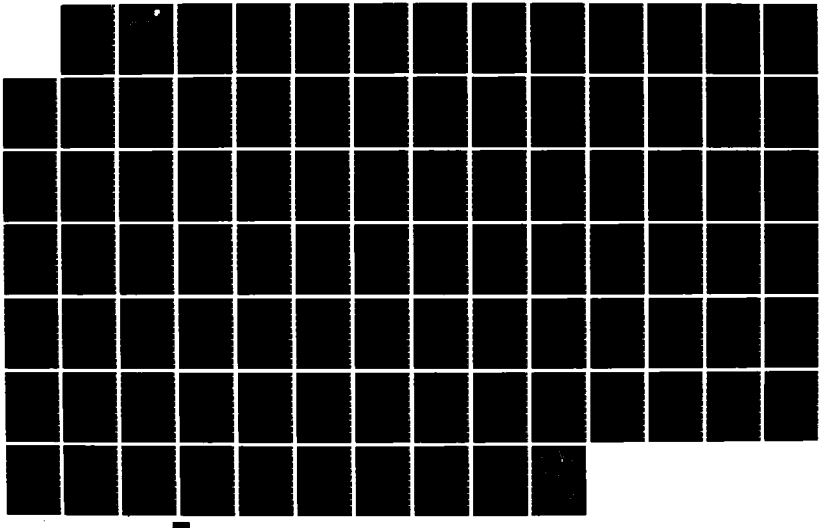

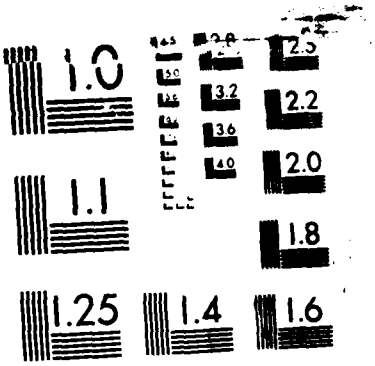

RADC-TR-86-28
Final Technical Report
March 1986

ELECTROMAGNETIC FIELD-TO-WIRE COUPLING IN THE SHF/EHF FREQUENCY RANGE

Syracuse University

A. T. Adams, Jose Perini, M. Miyabayashi, D. H. Shau
and K. Heidary

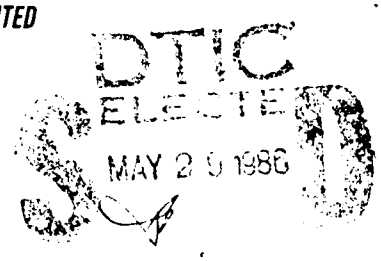

ROME AIR DEVELOPMENT CENTER
Air Force Systems Command
Griffiss Air Force Base, NY 13441-5700

This report has been reviewed by the RADC Public Affairs Office (PA) and is releasable to the National Technical Information Service (NTIS). At NTIS it will be releasable to the general public, including foreign nations.

RADC-TR-86-28 has been reviewed and is approved for publication.

APPROVED: Anthony J. Pesta

ANTHONY J. PESTA
Project Engineer

APPROVED: John J. Bart

JOHN J. BART
Technical Director
Reliability & Compatibility Division

FOR THE COMMANDER: John A. Ritz

JOHN A. RITZ
Plans & Programs Division

If your address has changed or if you wish to be removed from the RADC mailing list, or if the addressee is no longer employed by your organization, please notify RADC (RBCT) Griffiss AFB NY 13441-5700. This will assist us in maintaining a current mailing list.

Do not return copies of this report unless contractual obligations or notices on a specific document requires that it be returned.

UNCLASSIFIED

SECURITY CLASSIFICATION OF THIS PAGE

REPORT DOCUMENTATION PAGE

1a REPORT SECURITY CLASSIFICATION UNCLASSIFIED	1b RESTRICTIVE MARKINGS N/A
2a SECURITY CLASSIFICATION AUTHORITY N/A	3 DISTRIBUTION / AVAILABILITY OF REPORT Approved for public release; distribution unlimited.
2b DECLASSIFICATION / DOWNGRADING SCHEDULE N/A	
4 PERFORMING ORGANIZATION REPORT NUMBER(S) N/A	5 MONITORING ORGANIZATION REPORT NUMBER(S) RADC-TR-86-28
6a NAME OF PERFORMING ORGANIZATION Syracuse University 6b OFFICE SYMBOL (If applicable)	7a NAME OF MONITORING ORGANIZATION Rome Air Development Center (RBCT)
6c ADDRESS (City, State, and ZIP Code) Skytop Office Building Skytop Rd, Syracuse NY 13210	7b ADDRESS (City, State, and ZIP Code) Griffiss AFB NY 13441-5700
8a NAME OF FUNDING / SPONSORING ORGANIZATION Rome Air Development Center 8b OFFICE SYMBOL (If applicable) RBCT	9 PROCUREMENT INSTRUMENT IDENTIFICATION NUMBER F30602-81-C-0169
8c ADDRESS (City, State, and ZIP Code) Griffiss AFB NY 13441-5700	10 SOURCE OF FUNDING NUMBERS PROGRAM ELEMENT NO: 62702F; PROJECT NO: 2338; TASK NO: 03; WORK UNIT ACCESSION NO: PK

11 TITLE (Include Security Classification)
ELECTROMAGNETIC FIELD-TO-WIRE COUPLING IN THE SHF/EHF FREQUENCY RANGE

12 PERSONAL AUTHOR(S)
A.T. Adams, Jose Perini, M. Miyabayashi, D.H. Shau, K. Heidary

13a TYPE OF REPORT	13b TIME COVERED	14 DATE OF REPORT (Year, Month, Day)	15 PAGE COUNT
Final	FROM May 85 TO Oct 85	March 1986	96

16 SUPPLEMENTARY NOTATION
N/A

17 COSATI CODES			18 SUBJECT TERMS (Continue on reverse if necessary and identify by block number)	
FIELD	GROUP	SUB GROUP	Electromagnetic Coupling	Field-to-Wire Coupling
09	02		Transmission Lines	Scattering Analysis
			Radiation Analysis	SHF/EHF Frequencies

19 ABSTRACT (Continue on reverse if necessary and identify by block number)

A feasibility study has been conducted to examine methods of treating field-to-wire coupling in the SHF/EHF frequency range. In this region, transmission line lengths and wire separations become very large electrically, and field-to-wire coupling problems become intractable.

Several types of transmission lines have been examined in the SHF/EHF range, including uniform and non-uniform transmission lines, coaxial transmission lines, and multi-conducter transmission lines. Current distributions are predominantly of the standing-wave or traveling-wave form. The higher order modes are not significant for those cases examined.

Bounds may be obtained for induced currents in the field-to-wire problem by considering the transmission line as an antenna and using the equivalent circuit of the receiving antenna which has been extended to multiport receivers. A method has thus been —

20 DISTRIBUTION AVAILABILITY OF ABSTRACT	21 ABSTRACT SECURITY CLASSIFICATION
☒ UNCLASSIFIED/UNLIMITED ☐ SAME AS RPT ☐ DTIC USERS	UNCLASSIFIED

22a NAME OF RESPONSIBLE INDIVIDUAL	22b TELEPHONE (Include Area Code)	22c OFFICE SYMBOL
ANTHONY J. PESTA	(315) 330-7642	RADC (RBCT)

DD FORM 1473, 84 MAR — 83 APR edition may be used until exhausted. All other editions are obsolete.

SECURITY CLASSIFICATION OF THIS PAGE
UNCLASSIFIED

TABLE OF CONTENTS

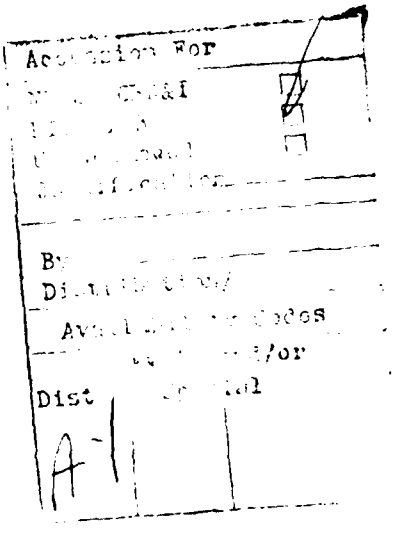

LIST OF ILLUSTRATIONS

LIST OF TABLES

CHAPTER I

INTRODUCTION

Transmission line analysis has advanced steadily over the last few decades and, as a result, a number of analyses and computer codes are now available for the treatment of a variety of transmission line problems. High-frequency problems, however, remain intractable. Lumped-circuit models which are currently available (such as those of IEMCAP) are not applicable to SHF/EHF coupling analysis because of limitations due to assumptions made in those models. The moment-method codes are limited by the number of unknowns which can be treated and by thin-wire assumptions.

Figs. 1-1 to 1-4 show four typical problems to be considered in the SHF/EHF region. Fig.1-1 shows electric fields incident upon a loaded transmission line. The transmission line consists of a wire of radius a and length L mounted a distance d above a ground plane. A load Z_L is attached between wire and ground plane. At SHF/EHF frequencies, L may be many wavelengths long, d may be several wavelengths, and radius a may or may not be large electrically. The current induced in the load Z_L is to be determined. Fig. 1-2 shows electric fields incident upon a non-uniform (spherical) transmission line consisting of a wire of length L and radius a mounted above a ground plane at an angle α to the ground plane. A load Z_L is attached between wire and ground plane. Coaxial and multiconductor lines were also considered. Figure 1-3 shows electric fields incident upon a coaxial transmission line of length L_1 mounted at an angle α above a ground plane. The center conductor of the

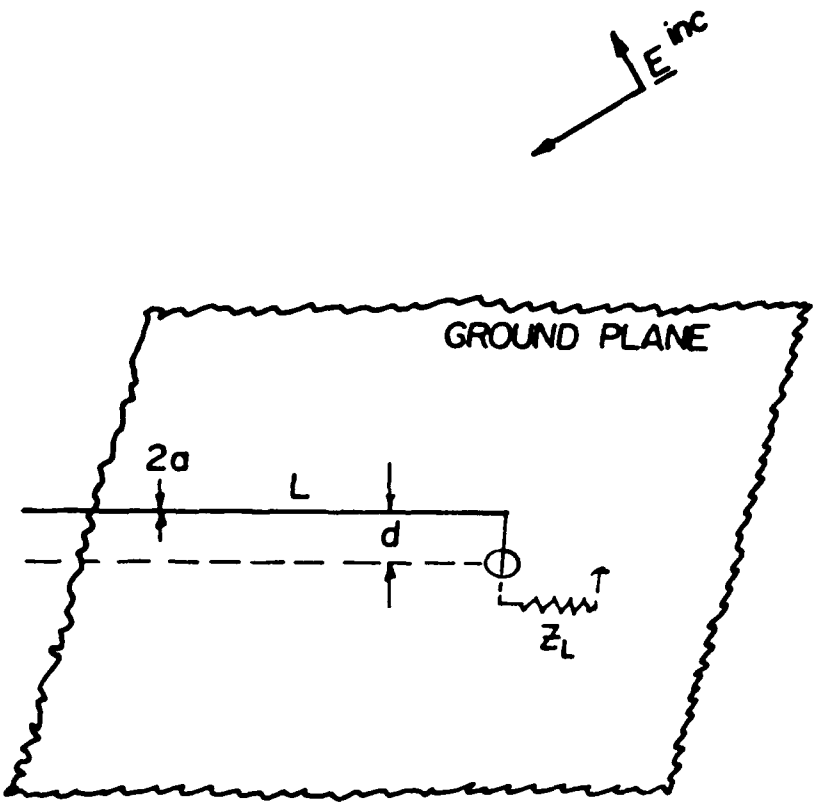

Fig. 1-1. Coupling to a Uniform Transmission Line.

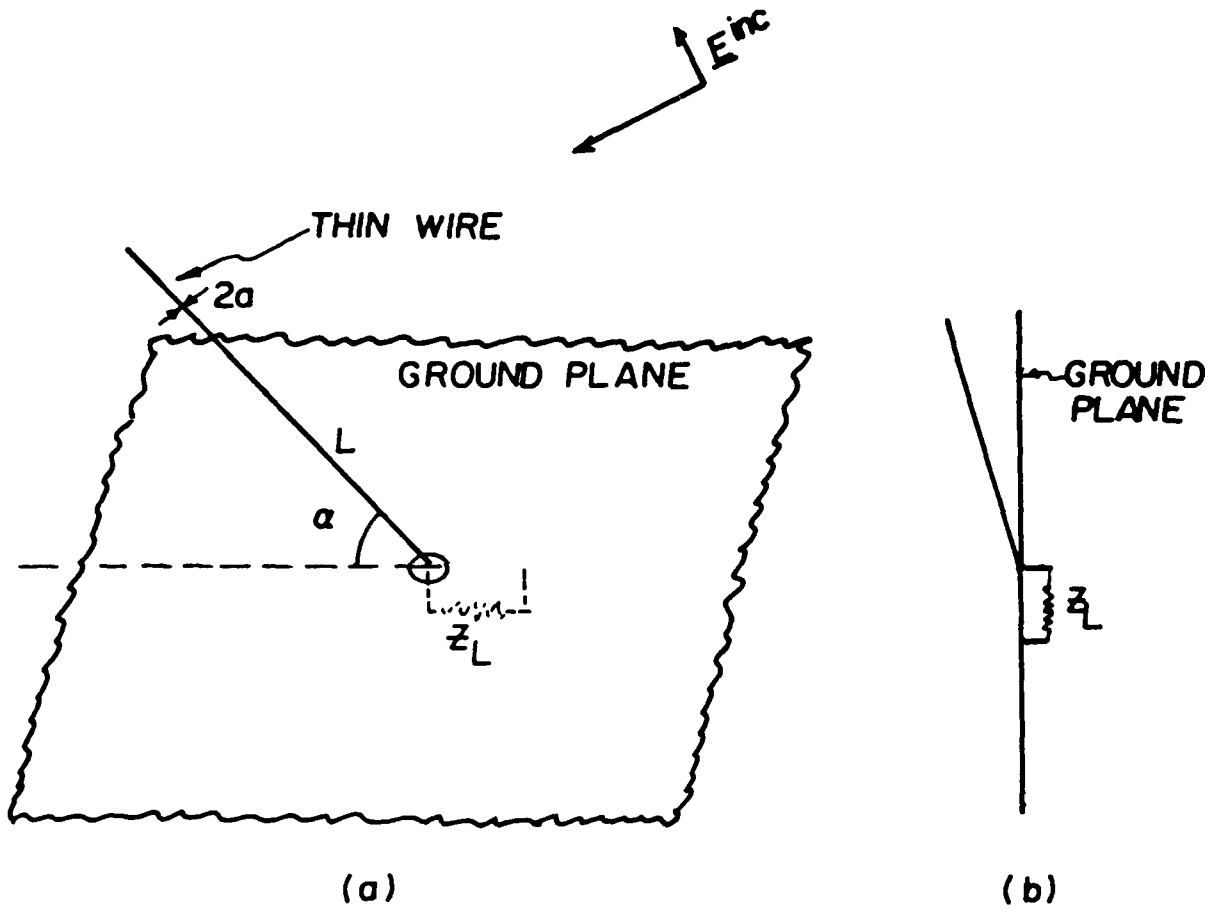

Fig. 1-2. Coupling to a non-uniform (vee) transmission line.

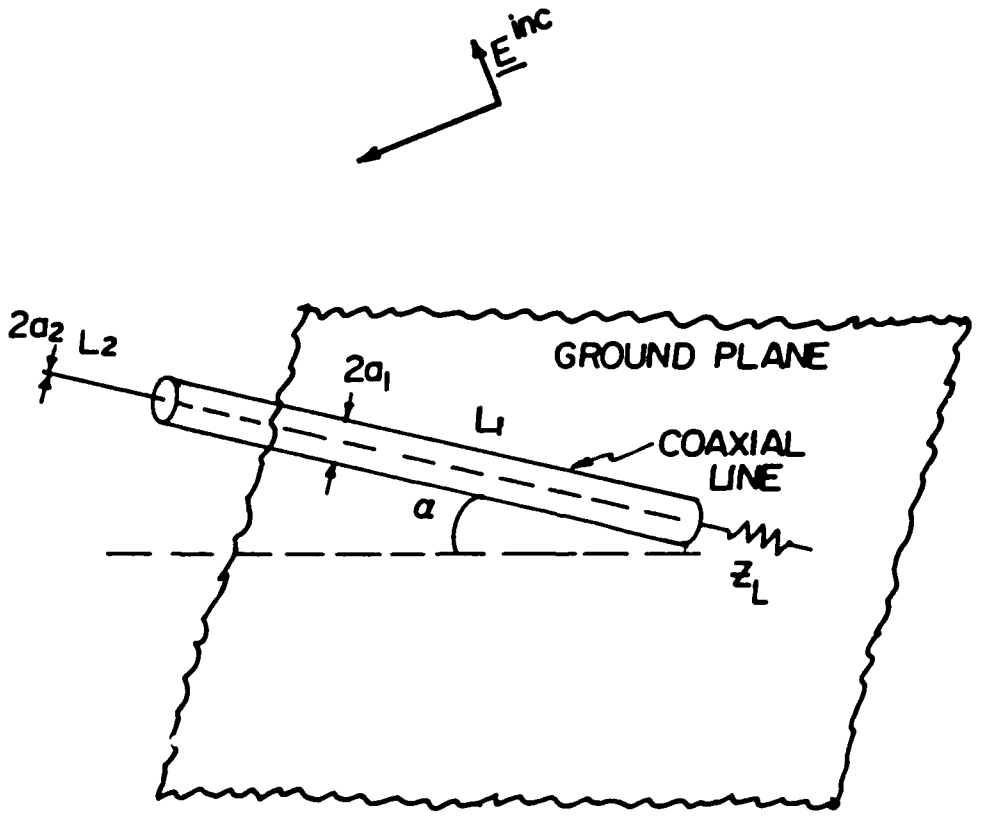

Fig. 1-3. Coupling to a coaxial transmission line.

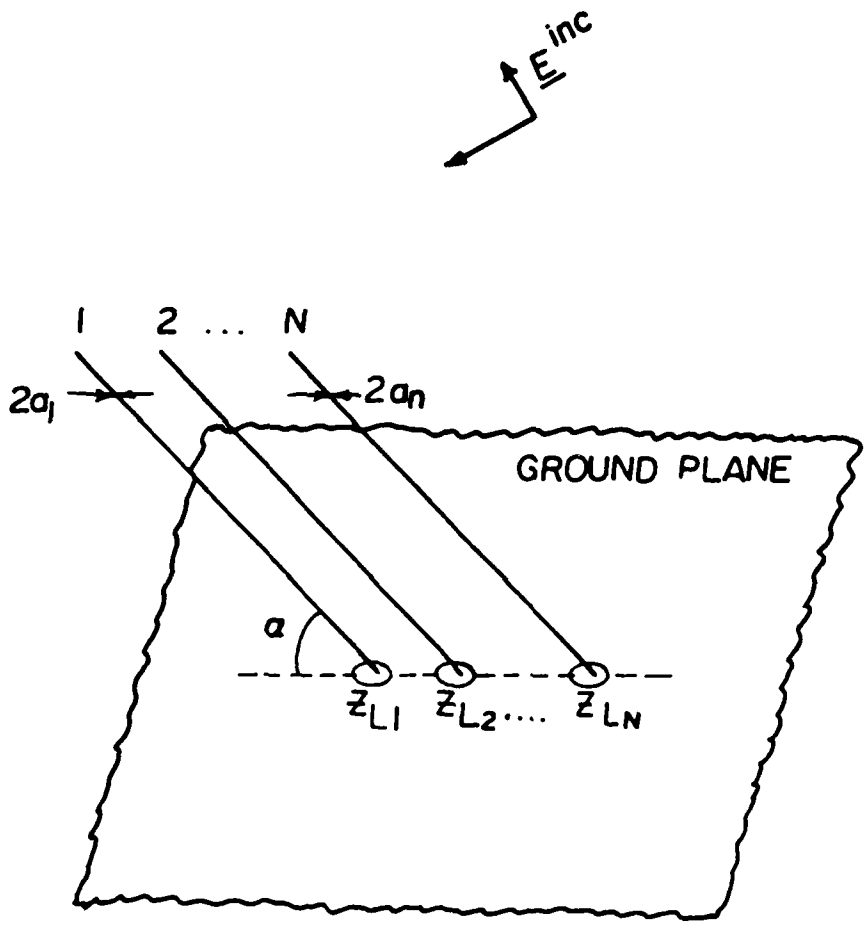

Fig. 1-4. Coupling to a multiconductor transmission line.

coaxial line extends a distance L_2 beyond the outer conductor. Radii of inner and outer conductors are a_2, a_1 respectively. A load Z_L is attached between coaxial line and ground plane (the load may also be underneath the ground plane). The current induced in the load Z_L is to be determined. Fig. 1-4 shows a multiconductor non-uniform (spherical) transmission line mounted at an angle α above a ground plane with loads Z_{L1}, Z_{L2},...Z_{Ln} attached between wire and ground plane. The currents induced in loads are to be determined.

At SHF/EHF frequencies, transmission line lengths become very long electrically. At 30 GHz the wavelength is one centimeter and a wire of one meter length is 100 wavelengths long. As frequency increases, eventually wire transmission line separation (2d of Figure 1-1) becomes electrically large and higher order modes are permitted. Finally, at even higher frequencies, wire diameter (2a of Figure 1-1) becomes electrically large and thin-wire limitations are no longer applicable.

In this report, we conduct a feasibility study concerning SHF/EHF field-to-wire coupling analysis. Our first concern is with current distributions that arise in radiation and scattering problems in the SHF/EHF region. Numerous radiation and scattering problems of various different types including those of Figs. 1-1 to 1-4 are treated and the current distributions are studied. Both uniform and non-uniform (spherical) transmission lines are considered. The radiation currents are predominantly of a form consisting of standing waves and traveling waves. The scattering currents are of more complicated form but these complications can also be explained in terms of standing and traveling waves. The higher-order modes do not appear to be very important, even when transmission line wire separation (2d of Fig. 1-1) is several

wavelengths. The current distributions obtained can be explained approximately without taking higher-order modes into account. The higher order modes are undoubtedly excited to some degree, but their effect does not appear to be significant in those cases treated.

The transmission line may also be considered as a receiving antenna. In order to determine the current induced in load Z_L of Figs. 1-1 to 1-4, the impedance Z_a of the antenna when excited as a transmitter, and the open-circuit voltage V_{oc} of the receiving antenna, are required. Bounds to both Z_a and V_{oc} may be obtained, and, as a result, the induced current may be bounded. Equivalent circuits for N-port receiving antennas are also derived; these may be applied to multiconductor transmission lines.

As a result of the feasibility study, a method has been outlined for obtaining bounds to field-to-wire coupling in some uniform and non-uniform transmission lines at SHF/EHF frequencies where previous methods are unsuitable.

Chapter Two

CURRENT DISTRIBUTIONS FOR RADIATION AND SCATTERING PROBLEMS

2.1 INTRODUCTION

In this chapter current distributions are computed for a wide variety of radiators and scatterers related to the basic problems of Figs. 1-1 thru 1-4. Both amplitude and phase are plotted and most lengths are fixed at 10 wavelengths. Previous computations (not shown) have been carried out for a variety of lengths and spacings and to check the computations, which were performed using the moment code WRSMOM [1,2]. Copper losses were included in the computations, but their effect was negligible.

2.2 RECIPROCITY FOR SCATTERING PROBLEMS

Fig. 2-1a shows a problem such as those of Figs. 1-1 through 1-4. It may be regarded as a scattering problem if port two is excited, and a radiation problem if port one is excited. By reciprocity ($Z_{12} = Z_{21}$), the scattering problem of Fig. 2-1b can be replaced with either of the radiation problems of Fig. 2-1c. Similarly, by reciprocity ($Y_{12} = Y_{21}$) the scattering problem of Fig. 2-1d may be replaced by the radiation problem of Fig. 2-1e. Note that Z_L in Fig. 2-1e does not affect the normalized current distribution or the normalized beam pattern, but it does affect the absolute level of the radiated field.

Z_L may represent any load in Fig. 2-1. If $Z_L = \infty$, then V_1 of Fig. 2-1b represents open circuit voltage. If $Z_L = 0$, then I_1 of Fig. 2-1d represents

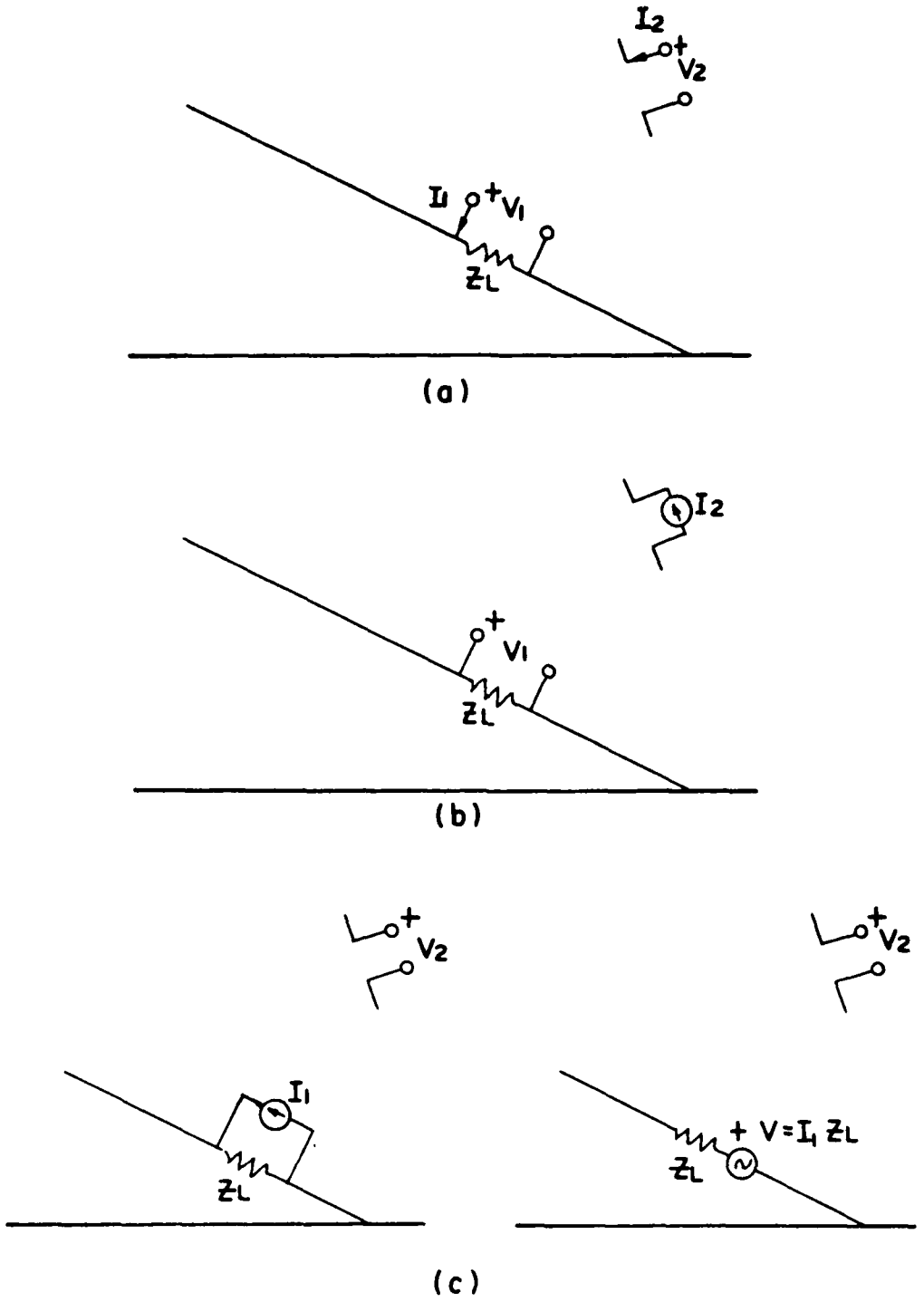

Fig. 2-1. Reciprocity for field-to-wire coupling
(a) Basic problem #1 (b) Scattering problem #1
(c) Radiation problem #1

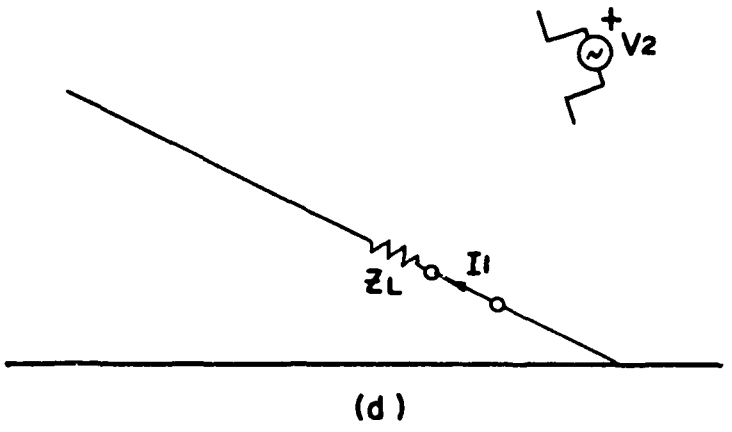

(d)

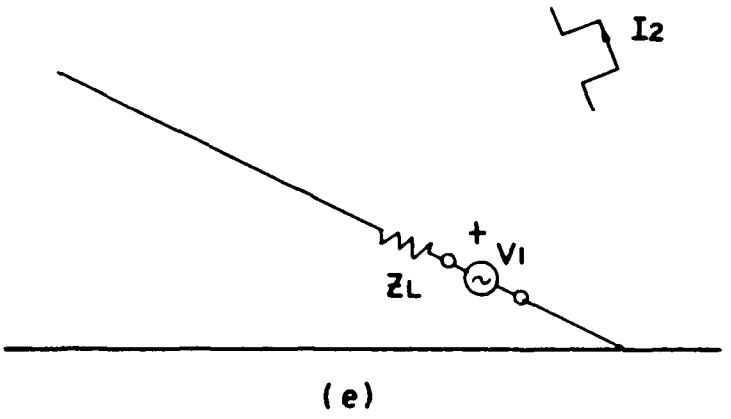

(e)

Fig. 2-1. (d) Scattering problem #2
(e) Radiation problem #2

short circuit current. Thus if induced current I_1 is desired in a scattering problem (see Fig. 2-1d), we may replace the scattering problem with a radiation problem of Fig. 2-1e. The voltage source is applied (in Fig. 2-1e) at the point where we are interested in the induced current (in Fig. 2-1d). This last form of the reciprocity theorem will be used in computing induced currents in Chapter Four.

2.3 CURRENT DISTRIBUTIONS

Fig. 2-2 shows the geometry for transmission line radiation (Fig. 2-2a) and scattering (Fig. 2-2b), including the image representations. Fig. 2-3 shows plots of the current distribution on a transmission line with length $L = 5\lambda$ and variable transmission line spacing 2d. The transmission line is terminated in an open circuit. A standing-wave pattern is observed in all cases. The standing-wave ratio decreases somewhat as spacing 2d increases to one wavelength, due to increased radiation from the end (open circuit). Figs. 2-4 thru 2-13 show current distributions for transmission lines of length 10λ, with variable spacing and terminations. Figs. 2-4, 2-5 show distributions for 0.1λ separation and $Z_t = 160\Omega, \infty$, respectively. 160Ω represents a transmission line which is terminated in a nearly-matched load. It should be pointed out that a matched load would be a complex impedance. The magnitude plot shows a small standing wave ratio. The phase is almost exactly linear, as would be expected from a traveling wave. The phase distribution turns out to be a very sensitive indicator of the difference between traveling and standing waves, as will be brought out in figures 2-4 thru 2-26. Fig. 2-5 involves an open-circuit termination and accordingly shows a standing-wave pattern. The pattern has 21 peaks

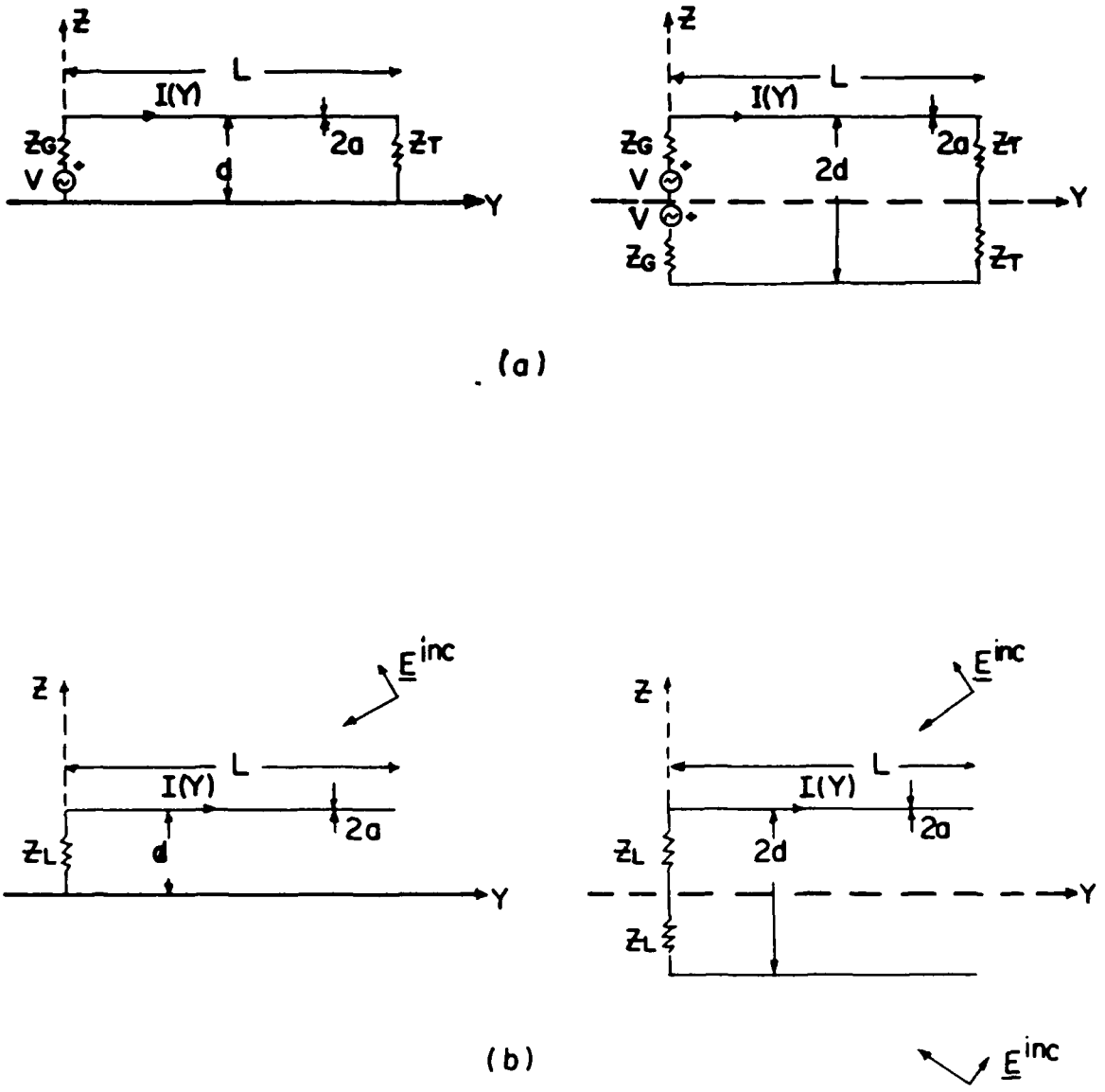

Fig. 2-2. Geometry for a uniform transmission line.
(a)Radiator (b) Scatterer

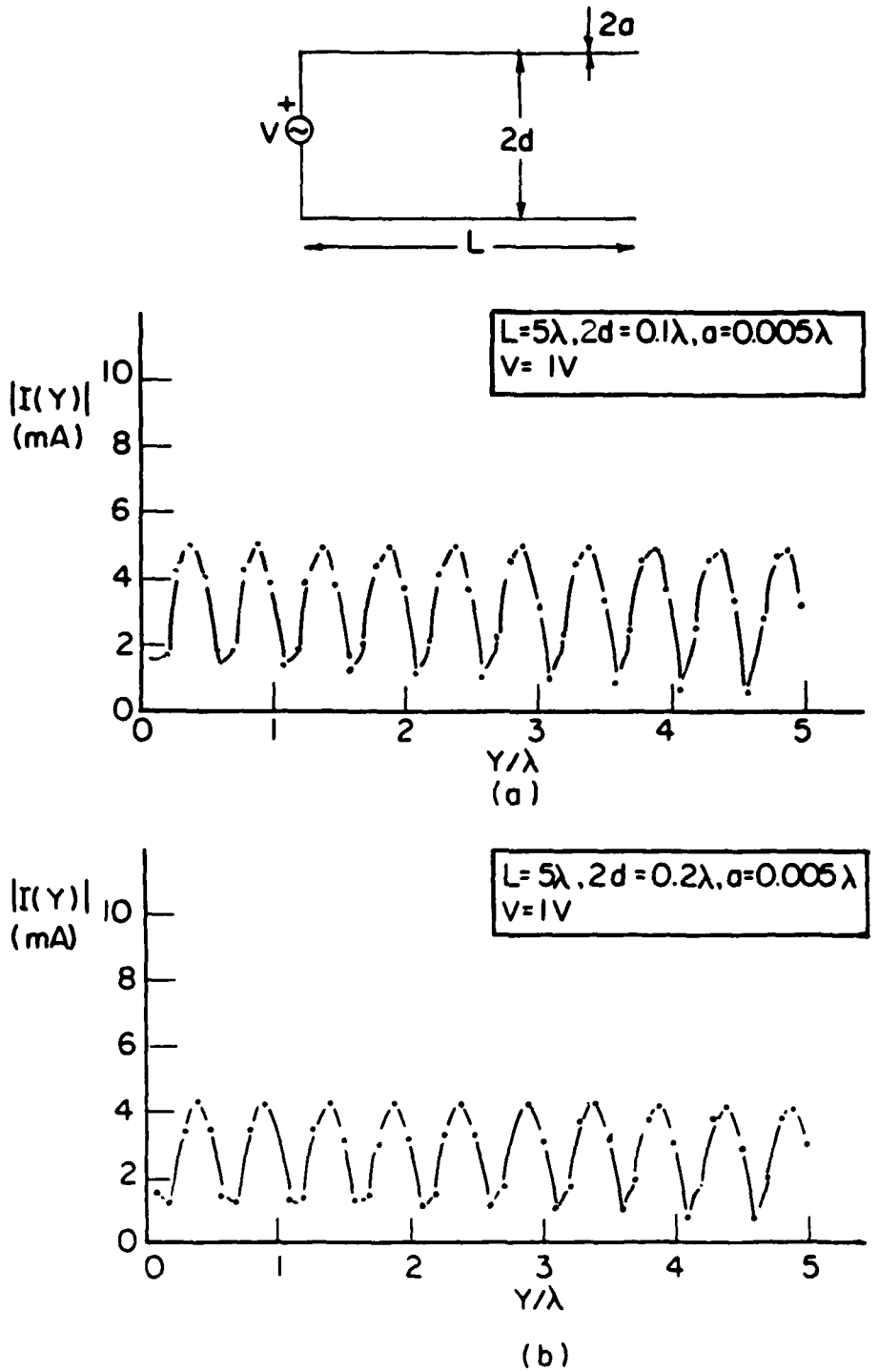

Fig. 2-3. Current distributions for an open-circuited uniform transmission line radiator
(a) 2d = 0.1λ (b) 2d = 0.2λ

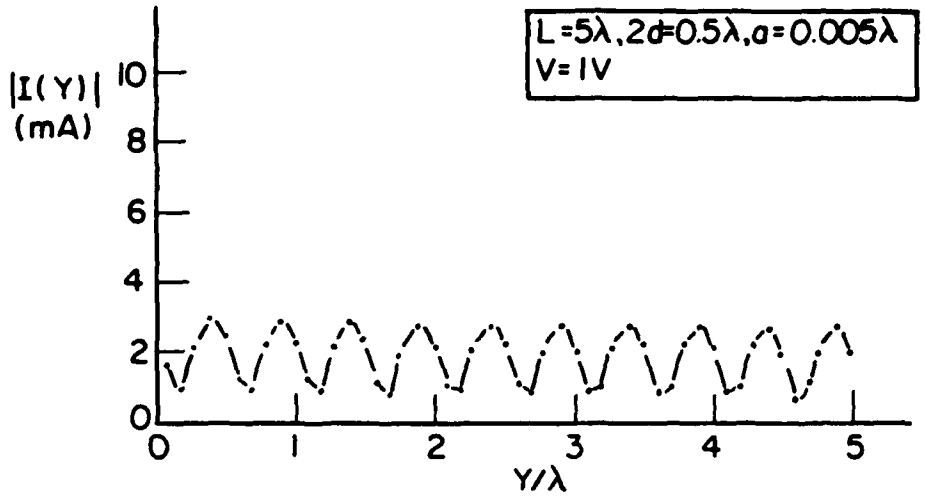

(c)

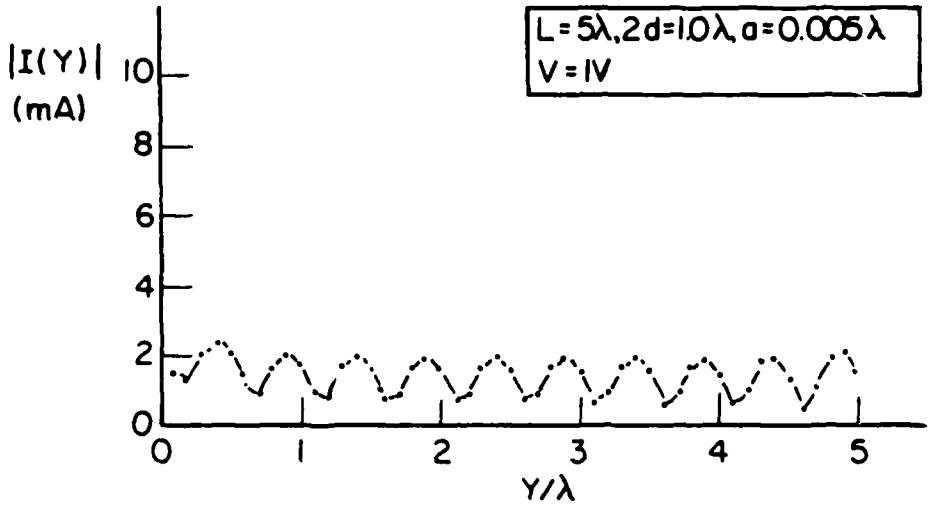

(d)

Fig. 2-3. (c)2d = 0.5λ (d)2d = 1.0λ

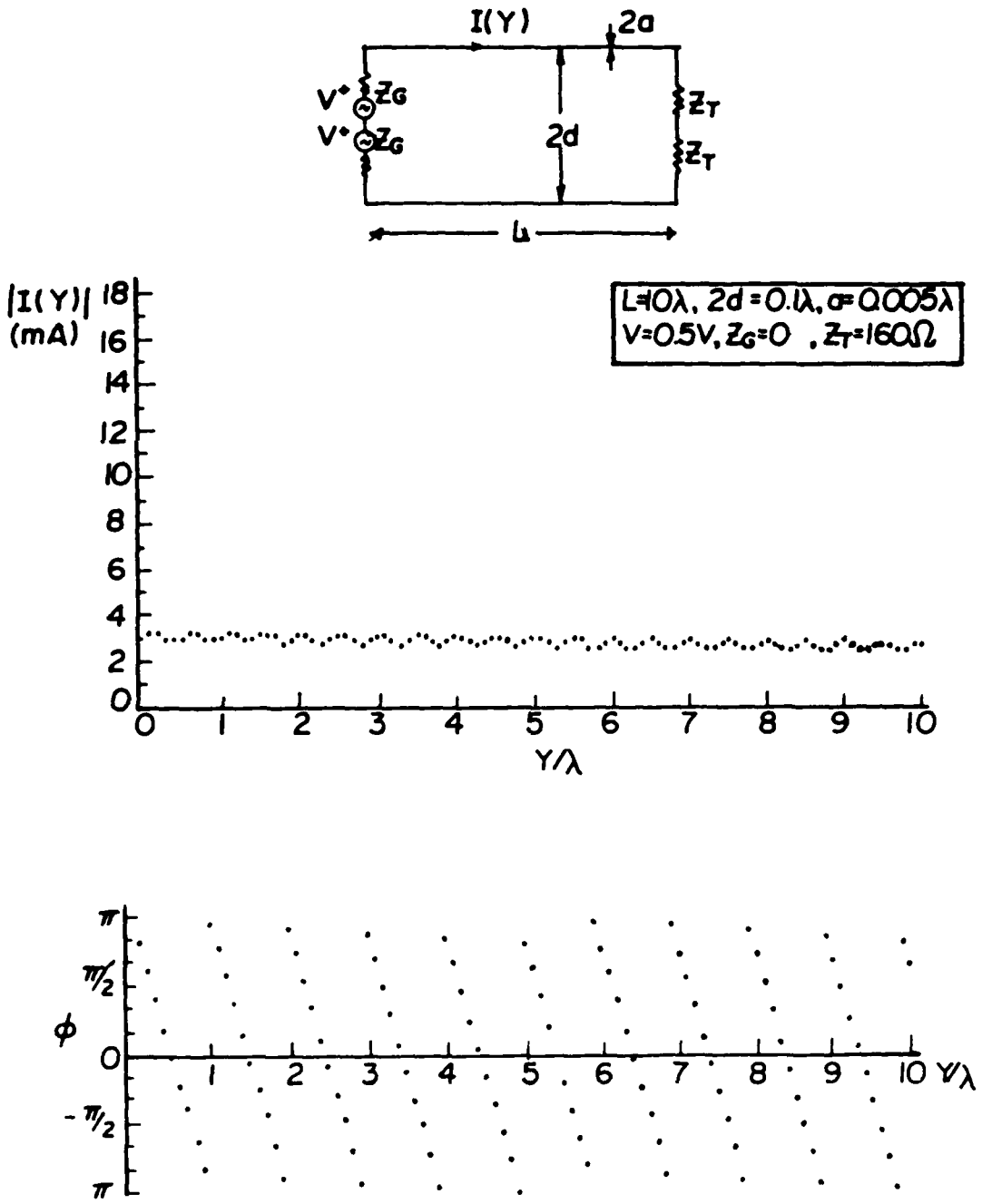

Fig. 2-4. Current distribution for a transmission line radiator ($2d=0.1\lambda$, $Z_t = 160\ \Omega$)

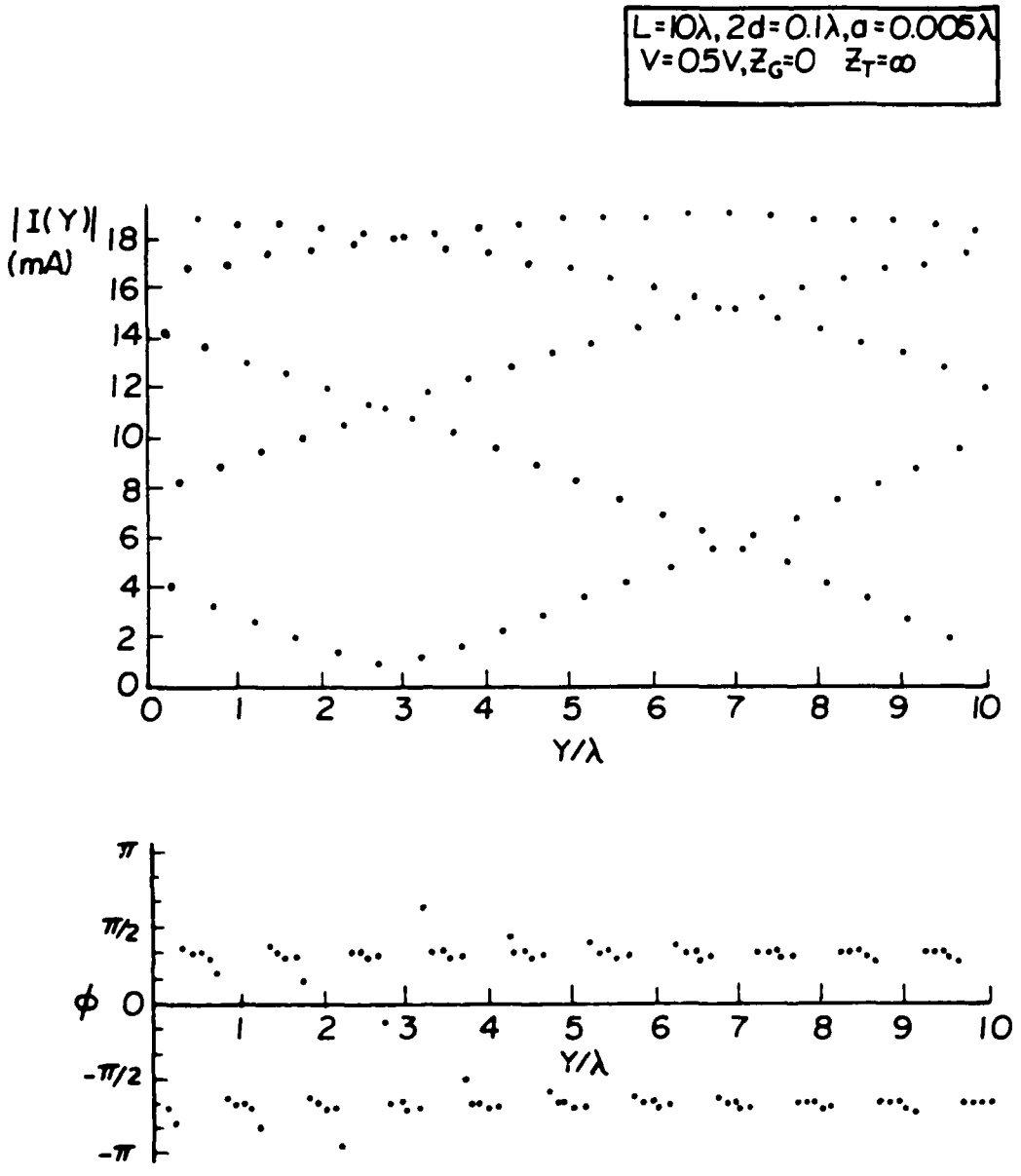

Fig. 2-5. Current distribution for a transmission line radiator ($2d = 0.1\lambda$, $Z_t = \infty$)

and if the points were connected, the standing-wave pattern would be clear. The phase plot shows a nearly perfect periodic step function which jumps 180° at zero crossings, as would be expected for a standing wave pattern. Figs. 2-6, 2-7 show plots for separation $2d = 0.25\lambda$, and represent traveling, standing waves, respectively, with slightly greater departures from perfect phase performance. Figs. 2-8, 2-9 show greater departures in phase. As spacing increases to 1.0λ (Figs. 2-10, 2-11) and to 2.0λ (Figs. 2-12, 2-13), the departure from perfect phase behavior becomes significant. Note especially that open-circuit cases may be said to represent a combination of standing-and traveling-wave performance, the behavior shifting more toward a standing-wave performance near the open circuit.

Fig. 2-14 shows the geometry for transmission-line scattering problems, including the image representation. Fig. 2-15 shows current distributions for transmission-line lengths of $1, 5, 10\lambda$. A plane wave is incident in the plane of the transmission line and image at an angle of 45°. Note that the current distributions differ significantly from those of the transmitting problem. It is interesting to note that the current distribution can be explained in terms of two waves, one the incident wave and the other a wave excited at the end of the line and traveling down the line at the speed of light. Such a combination of two waves produces exactly the slightly more than three periods shown in the case $L = 10\lambda$. One can explain such current distributions but it will not be necessary in our computations because we use reciprocity and consider only the radiating case.

Fig. 2-16 shows the geometry for the vee antenna as a radiator and scatterer and Figs. 2-17 thru 2-24 show current distributions. Fig. 2-17 shows the characteristics of the radiator of angle $\alpha = 45°$ and length $L = 10\lambda$.

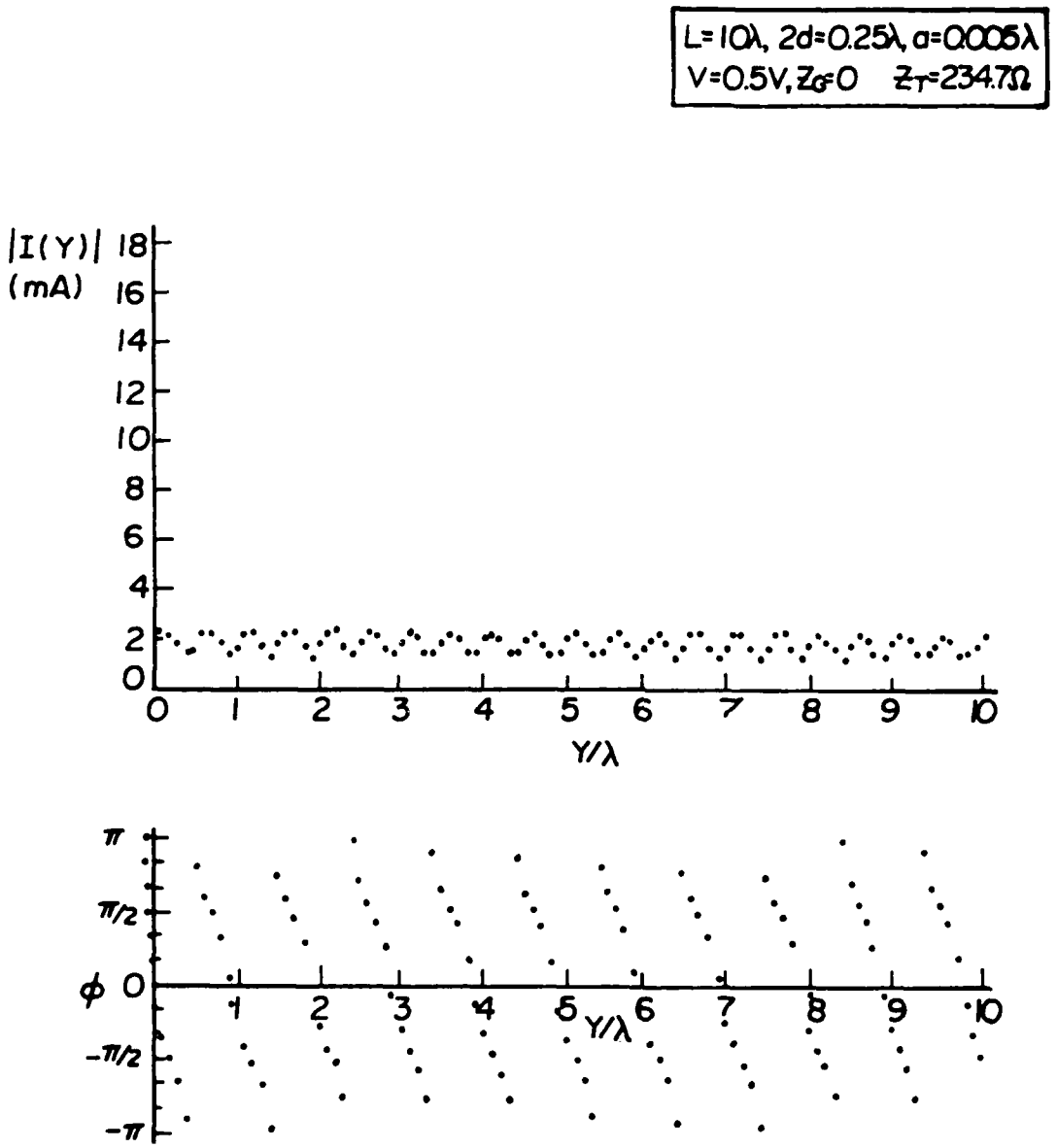

Fig. 2-6. Current distribution for a transmission line radiator ($2d=0.25\lambda$, $Z_t = 234.7\Omega$)

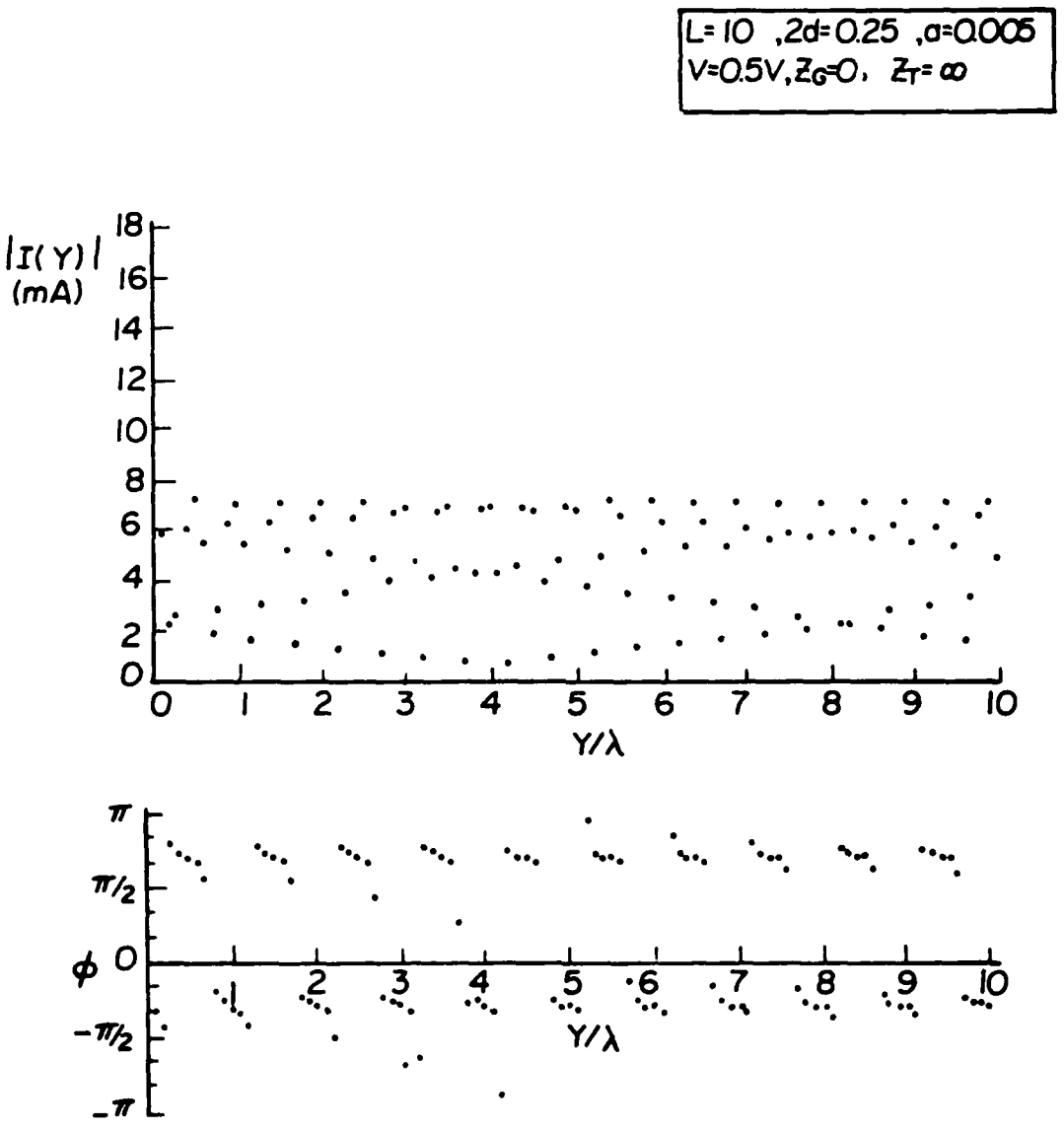

Fig. 2-7. Current distribution for a transmission line radiator ($2d=0.25\lambda$, $Z_t = \infty$)

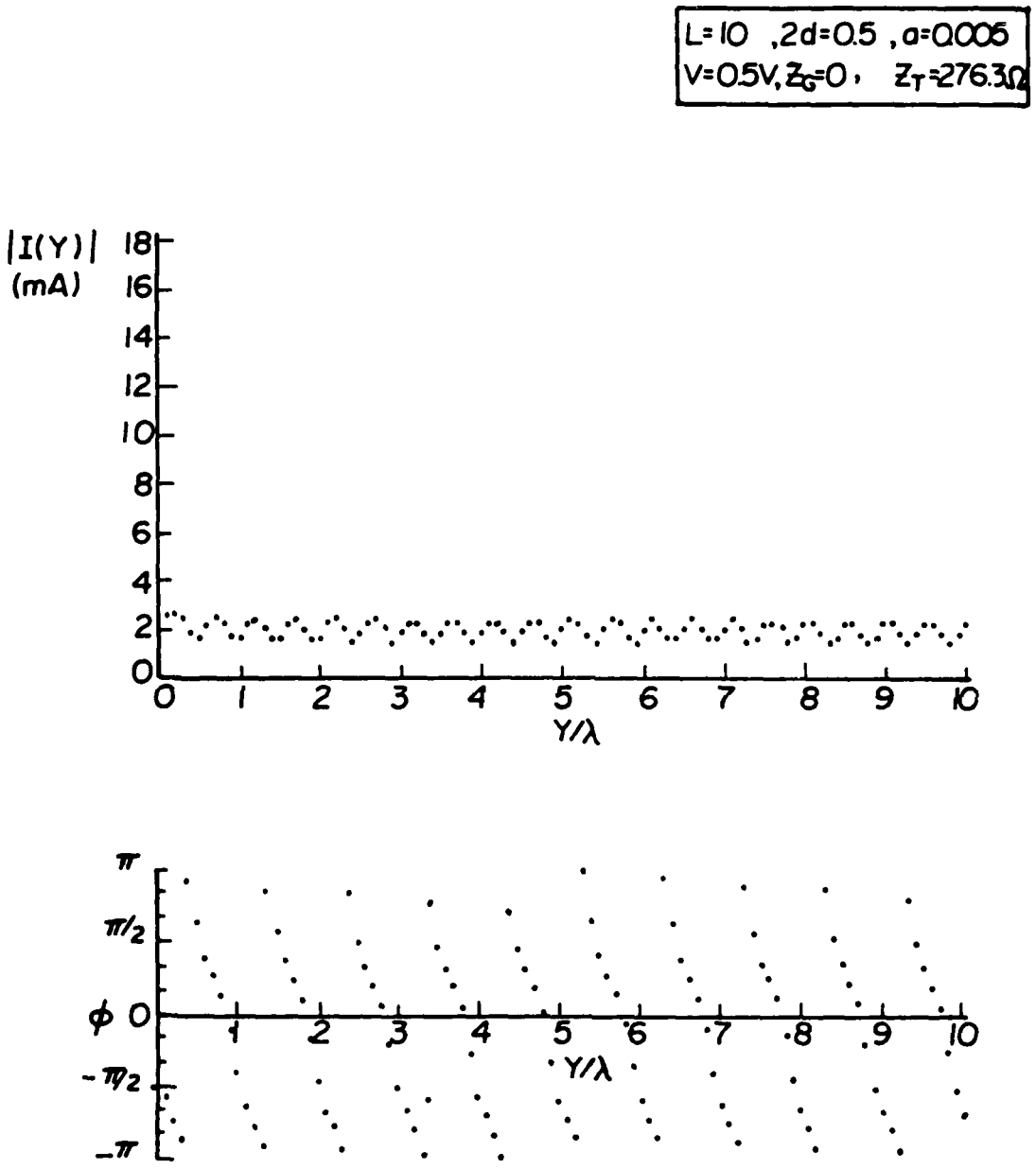

Fig. 2-8. Current distribution for a transmission line radiator ($2d=0.5\lambda$, $Z_t = 276.3\Omega$)

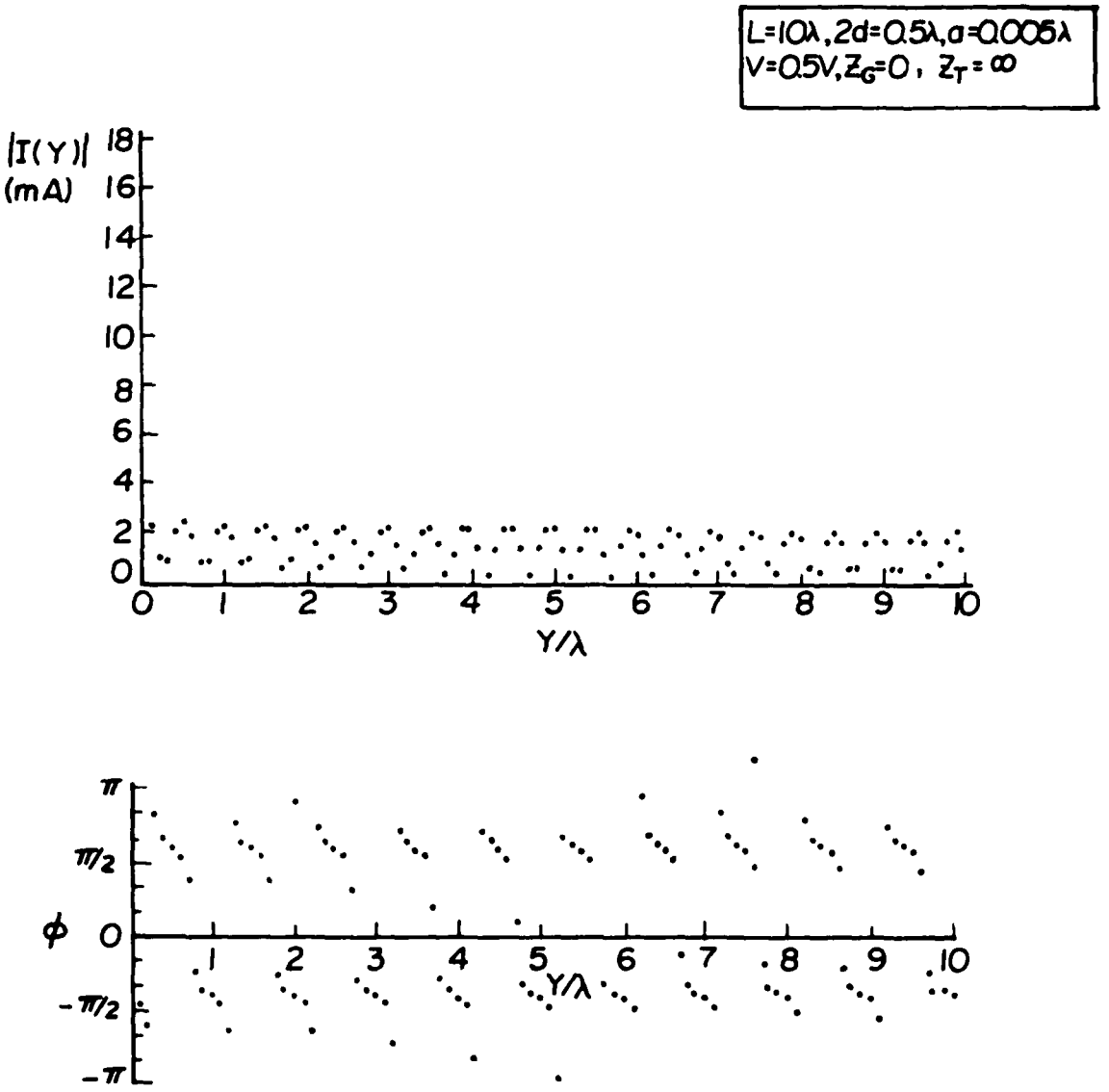

Fig. 2-9. Current distribution for a transmisson line radiator ($2d=0.5\lambda$, $Z_t = \infty$).

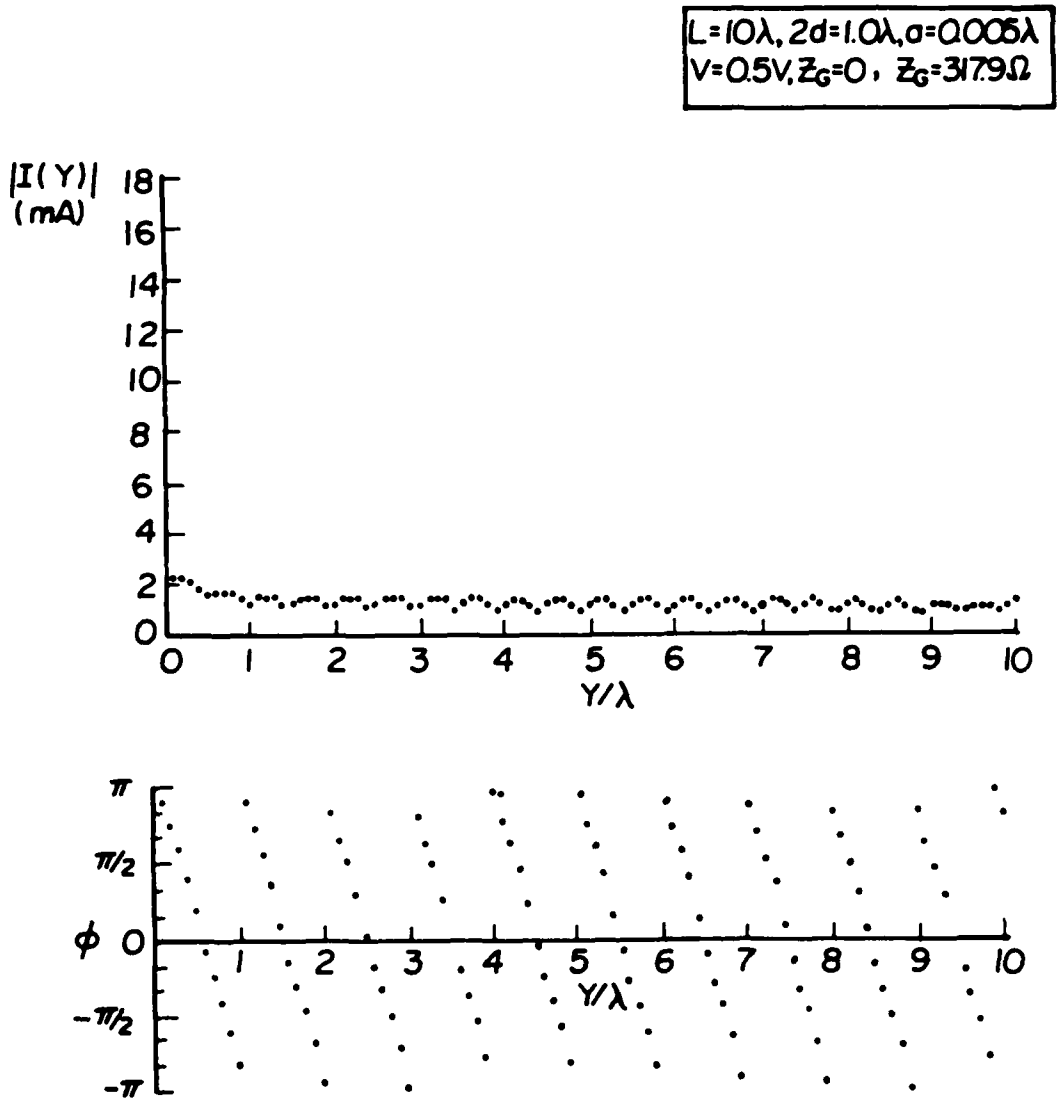

Fig.2-10. Current distribution for a transmission line radiator ($2d=1.0\lambda$, $Z_t = 317.9\Omega$)

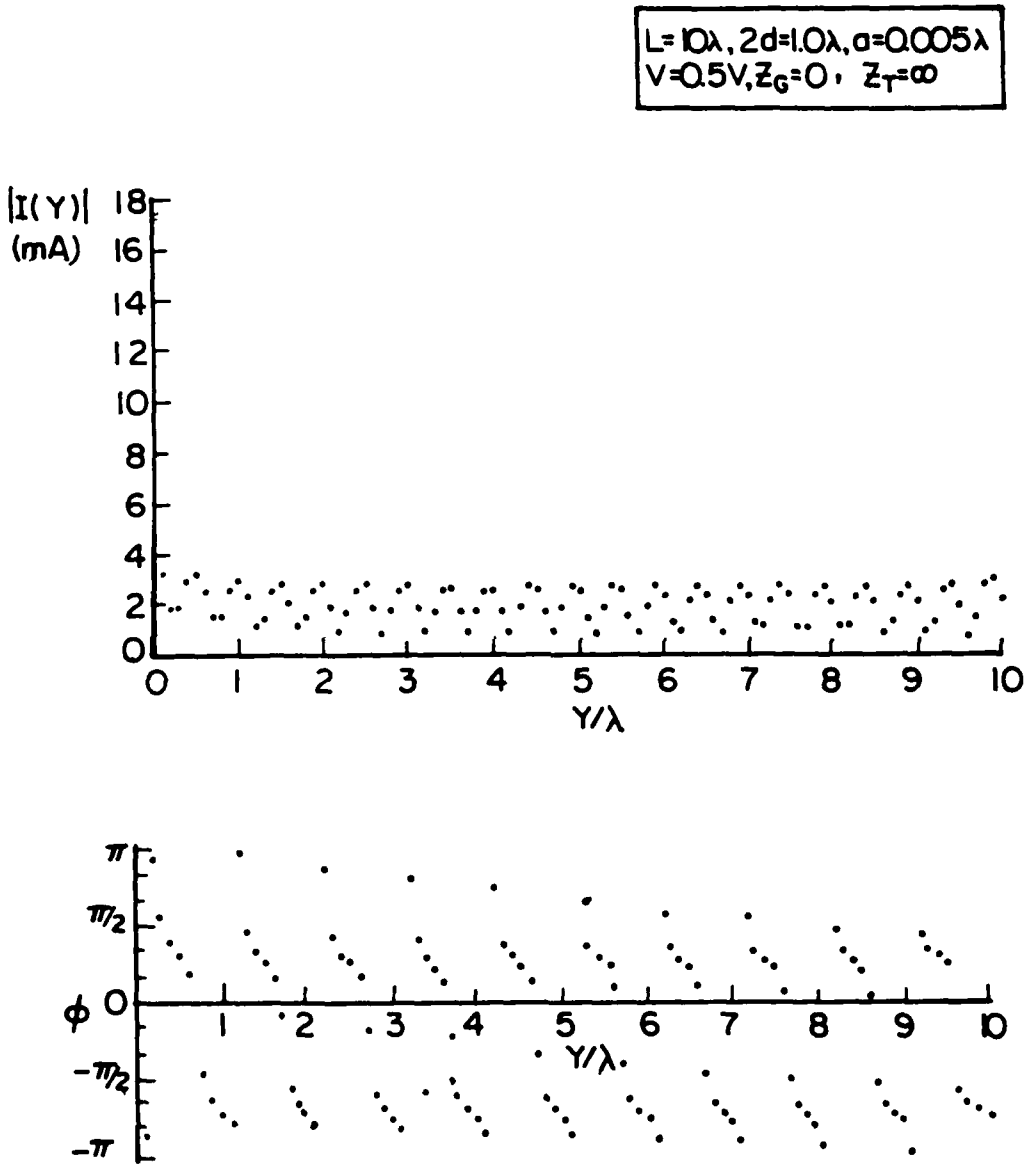

Fig. 2-11. Current distribution for a transmission line radiator ($2d = 1.0\lambda$, $Z_t = \infty$).

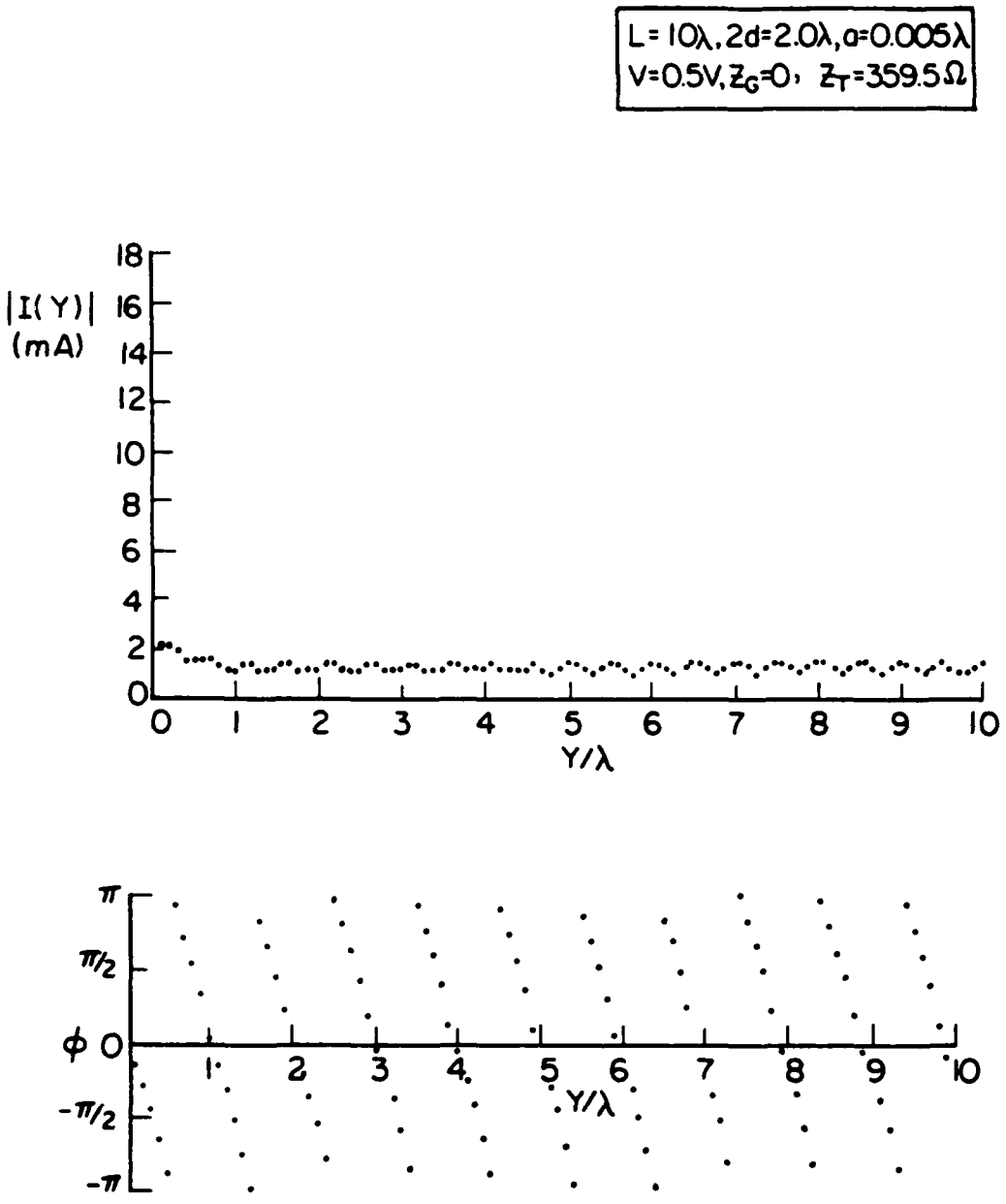

Fig. 2-12. Current distribution for a transmission line radiator ($2d = 2.0\lambda$, $Z_t = 359.5\Omega$).

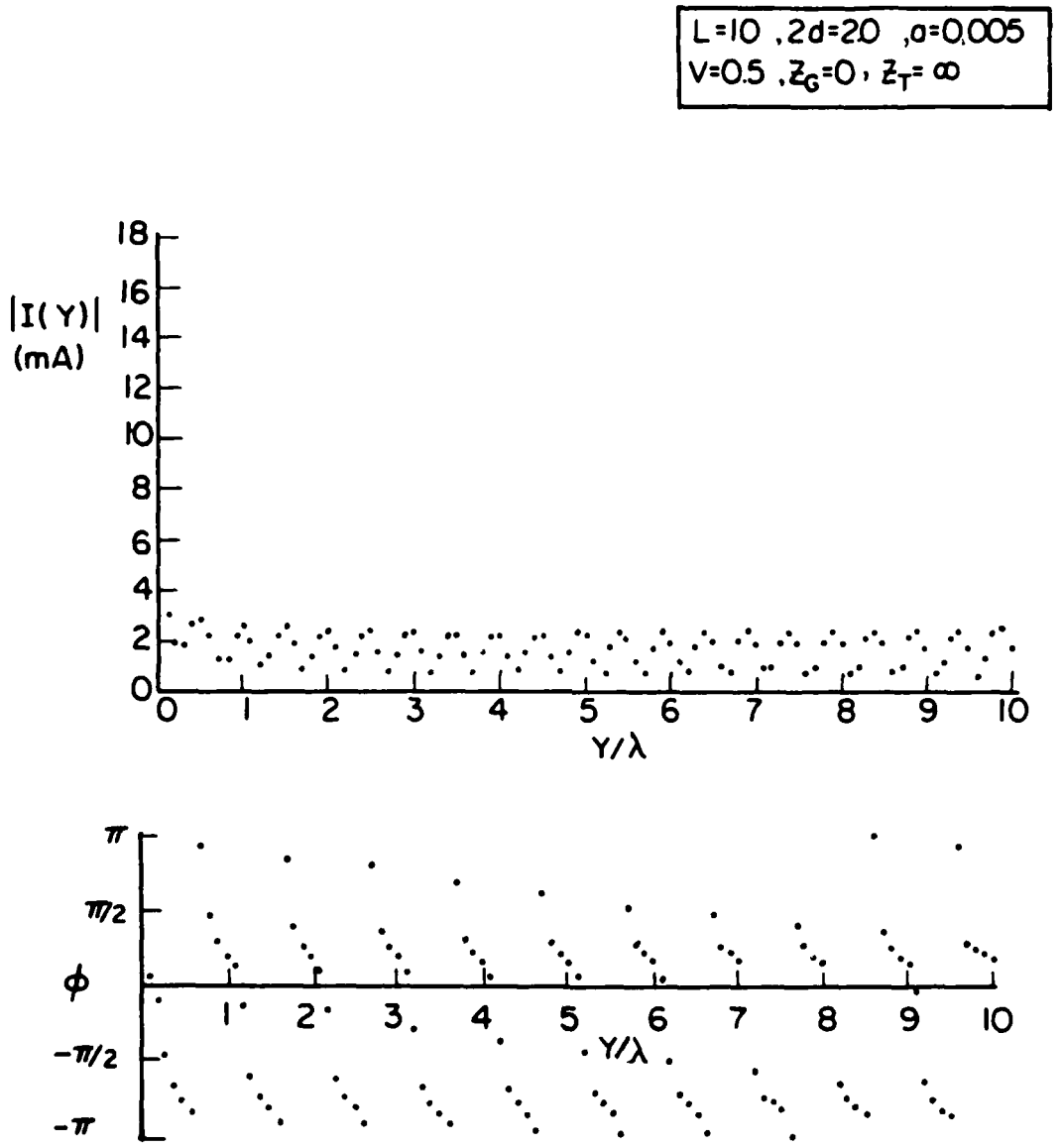

Fig. 2-13. Current distribution for a transmission line radiator ($2d = 2.0\lambda$, $Z_t = \infty$).

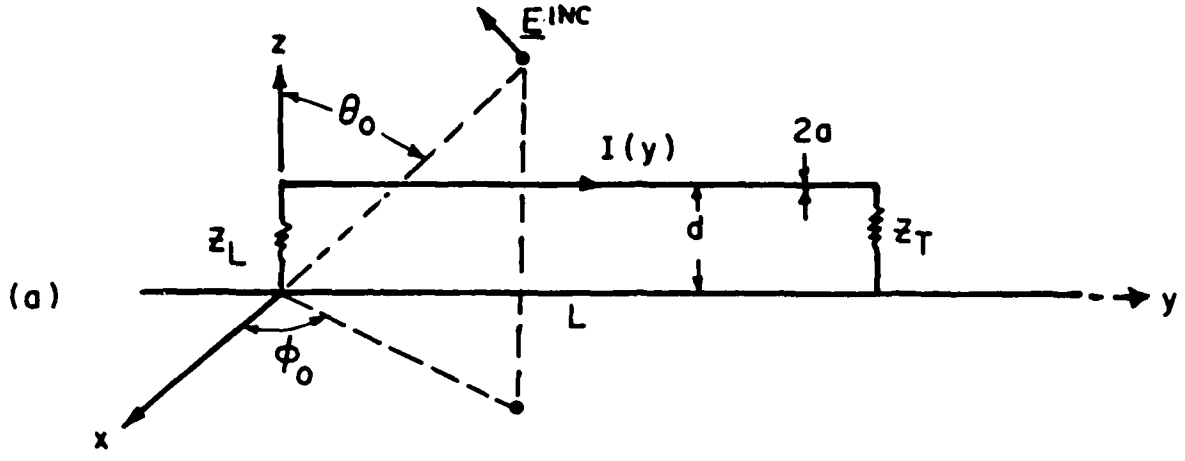

(a) wire/ground plane

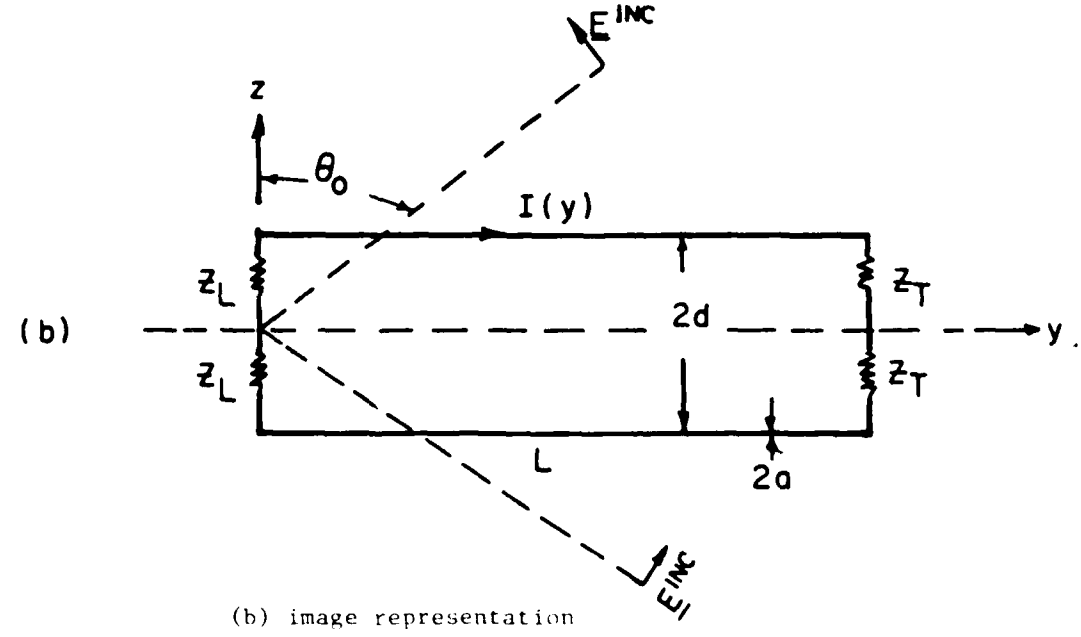

(b) image representation

Fig. 2-14. Geometry for transmission line scattering

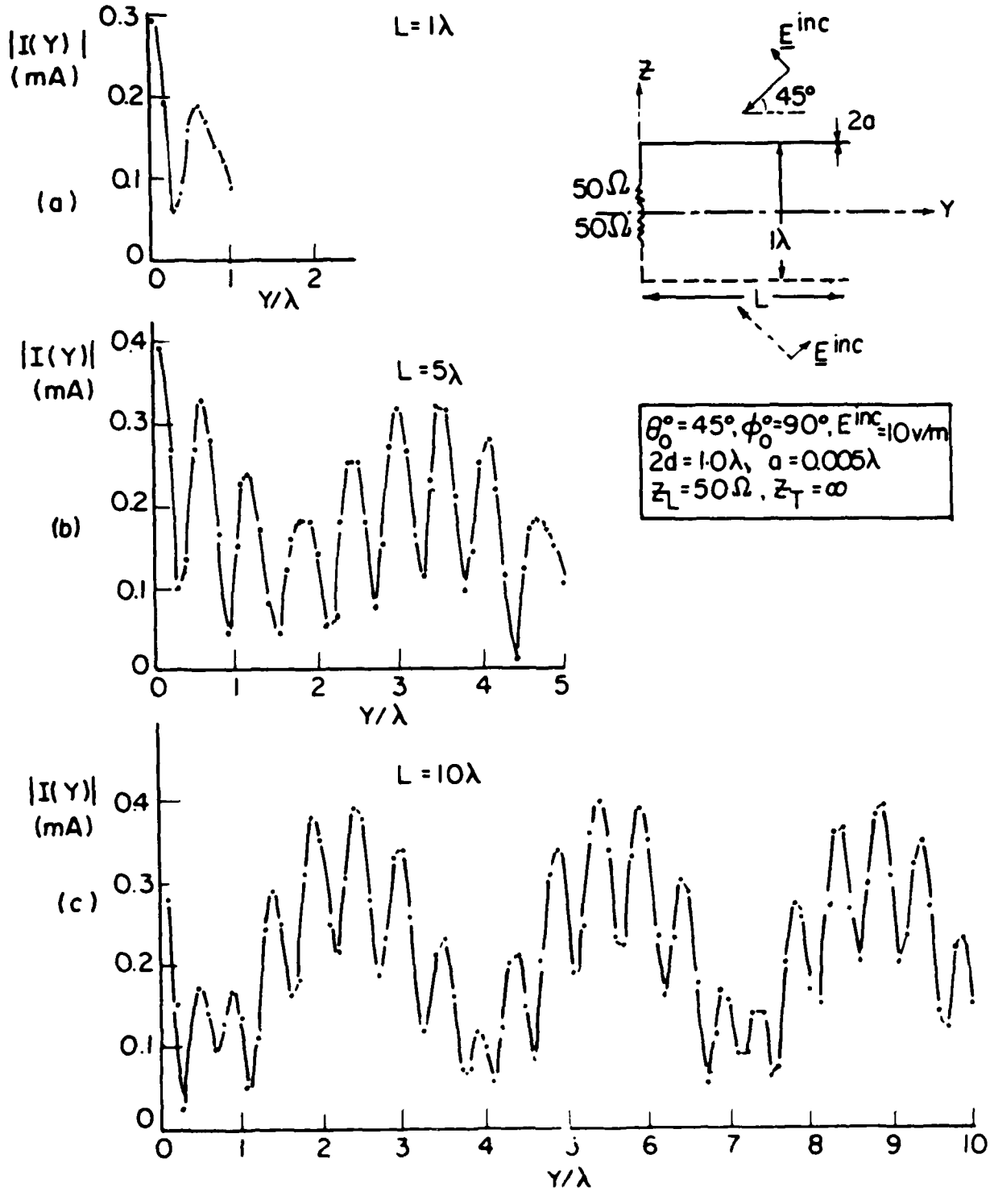

Fig. 2-15. Current distribution for a transmission line scatterer. (a) L = 1. (b) L = 5. (c) L = 10.

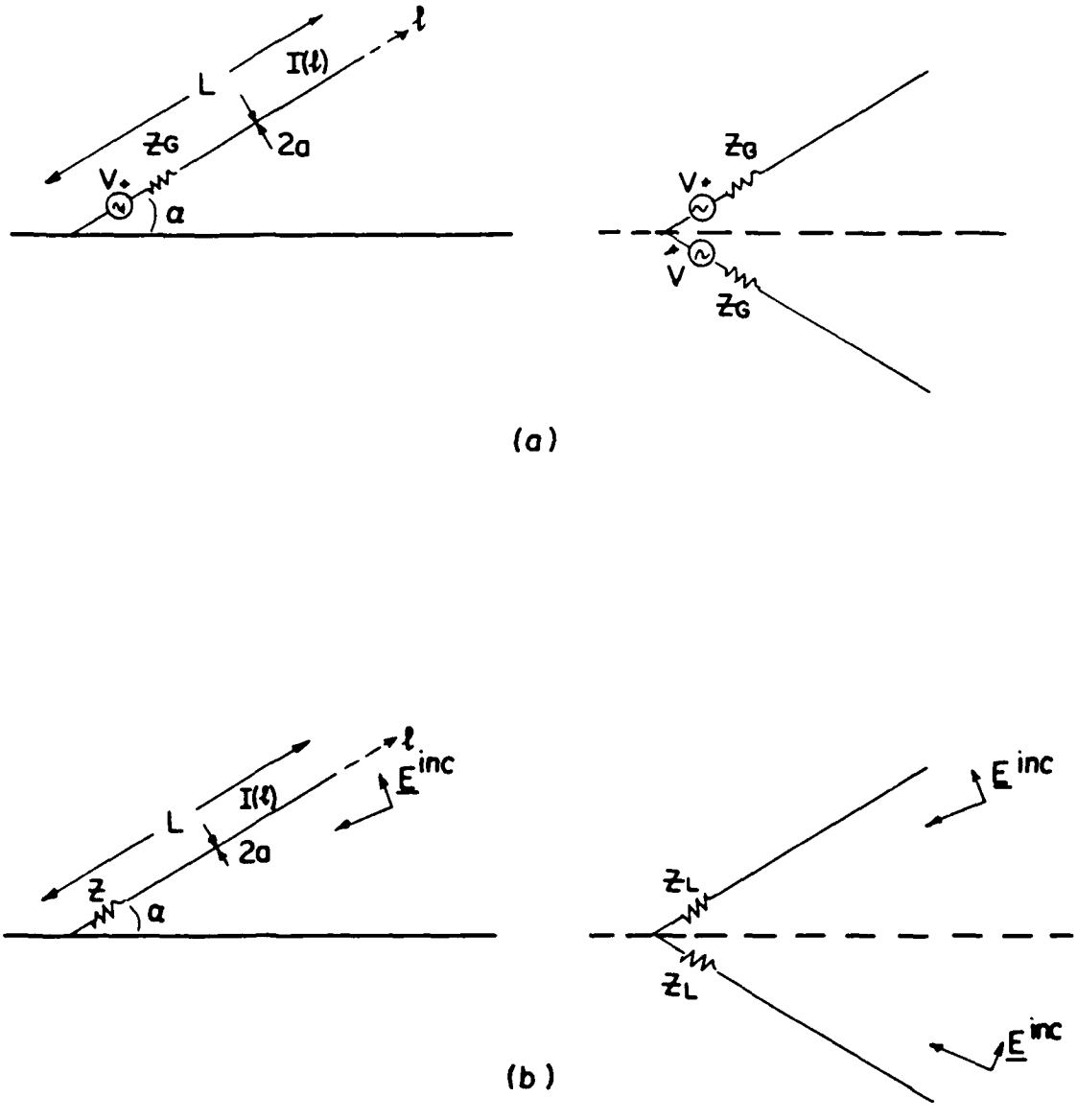

Fig. 2-16. Geometry for a non-uniform transmission line.
(a) radiator (b) scatterer

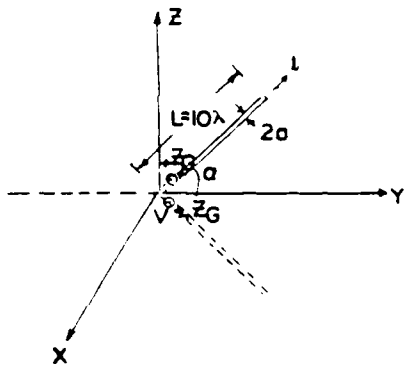

$Z_G = 50\Omega$ $a = 0.02\lambda$

$\alpha = 45°$

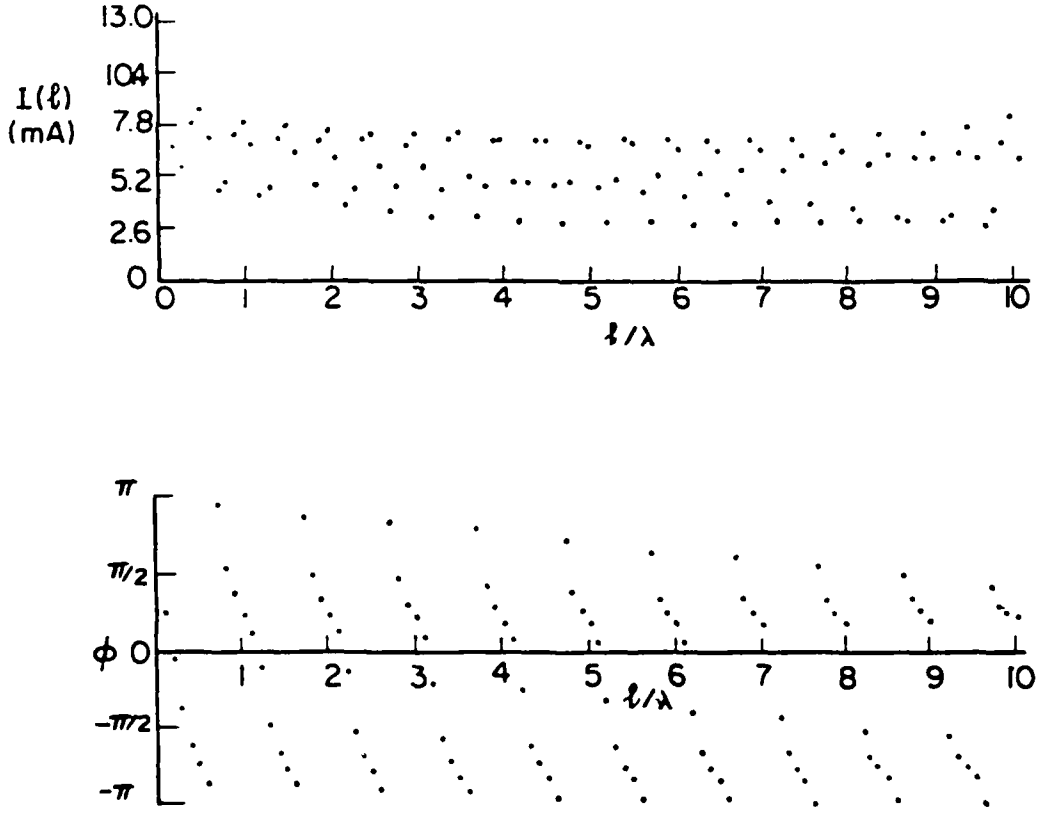

Fig.2-17. Current distribution for a VEE radiator.

Note a combination of traveling - and standing-wave effects. Figs. 2-18 thru 2-22 show the current distributions in scattering problems with the fields incident from $\theta_0 = 90°$, $45°$ ($\phi_0 = 90°$), $\theta_0 = \phi_0 = 0$, and $\theta_0 = 45°$, $90°$ ($\phi_0 = 270°$), respectively Figs. 2-18, 2-20, 2-22 show the three-period pattern of Fig. 2-15. The phase indicates the presence of different phase progressions as discussed previously. Figs. 2-19, 2-21 show less phase variation as expected for normal incidence (consider the direct wave, image vee). Figs.2-23, 2-24 show the scattering problem for the vee antenna with $\alpha = 90°$, $L = 10\lambda$. Normal incidence (Fig. 2-24) leads to less phase variation and Fig. 2-23 shows the familiar three-period pattern. Finally, Figs. 2-25 and 2-26 show current distributions of a curved semicircular structure of length $\ell_1 = 10\lambda$, and separation $d = 0.1\lambda$, 0.5λ, respectively. The closely-spaced wires of Fig. 2-25 exhibit little or no attenuation, whereas the distribution of Fig. 2-26 is highly attenuated.

The current distributions of this chapter exhibit certain consistent trends. First, the patterns of the radiators and scatterers can be explained approximately in terms of standing-and traveling-waves. Attenuated higher-order modes are undoubtedly present, but a first-order approximation can ignore their effects. It would be very interesting to determine (with more complex codes) to what extent these trends hold up as line length and wire separations increase, i.e., as frequency increases.

2.4 REFERENCES FOR CHAPTER FOUR

[1] D. E. Warren, T. E. Baldwin, A. T. Adams, "Near Electric and Magnetic Fields of Wire Antennas," IEEE Transactions on Antennas and Propagation, Vol. AP-22, No. 2, p. 364, March 1974.

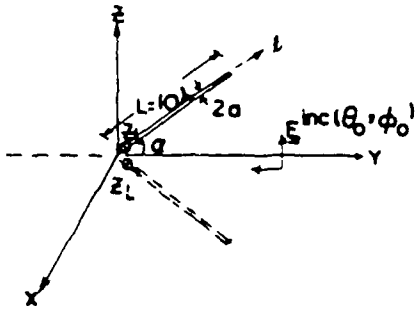

$Z_L = 50\Omega$ $a = 0.02\lambda$ $\alpha = 45°$
$\theta_0 = 90°$, $\phi_0 = 90°$

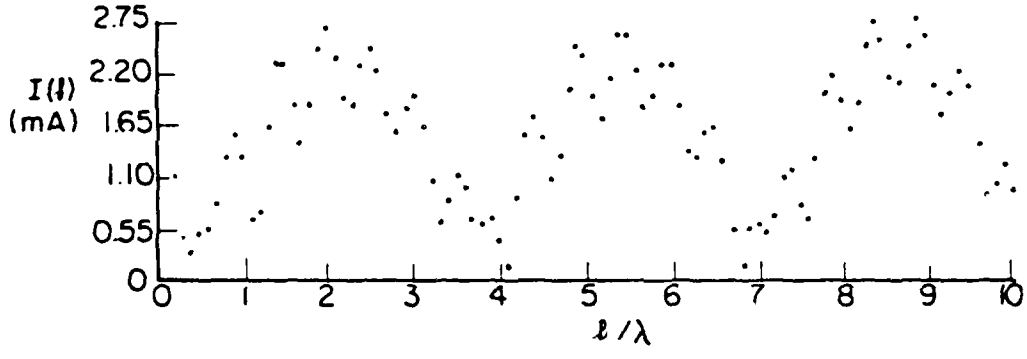

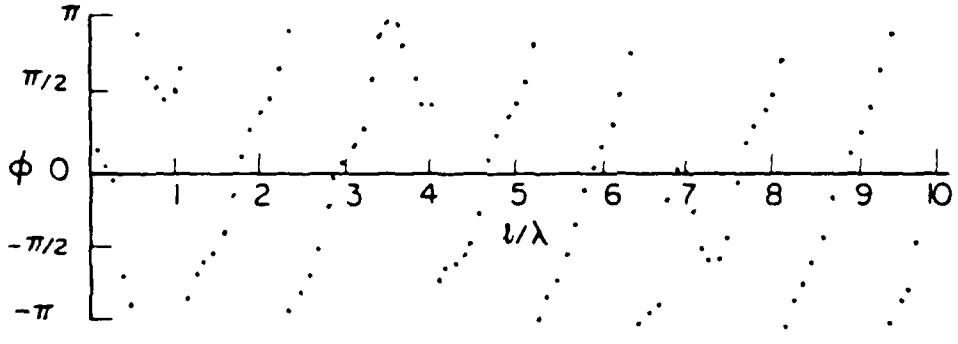

Fig. 2-18. Current distribution for a VEE scatterer (θ_0 = ϕ_0 = 90°).

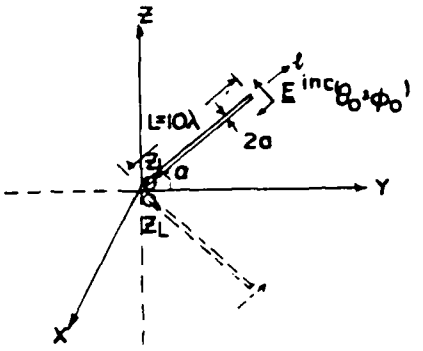

$Z = 50\,\Omega$ $a = 0.02\lambda$ $\alpha = 45°$
$\theta_0 = 45°$ $\phi_0 = 90°$

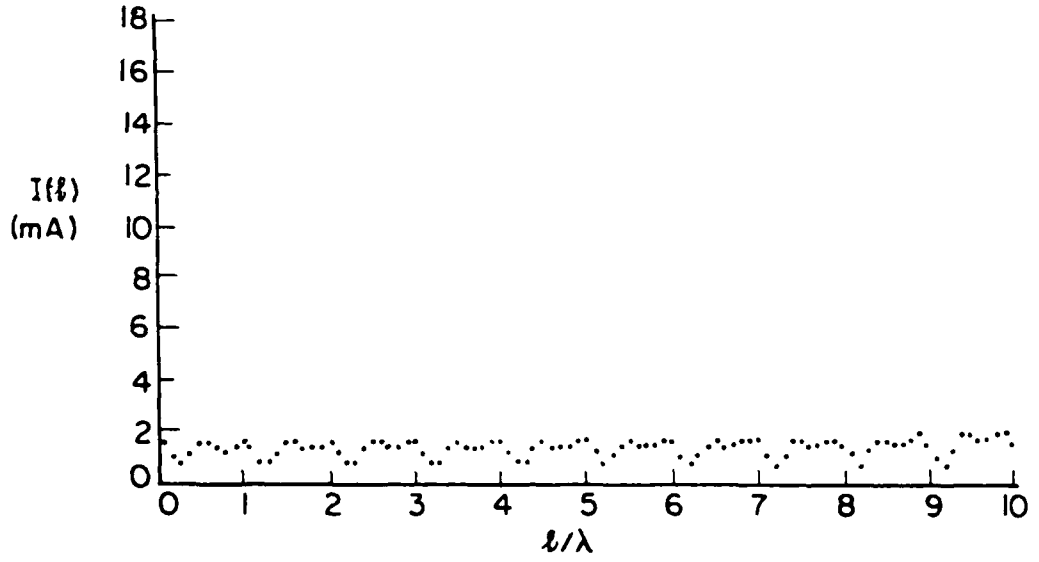

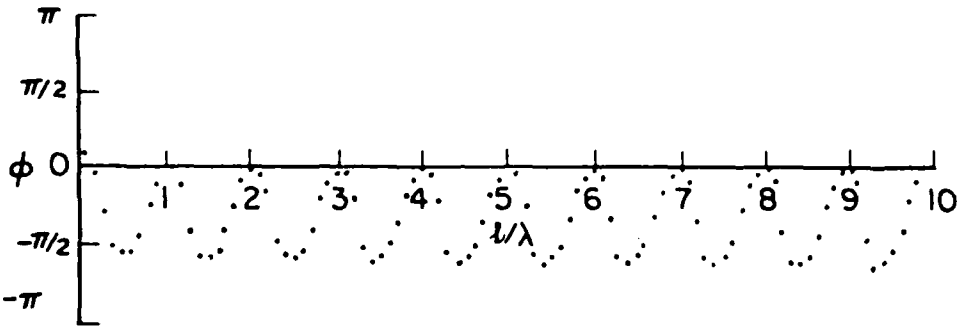

Fig. 2-19. Current distribution for a VEE scatterer ($\theta_o = 45°, \Phi = 90°$)

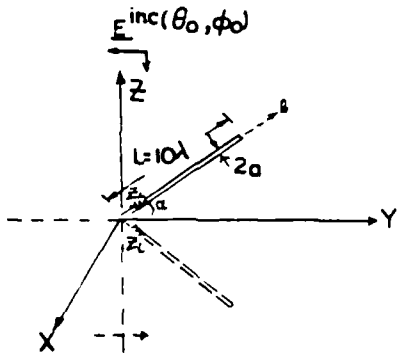

$Z_L = 50\Omega$ $a = 0.02\lambda$ $\alpha = 45°$
$\theta_0 = 0°$ $\phi_0 = 0°$

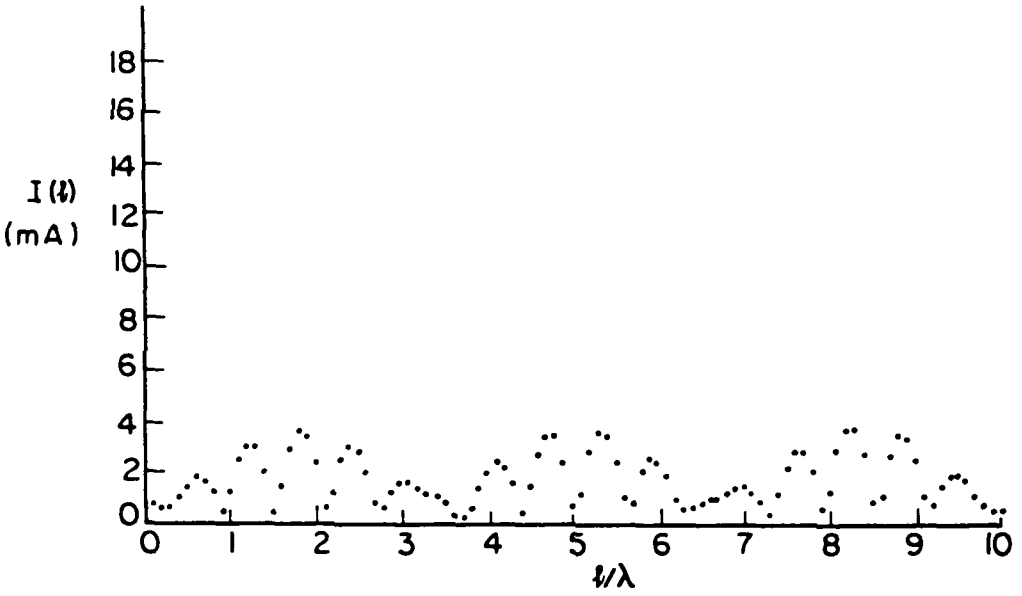

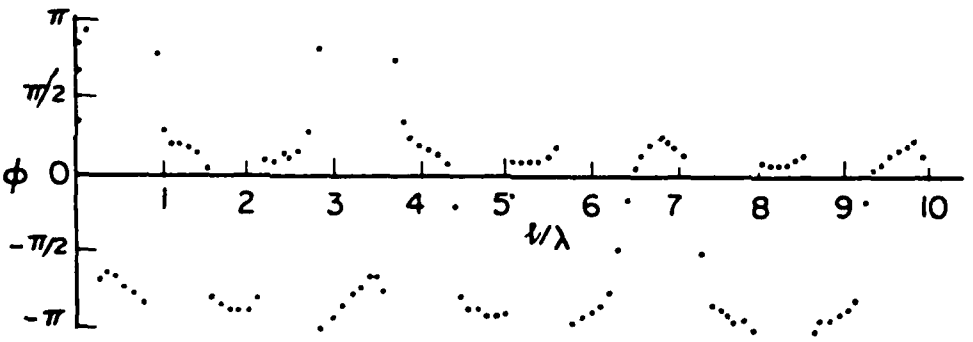

Fig. 2-20. Current distribution for VEE scatterer ($\theta_o = \phi_o = 0°$)

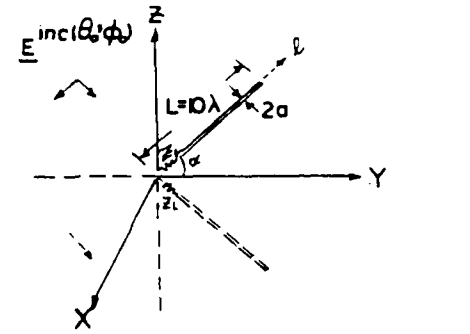

$Z_L = 50\Omega$ $a = 0.02\lambda$ $\alpha = 45°$
$\theta° = 45°$ $\phi_0 = 270°$

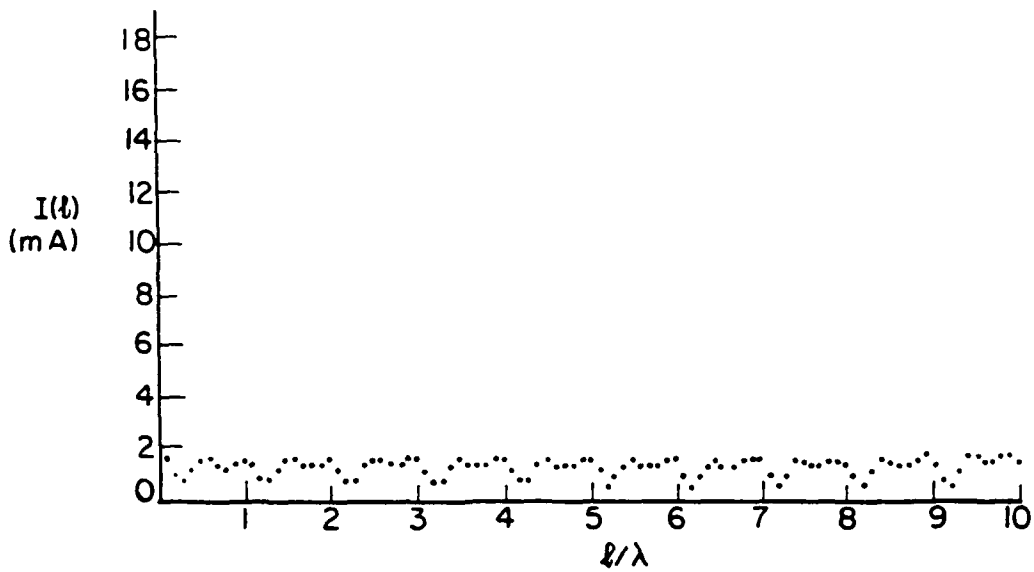

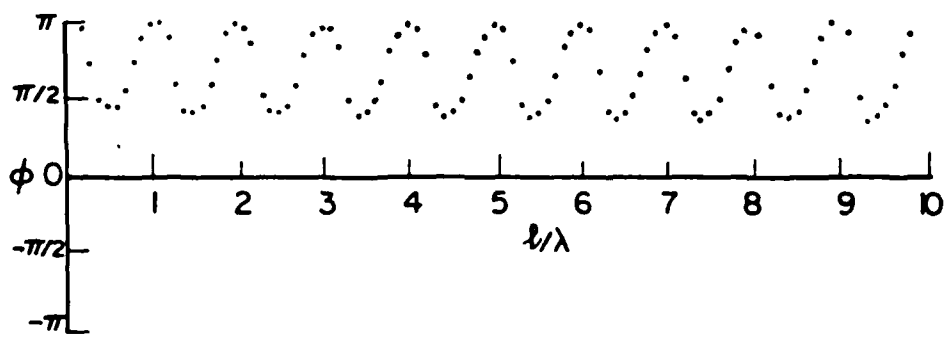

Fig. 2-21. Current distribution for a VEE scatterer ($\theta_o = 45°$, $\phi_o = 270°$)

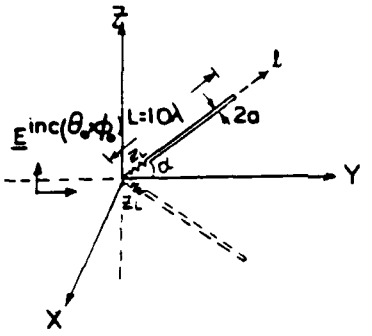

$z_L = 50\Omega$ $a = 0.02\lambda$ $\alpha = 45°$
$\theta_o = 90°$ $\phi_o = 270°$

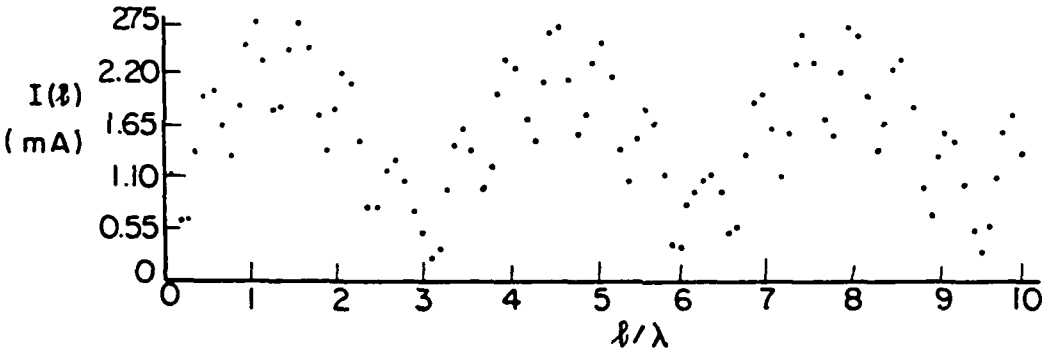

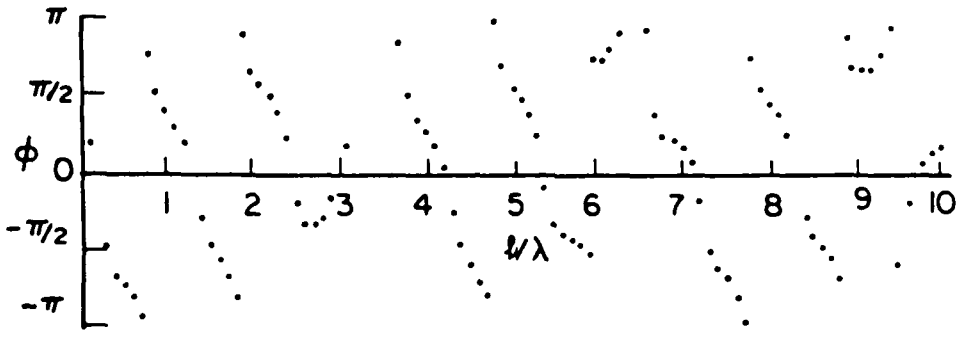

Fig. 2-22. Current distribution for a VEE scatterer (θ_o = 90°, ϕ_o = 270°)

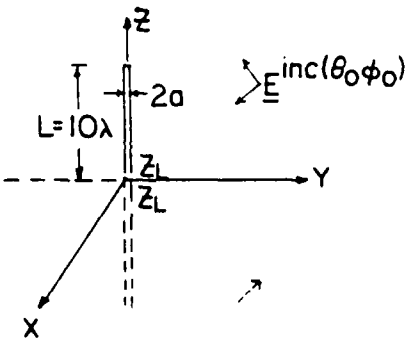

$Z_L = 50\Omega$ $a = 0.02\lambda$
$\theta_0 = 45°$ $\phi_0 = 270°$

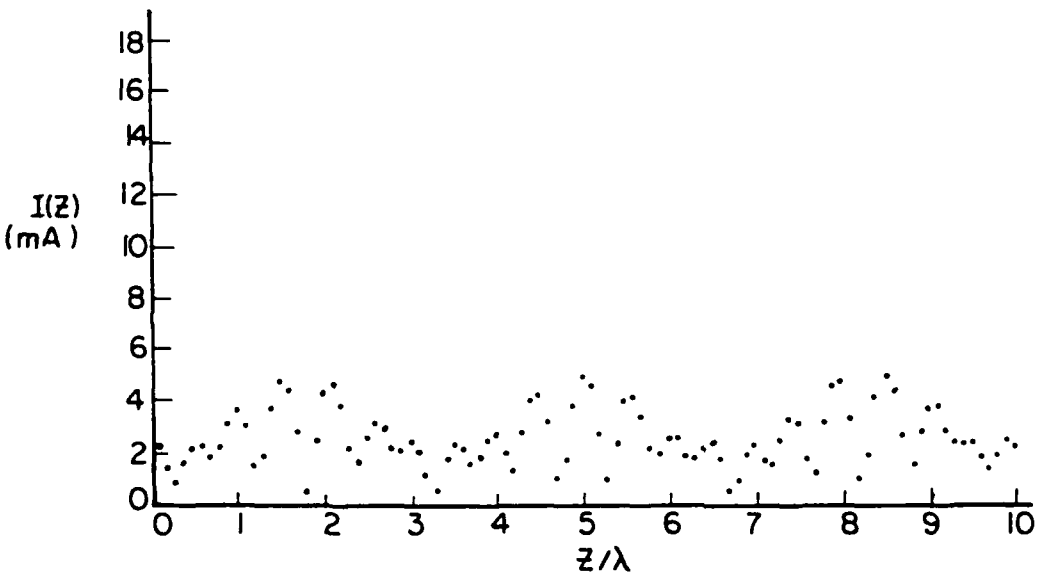

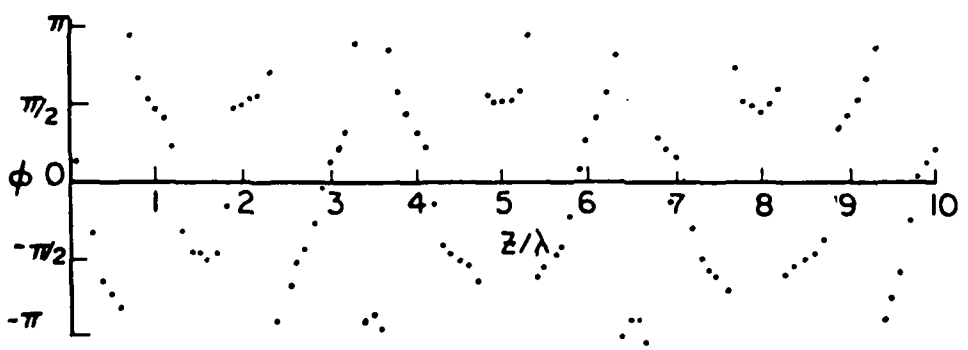

Fig. 2-23. Current distribution for a dipole scatterer (θ_o = 45°, ϕ_o = 270°)

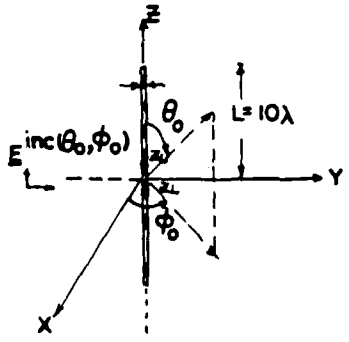

$Z_L = 50\Omega$	$a = 0.02\lambda$
$\theta_0 = 90°$	$\phi_0 = 270°$

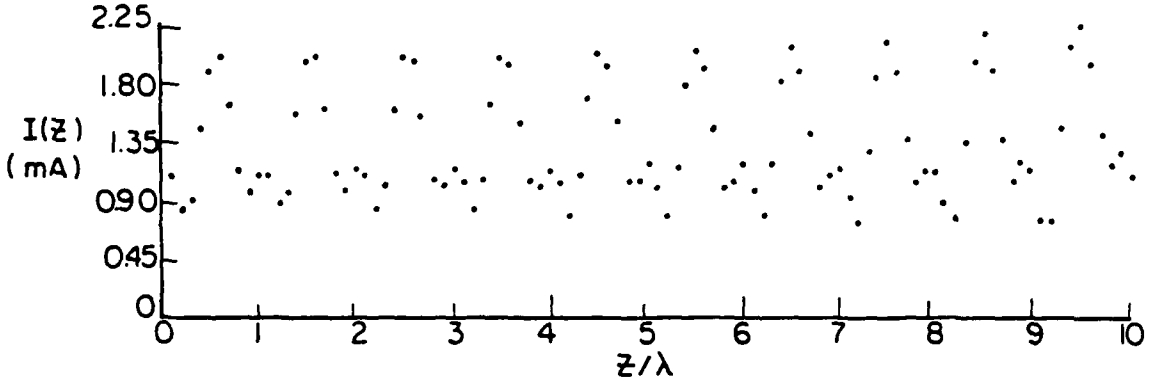

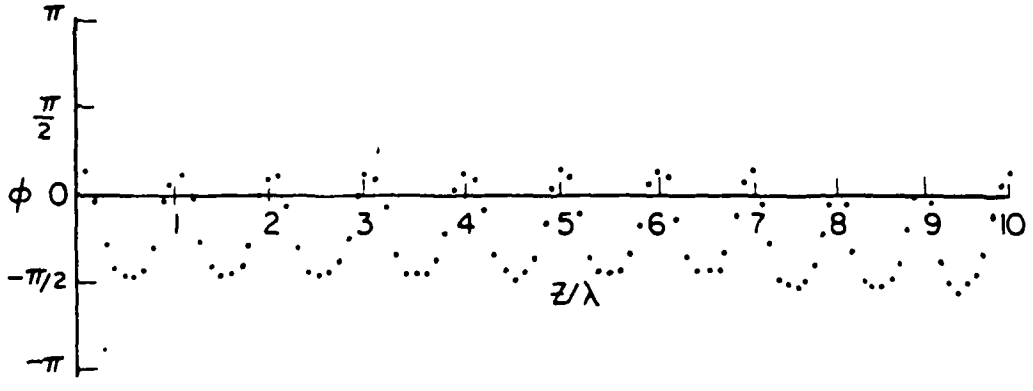

Fig. 2-24. Current distribution for a dipole scatterer ($\theta_0 = 90°$, $\phi_0 = 270°$)

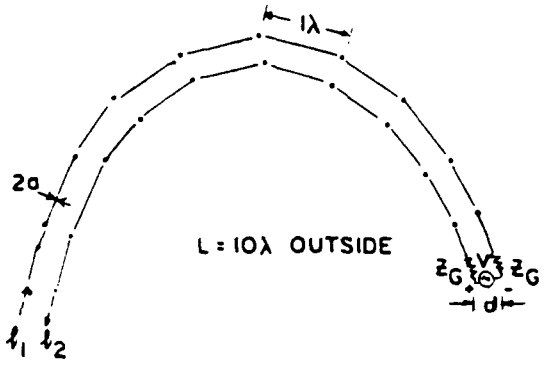

$z_G = 50\Omega$ $a = 0.02\lambda$
$d = 0.1\lambda$

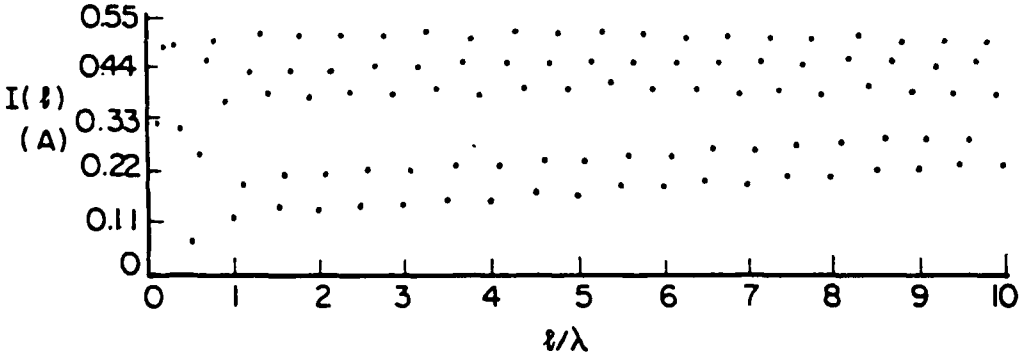

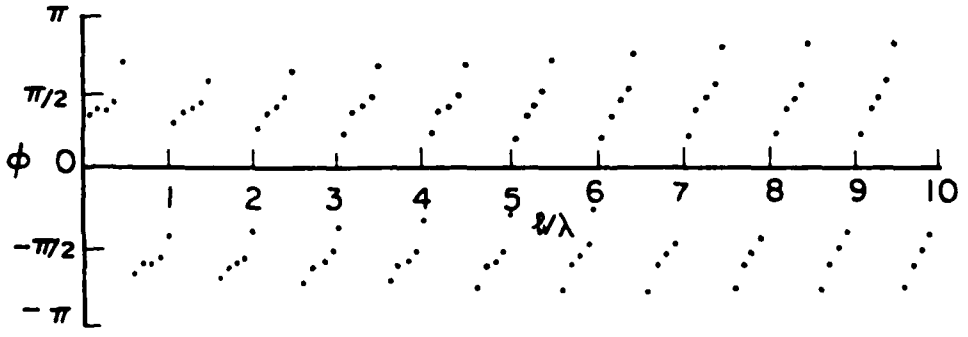

Fig. 2-25. Current distribution for a curved transmission line (d = 0.1λ)

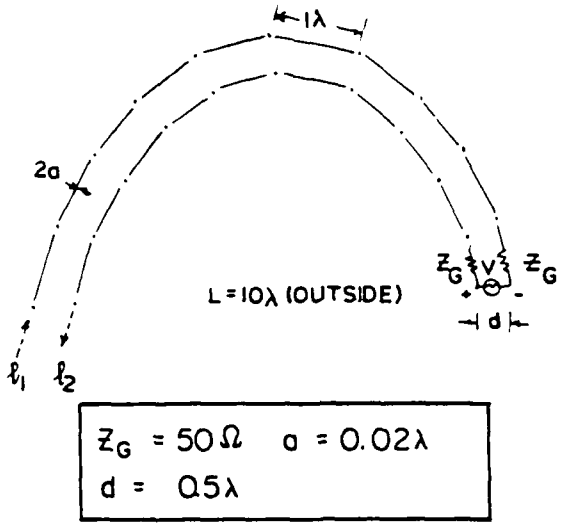

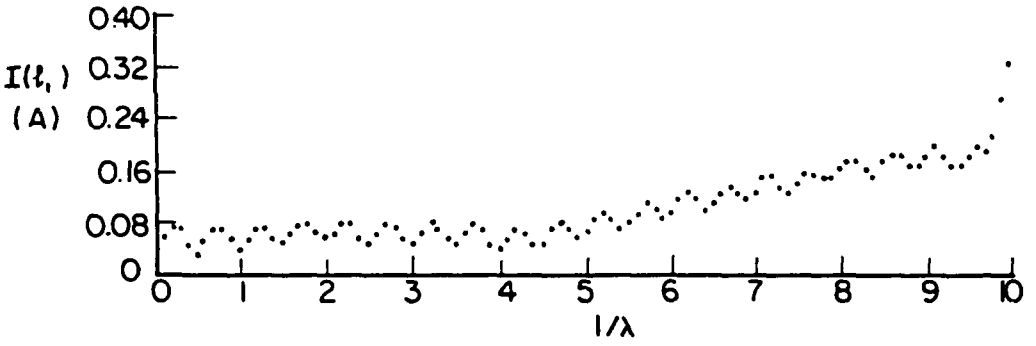

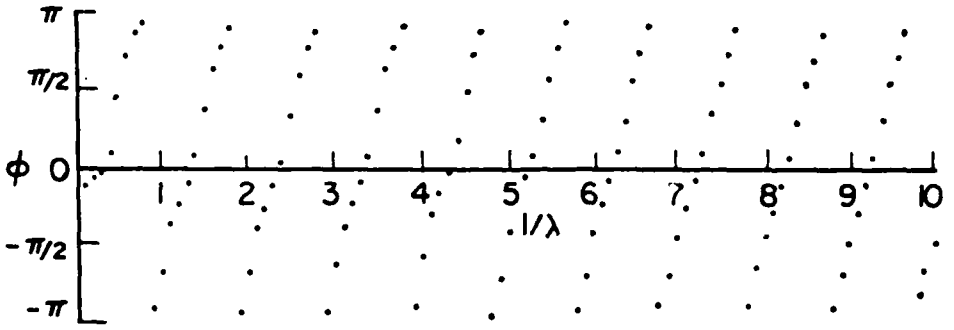

Fig. 2-26. Current distribution for a curved transmission line (d = 0.5λ)

[2] A. T. Adams, B. J. Strait, D. E. Warren, D. C. Kuo, T. E. Baldwin, "Near Fields of Wire Antennas by Matrix Methods," IEEE Transactions on Antennas and Propagation, vol. AP-21, No.5, pp.602-610, Sept. 1973.

CHAPTER 3

EQUIVALENT CIRCUITS FOR N-PORT RECEIVING ANTENNAS

3-1 EQUIVALENT CIRCUITS FOR THE ONE-PORT RECEIVING ANTENNA

Figure 3-1 shows a one-port antenna acting as transmitter (Fig.3-1a) or receiver (Fig. 3-1b) and the Thevenin's (Fig. 3-1c) and Norton's (Fig. 3-1d) equivalent circuits of the receiving antenna. V,I represent terminal voltage, current when the antenna is excited as a transmitter. Z_a, $\underline{J}_t$ represent the impedance, vector current density respectively when excited as a transmitter. V_{oc}, I_{sc} represent open-circuit ($Z_L = \infty$) terminal voltage and short-circuit ($Z_L = 0$) terminal current of the receiving antenna.

The following relationships may be derived [1]

$$V_{oc} = \frac{1}{I} \iiint \underline{E}^{inc} \cdot \underline{J}_t \, dv \tag{3-1}$$

where $\underline{J}_t$ is the antenna current distribution when excited as a transmitter.

$$V_{oc} = I_{sc} Z_a \tag{3-2}$$

$$Z_a = V/I \tag{3-3}$$

3-2 EQUIVALENT CIRCUITS OF MULTIPORT LINEAR DEVICES

In this section, the Thevenin's and Norton's equivalent circuits for one-port active linear devices [2,3] are generalized to obtain equivalent circuits for N-port active linear devices. Three general representations are obtained with voltage, current, and mixed sources, respectively.

Consider the two-port active linear device (Fig.3-2a) with passive

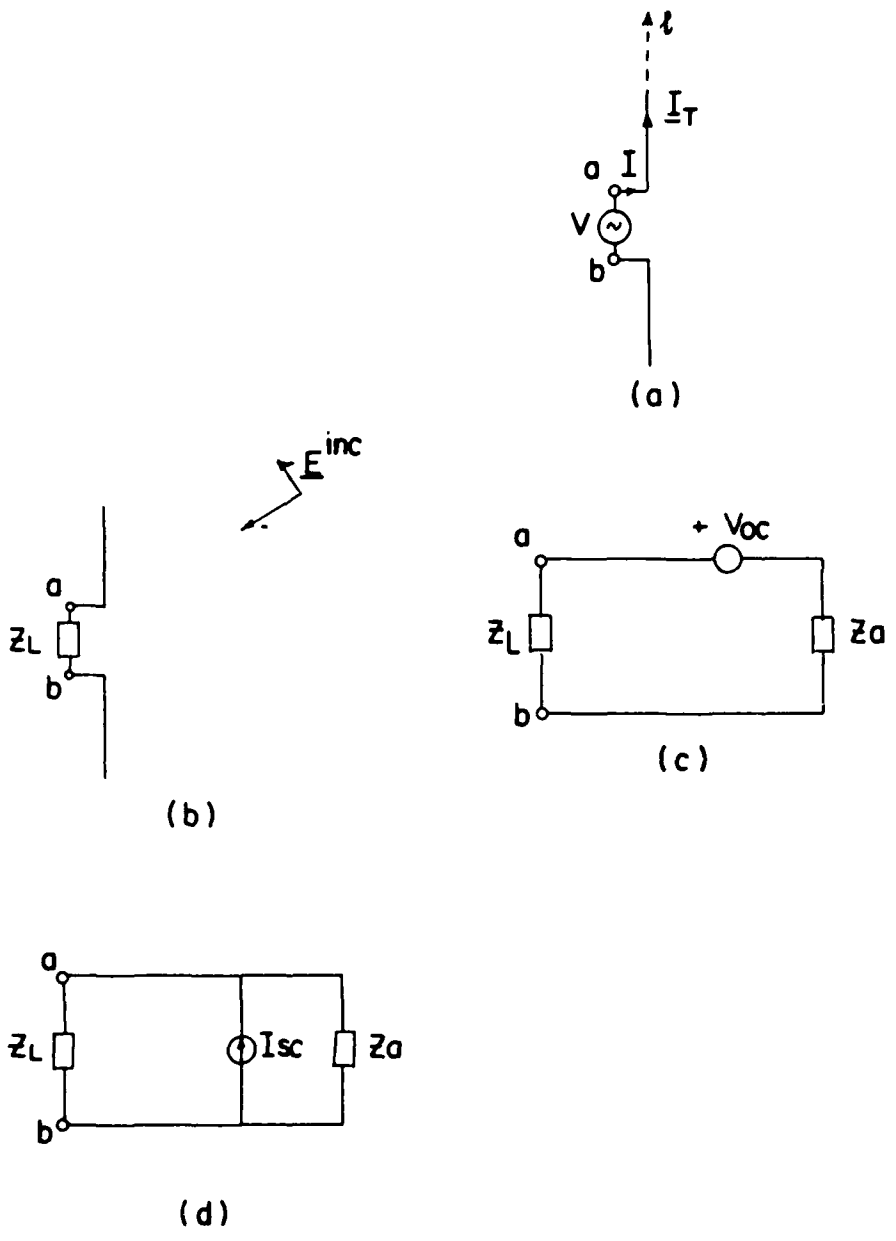

Fig. 3-1. The one-port antenna (a) transmitter (b) receiver (c) Thevenin's equivalent circuit (d) Norton's equivalent circuit.

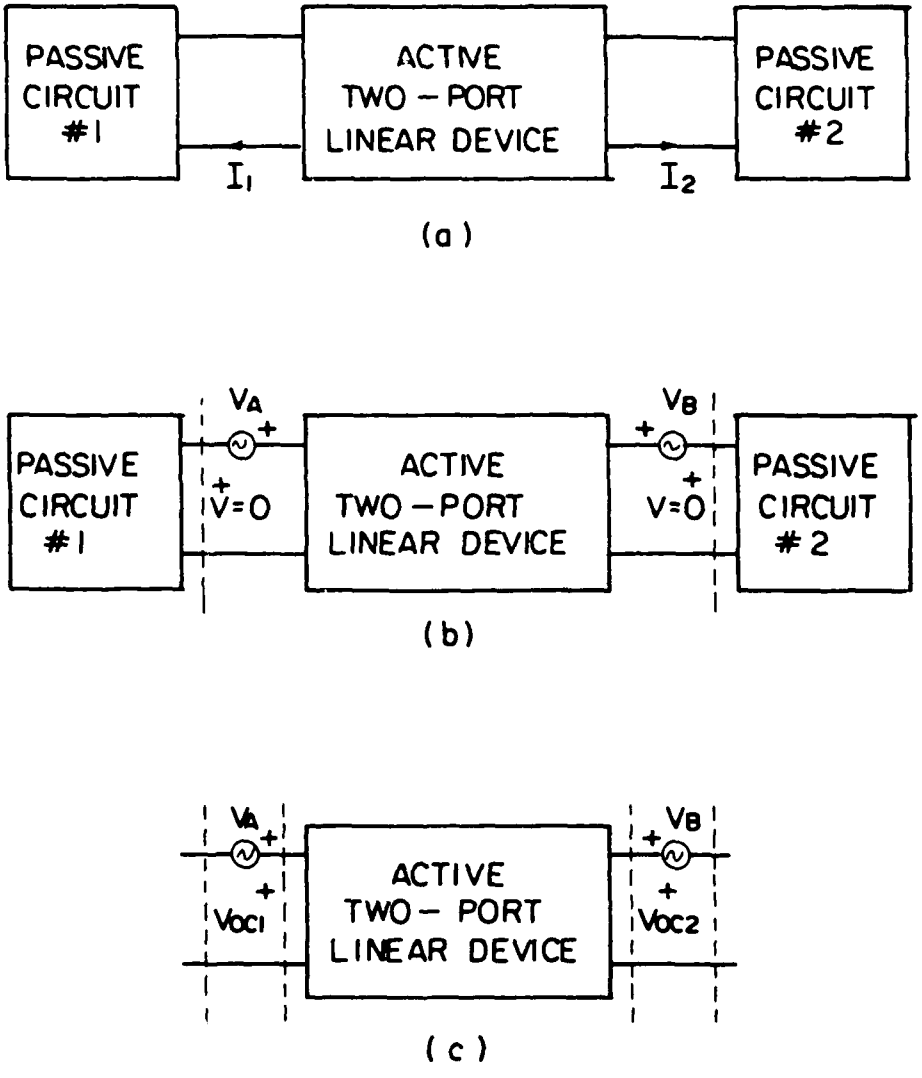

Fig. 3-2. The two-port equivalent circuit (a) general circuit (b) generators added (c) Passive circuits removed

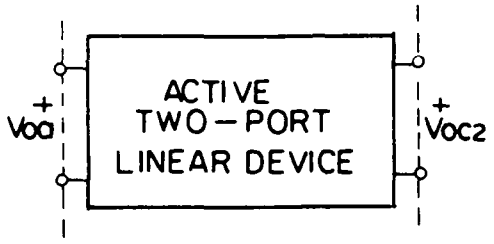

(d)

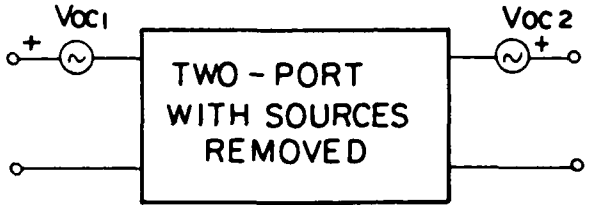

(e)

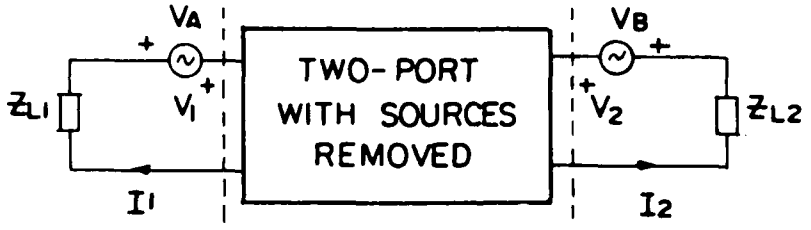

(f)

Fig. 3-2. (d) generators removed
(e) equivalent circuit
(f) conditions for zero currents

circuits to left and right. Currents I_1 and I_2 flow as a result of active internal sources in the two-port. Now add ideal voltage sources V_a, V_b (Fig. 3-2b) and assume (to be verified later) that it is possible to adjust V_a, V_b such that currents passing thru V_a, V_b are both zero. The voltages across terminals of the passive networks are thus zero. One may disconnect the passive circuits (Fig. 3-2c) without changing any voltages or currents. The generators V_a, V_b may also be disconnected (Fig. 3-2d). The voltages across the two-port are V_{oc1}, V_{oc2}, i.e., the open circuit voltages of the two-port when both ports are simultaneously open-circuited. Then

$$V_a + V_{oc1} = 0 \tag{3-4}$$

$$V_b + V_{oc2} = 0 \tag{3-5}$$

V_a and V_b, together with internal sources, have produced zero currents. The effect of V_a, V_b without internal sources would be to produce currents $-I_1$, $-I_2$. If voltage sources V_a, V_b are reversed (Fig. 3-2c) the effect would be to produce original currents I_1, I_2. Fig. 3-2c is thus a valid equivalent circuit of the two-port.

Now consider whether it is possible to adjust V_a, V_b to produce zero currents. Alternatively, if internal sources are deactivated, is it possible to adjust $-V_a$, $-V_b$ to produce $+I_1$, $+I_2$? Consider the corresponding equivalent circuit as shown in Fig. 3-2f. The voltage-current relationships may be given as follows (the passive circuits are replaced with loads Z_{L1}, Z_{L2}, respectively):

$$V_1 = Z_{11}I_1 + Z_{12}I_2 = V_a - Z_{L1}\, I_1 \tag{3-6}$$

$$V_2 = Z_{21}\, I_1 + Z_{22}\, I_2 = V_b - Z_{L2}\, I_2 \tag{3-7}$$

Then

$$V_a = (Z_{11} + Z_{L1})\, I_1 + Z_{12}\, I_2 \tag{3-8}$$

$$V_b = Z_{21}\, I_1 + (Z_{22} + Z_{L2})\, I_2 \tag{3-9}$$

V_a, V_b are thus specified given I_1, I_2 and the two-port equivalent circuit (Fig.3-2e) is established.

The N-port device may be treated in a similar manner leading to the equivalent circuit shown in Fig. 3-3a. All ports are simultaneously open-circuited to obtain $V_{ocl} \ldots V_{ocn}$. A dual development leads to the equivalent circuit of Fig. 3-3b. All ports are simultaneously short-circuited to obtain $I_{scl} \ldots I_{scn}$. Finally, mixed source representations such as that of Fig. 3-3c may be obtained by using a combination of ideal voltage and current sources.

3.3 EQUIVALENT CIRCUITS FOR MULTIPORT RECEIVING ANTENNAS

Fig. 3-4a shows magnetic current sources $\underline{M}_{t1}$, $\underline{M}_{t2}$ and electric current source $\underline{J}_a$ in the presence of two conductors. $\underline{M}_{t1}$, $\underline{M}_{t2}$ enforce voltages V_1, V_2 at the two-port antenna terminals and are sources which excite the antennas as transmitters. $\underline{J}_a$ is the source of incident fields. Applying reciprocity [4] between sources t and a in the presence of the conductor yields

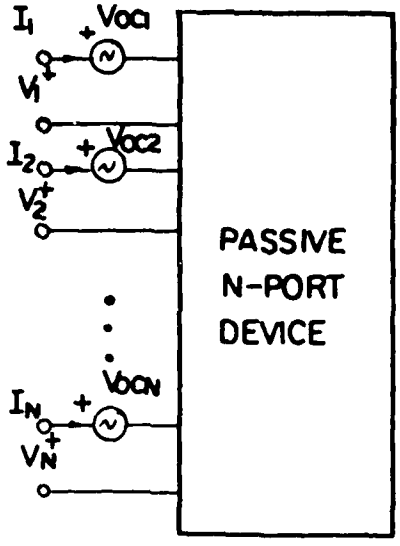

(a)

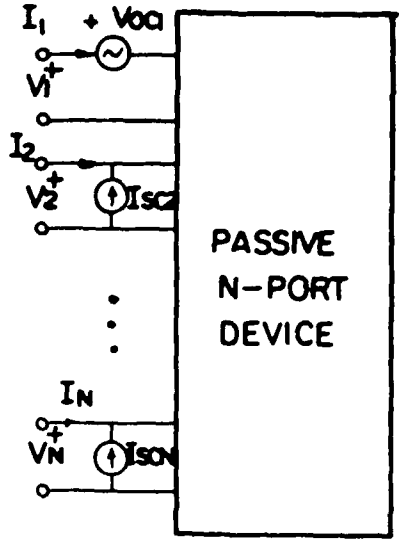

(c)

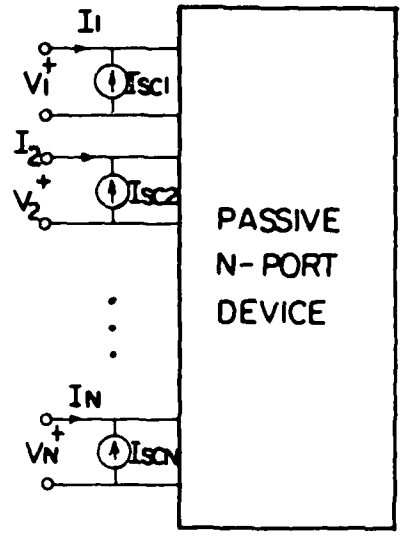

(b)

Fig. 3-3. N-port equivalent

(a) voltage sources (b) current sources (c) mixed sources

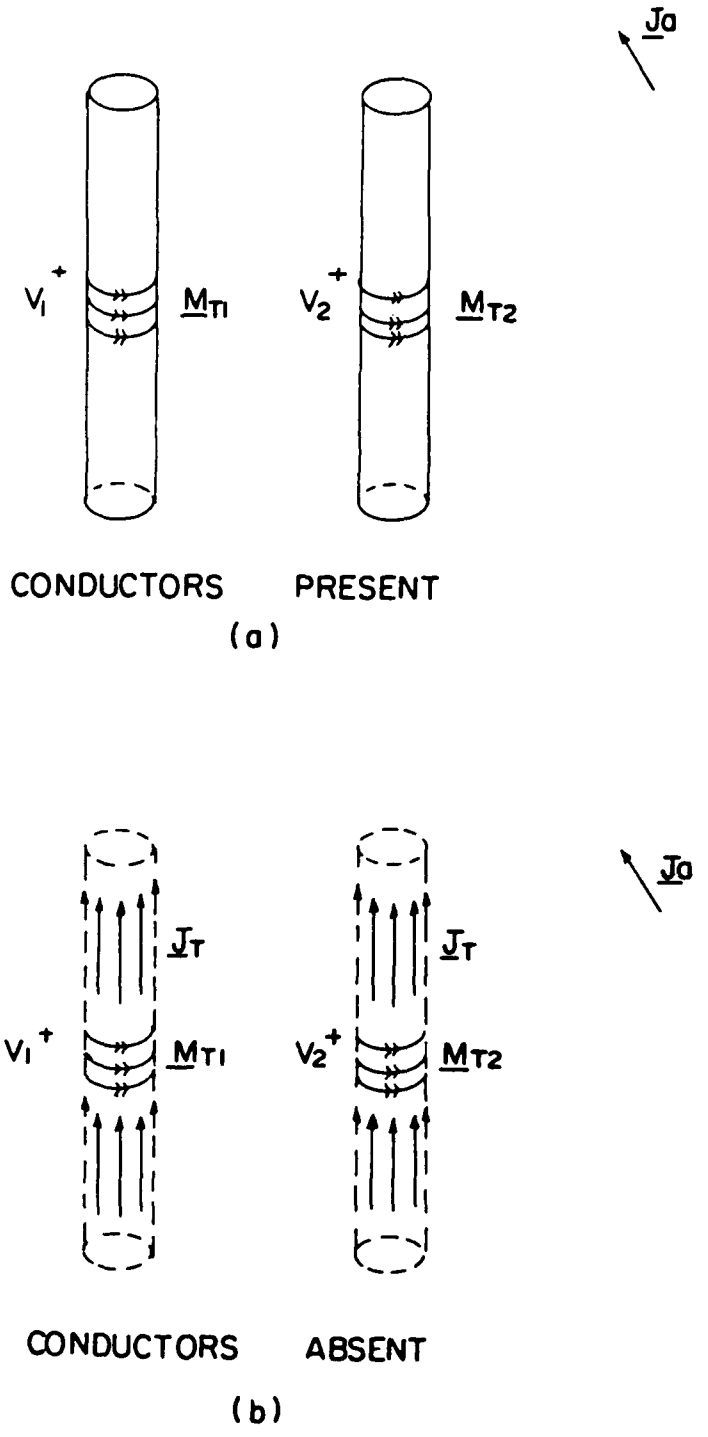

Fig. 3-4. The two-port receiving antenna with voltage sources (a) conductors present (b) conductors absent

$$\iiint \underline{E}_t \cdot \underline{J}_a \, dv = - \iiint \underline{H}_a \cdot \underline{M}_t \, dv$$

$$\approx V_1 \cdot I_{sc1} + V_2 \, I_{sc2} \tag{3-10}$$

where $\underline{M}_t = \underline{M}_{t1} + \underline{M}_{t2}$.

Fig. 3-4b shows applied sources $\underline{M}_t$ and induced electric current $\underline{J}_t$ in the absence of conductors (removed by equivalence [5]). Reciprocity is applied between sources t and a in the absence of conductor. $\iiint \underline{E}_t \cdot \underline{J}_a \, dv$ is unchanged and therefore

$$V_1 I_{sc1} + V_2 I_{sc2} = \iiint \underline{E}_t \cdot \underline{J}_a \, dv$$

$$= \iiint \underline{E}_a \cdot \underline{J}_t \, dv - \iiint \underline{H}_a \cdot \underline{M}_t \, dv \tag{3-11}$$

$$\approx \iiint \underline{E}_a \cdot \underline{J}_t \, dv = \iiint \underline{E}^{inc} \cdot \underline{J}_t \, dv$$

where $\underline{E}_a$ has been replaced with $\underline{E}^{inc}$, the incident fields. The integral $\iiint \underline{H}_a \cdot \underline{M}_t \, dv$ may be neglected for thin wires. Then

$$I_{sc1} = \frac{1}{V_1} \iiint \underline{E}^{inc} \cdot \underline{J}_t \, dv$$

$$= \frac{Y_{11}}{I_1} \iiint \underline{E}^{inc} \cdot \underline{J}_t \, dv \quad (\text{if } V_2 = 0) \tag{3-12}$$

$$I_{sc2} = \frac{Y_{22}}{I_2} \iiint \underline{E}^{inc} \cdot \underline{J}_t \, dv \quad (\text{if } V_1 = 0) \tag{3-13}$$

I_{sc1}, I_{sc2} represent terminal currents when both ports are simultaneously short-circuited. I_1, I_2 are terminal currents when antennas are excited as transmitters. $\underline{J}_t(V_2 = 0)$ represents currents on both antennas when port one

is excited with I_1 and port two is short-circuited and similarly for $\underline{J}_t$ $(V_1 = 0)$. The resulting equivalent circuit for the two-port is shown in Fig. 3-7b. The results may be extended to the N-port receiving antenna:

$$I_{sci} = \frac{Y_{ii}}{I_i} \iiint \underline{E}^{inc} \cdot \underline{J}_t \, dv \quad (V_j = 0, \; j \neq i) \tag{3-14}$$

where $\underline{J}_t(V_j = 0, \; j \neq i)$ represents the currents on all antennas when port i is excited with I_i and all other ports are shorted. The equivalent circuit is given in Fig. 3-3b.

A parallel development for electric current sources leads to the following results for the two-port problem (see fig. 3-5):

$$V_{oc1} = \frac{1}{I_1} \iiint \underline{E}_{inc} \cdot \underline{J}_t \, dv \quad (I_2 = 0) \tag{3-15}$$

$$V_{oc2} = \frac{1}{I_2} \iiint \underline{E}_{inc} \cdot \underline{J}_t \, dv \quad (I_1 = 0) \tag{3-16}$$

and the general result for the N-port is

$$V_{oci} = \frac{1}{I_i} \iiint \underline{E}^{inc} \cdot \underline{J}_t \, dv (I_j = 0, \; j \neq i) \tag{3-17}$$

V_{oci} is the open-circuit voltage at terminal i of the receiving antenna when all ports are simultaneously open-circuited.

$\underline{J}_t(I_j = 0), \; j \neq i)$ represents the currents on all antennas when port i is excited as a transmitter with current I_i and all other ports are open-circuited. The two-port and N-port equivalents are shown in Figs. 3-7a, 3-3a, respectively.

Finally a parallel development for the mixed-source representation of Fig. 3-6 yields

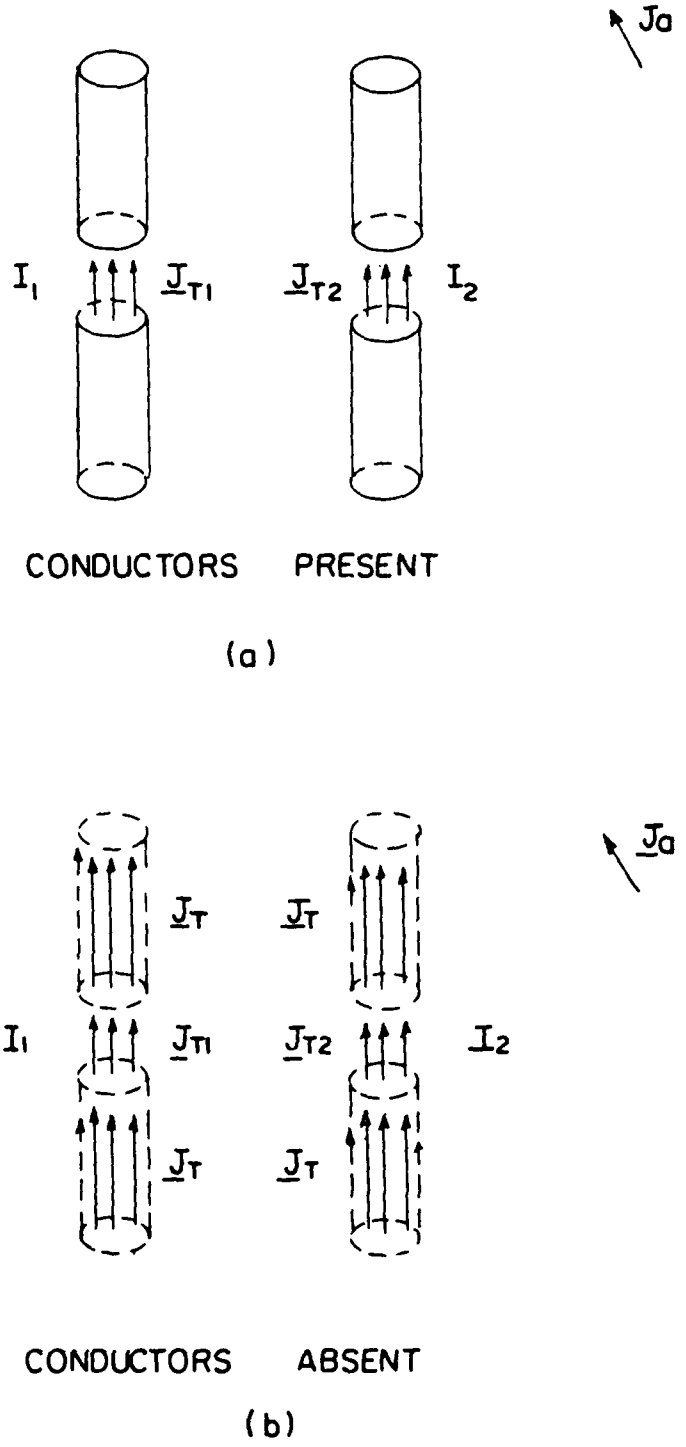

Fig. 3-5. The two-port receiving antenna with current sources (a) conductors present (b) conductors absent

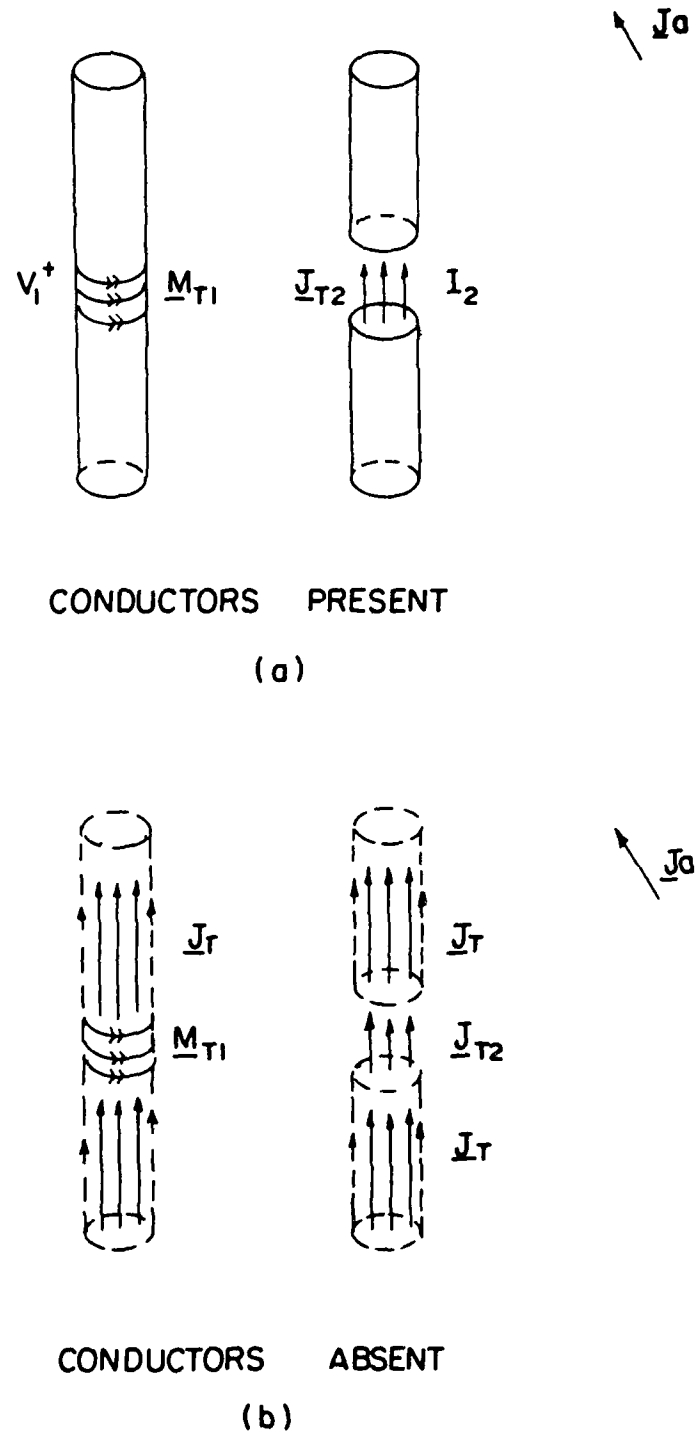

Fig. 3-6. The two-port receiving antenna with mixed sources (a) conductors present (b) conductors absent.

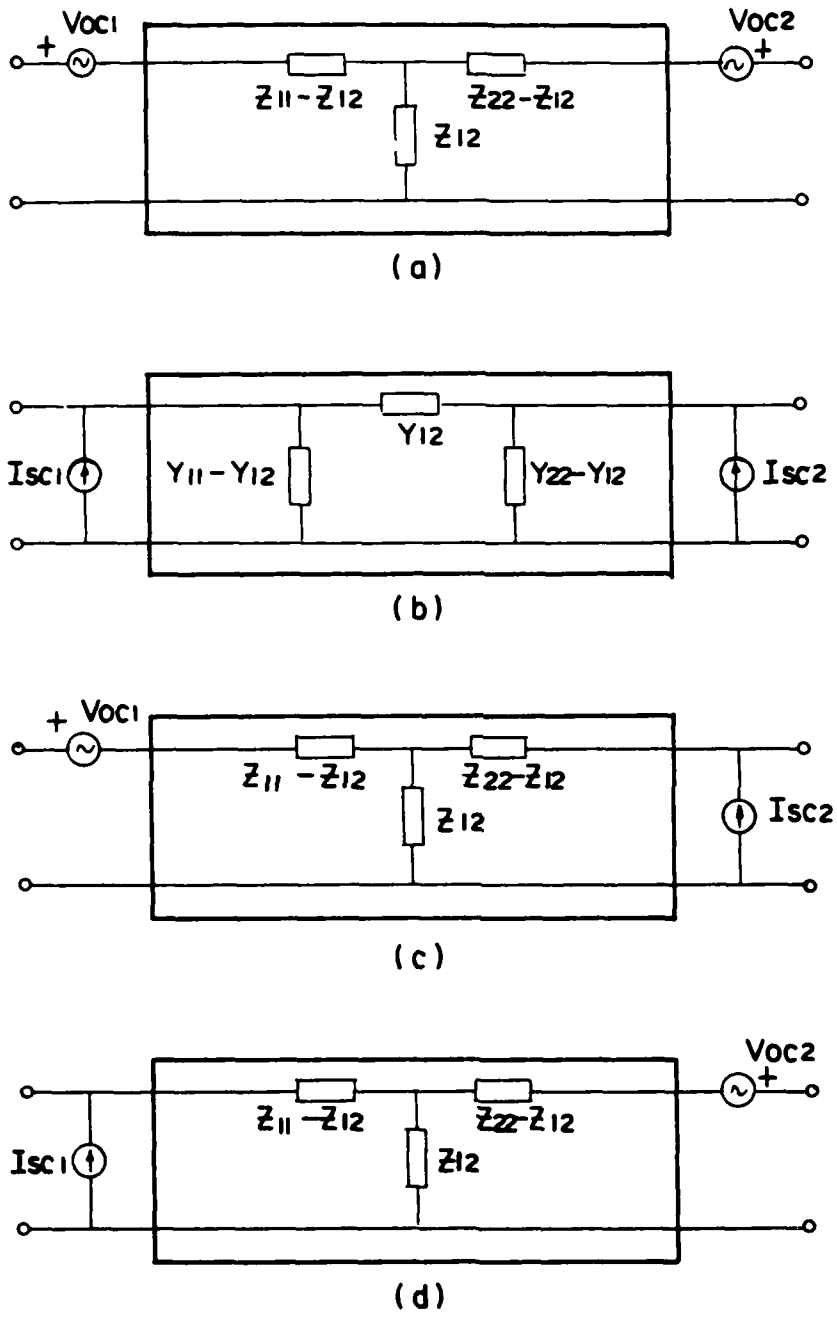

Fig. 3-7. Equivalent circuits of the two-port

(a) voltage sources (b) current sources

(c) voltage/current sources (d) current/voltage sources.

$$V_{oc2} = \frac{1}{I_2} \iiint \underline{E}^{inc} \cdot \underline{J}_t \, dv \quad (V_1 = 0) \tag{3-18}$$

$$I_{sc1} = \frac{1}{Z_{11} I_1} \iiint \underline{E}^{inc} \cdot \underline{J}_t \, dv \quad (I_2 = 0) \tag{3-19}$$

For a model (not shown) with current source at port one and voltage source at port two:

$$V_{oc1} = \frac{I}{I_1} \iiint \underline{E}^{inc} \cdot \underline{J}_t \, dv \quad (V_2 = 0) \tag{3-20}$$

$$I_{sc2} = \frac{1}{Z_{22} I_2} \iiint \underline{E}^{inc} \cdot \underline{J}_t \, dv \quad (I_1 = 0) \tag{3-21}$$

In Equation (3-18), V_{oc2} is the open-circuit voltage of the receiving antenna at port two when port one is short-circuited. $\underline{J}_t$ $(V_1 = 0)$ is the current on both antennas when operating as a transmitter with current I_2 at port two and port one is short circuited. The equivalent circuits are shown in Figs. 3-7c, 3-7d, 3-3c.

3.4 REFERENCES FOR CHAPTER THREE

[1] W. L. Weeks, Antenna Engineering McGraw-Hill, N.Y., 1968, Section 8.1, pp. 292-296.

[2] S. Seshu and N. Balabanian, Linear Network Analysis, John Wiley, 1959, Section 5.2, pp. 155-160

[3] M.E. Van Valkenburg, Network Analysis, 3rd Edition, 1974, Prentice-Hall, Section 9.5, pp. 259-270.

[4] R. F. Harrington, Time-Harmonic Electromagnetic Fields, McGraw-Hill, N.Y., 1961, Section 3.8, pp.116-120.

[5] Ibid, Section 3.5, pp. 106-110.

Chapter IV

BOUNDS FOR INDUCED CURRENT

4.1 INTRODUCTION

Each of the scattering problems of Figs. 1-1 thru 1-4 may be considered as a receiving antenna. The equivalent circuit of the receiving antenna is shown in Fig. 3-1. In order to determine the current induced in load Z_L, the antenna impedance Z_a of the antenna when excited as a transmitter and the open-circuit voltage V_{oc} of the receiving antenna are required. Alternatively, the minimum magnitude of Z_a and the maximum magnitude of V_{oc} will yield an upper bound on the magnitude of induced current in the load. Approximations and bounds are obtained for Z_a and V_{oc}, thus allowing one to obtain bounds or approximations for induced current. For very long antennas, the impedance upper and lower bounds converge so that the actual value of the impedance can be closely approximated. The absolute upper bound for Z_a can be obtained by treatment of a relatively short transmission line which may be modeled by moment methods. V_{oc} can be approximated by using simple models, i.e. standing or traveling waves, for the current $\underline{J}_t$ when the antenna is excited as a transmitter.

4.2 BOUNDS FOR ANTENNA IMPEDANCE Z_a

Kraus [1] has shown a plot of dipole impedance in the complex plane. His plot for the dipole exhibits a spiral-like pattern from which upper and lower bounds for the magnitude can be obtained. Numerous plots of transmission line impedance have been made for transmission lines similar to Figs. 1-1 thru 1-4. These plots all exhibit similar behavior; upper and

lower bounds to Z_a may be obtained from them.

Fig. 4-1 shows a dipole of length $2L_1$ and a transmission line of length L_2 and wire spacing $2d = .5\lambda$. The dipole and transmission line are treated separately, each in the absence of the other. The dipole and transmission line impedances are shown dotted, solid, respectively. The two plots coincide for a distance d. The magnitudes of the minimum and maximum values of the impedance may be found by drawing tangents to the curves from the origin. Both dipole and transmission line impedance plots exhibit the spiral-type structure. Both curves spiral into a tight circle within about two wavelengths ($L_1 = L_2 = 2\lambda$). Note that the absolute minimum magnitude of Z_a is about 30Ω. This value may be determined from a geometry of modest electrical size ($L_1 < 0.25\lambda$) even though the actual antenna or transmission line may be extremely large electrically and therefore unsuitable for moment methods. Note further that after a few turns ($L_1 > 2\lambda$), the dipole impedance has approached a circle with minimum value of about 50Ω and a maximum value of about 240Ω. Similarly, the transmission line impedance has an absolute minimum of about 30Ω and, for $L_2 > 2\lambda$, a minimum value of about 90Ω and a maximum value of about 350Ω. Figs. 4-2, 4-3 show a similar structure with wire spacing $2d = \lambda, 2\lambda$, respectively. The transmission line spirals into a relatively small circle. For $L_2 > 2\lambda$, the lower and upper bounds are about 80 , 150Ω for $d = 0.5\lambda$ and about 80 , 145Ω for $d = 1.0\lambda$.

Figs. 4-4 thru 4-9 show a two-conductor transmission line of length L, wire spacing 2d, and separations S which along with load Z_L, varies throughout the figures. These figures represent transmission problems of the type of Fig. 1-4. The voltage generator is located at the point where we are interested in the induced current. In all cases the spiral pattern is

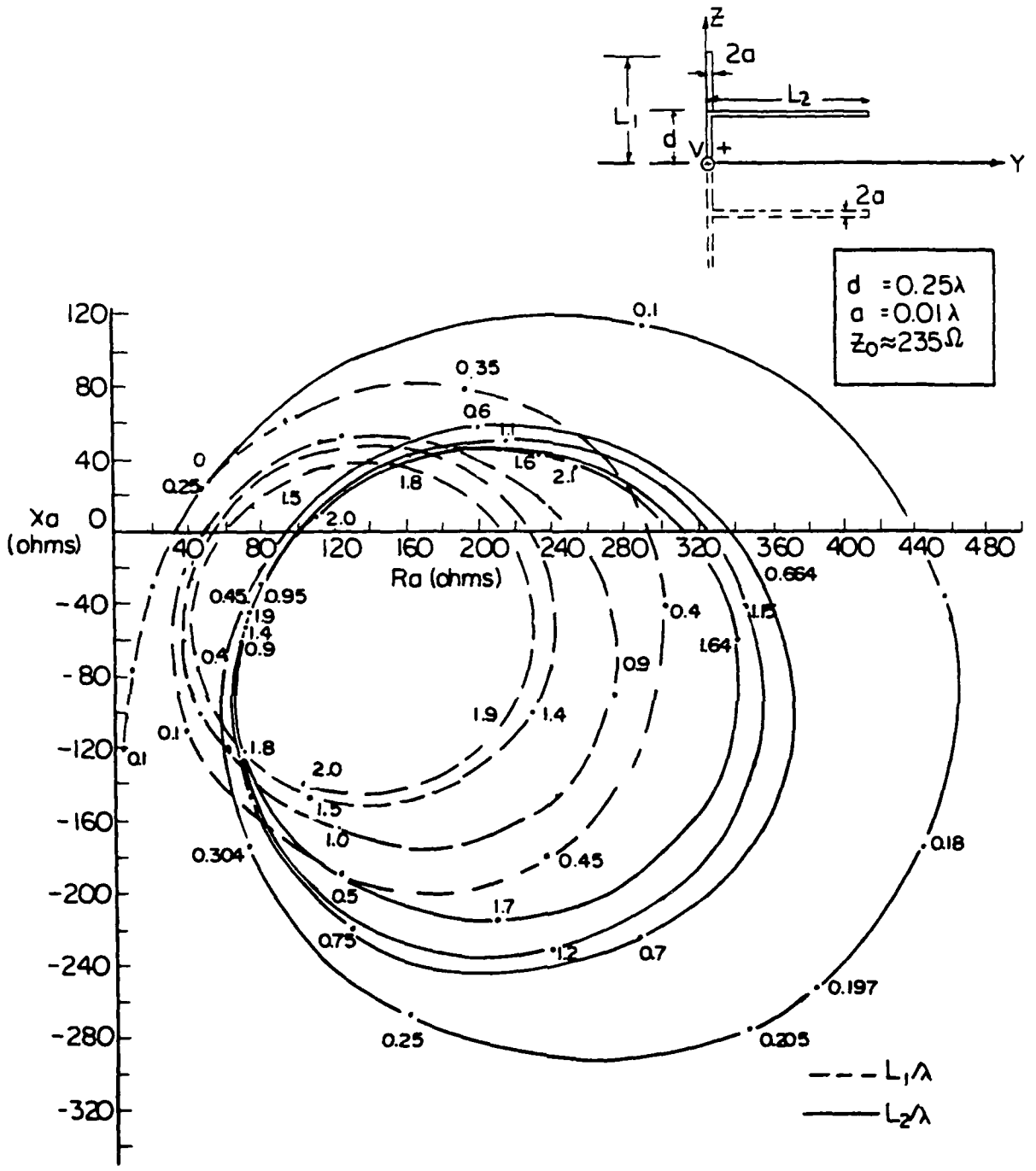

Fig. 4-1. Impedance of the dipole/transmission line (d = 0.25λ)

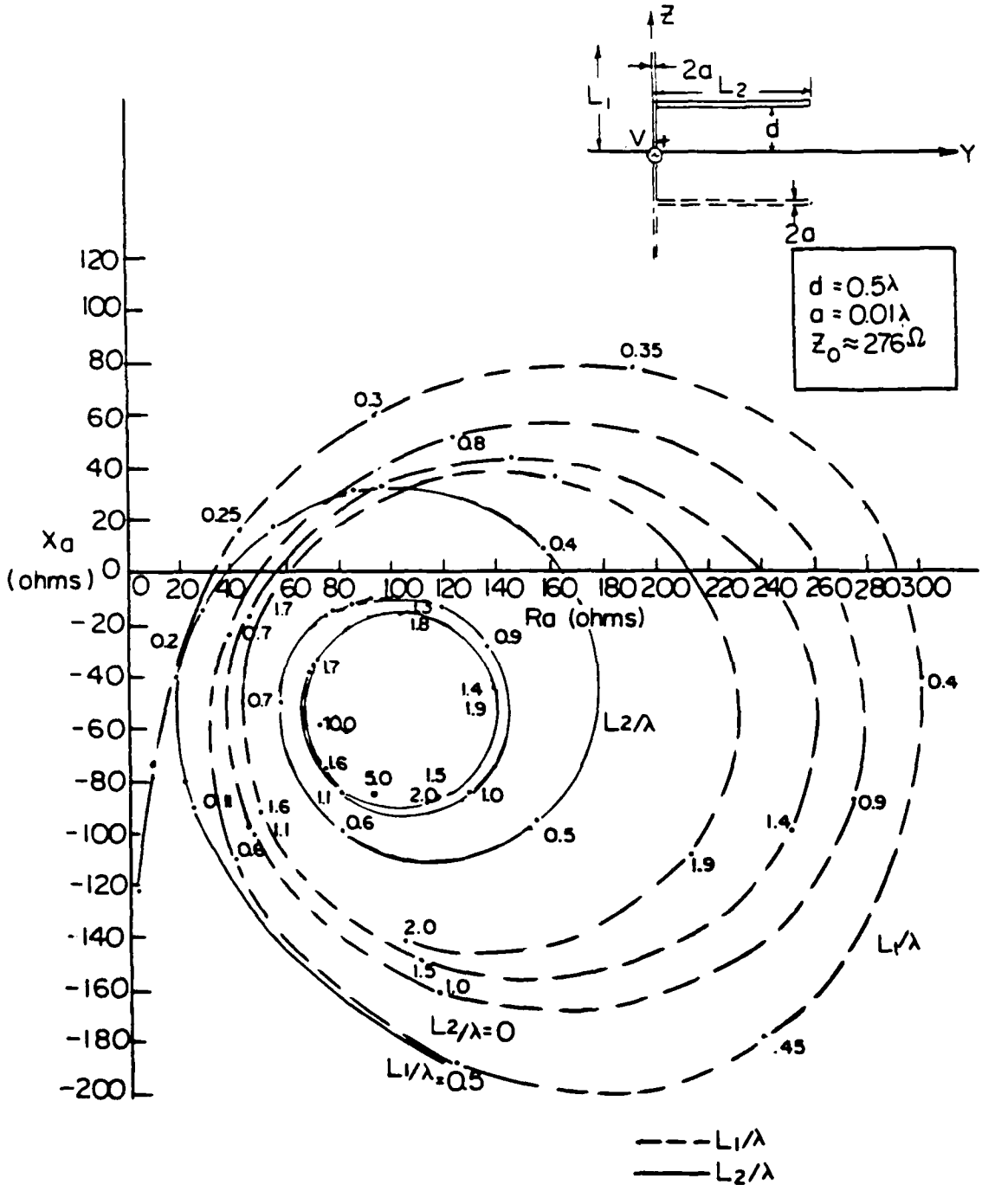

Fig. 4-2. Impedance of the dipole/transmission line (d = 0.5λ)

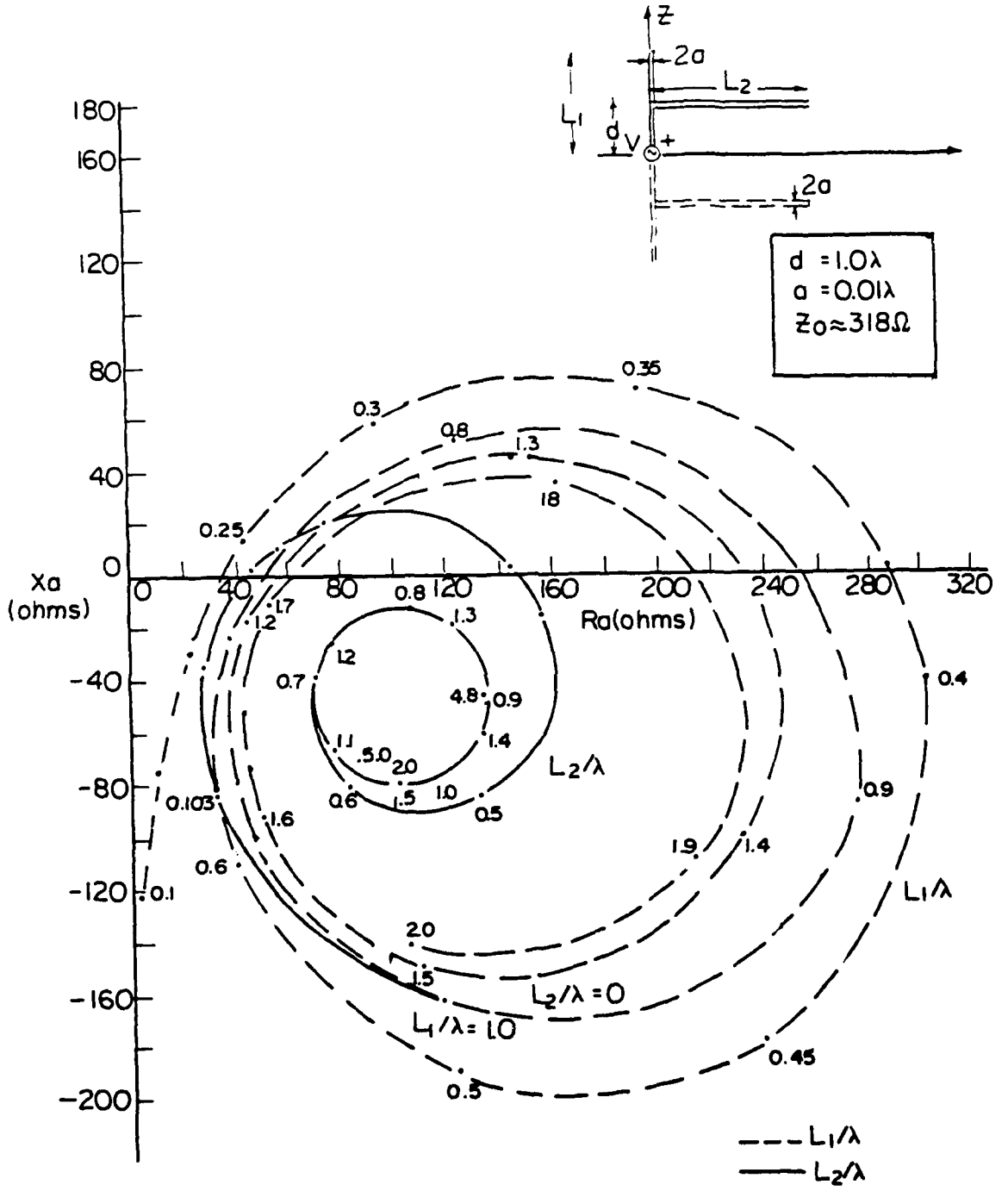

Fig. 4-3. Impedance of the dipole/transmission line (d = 1.0λ).

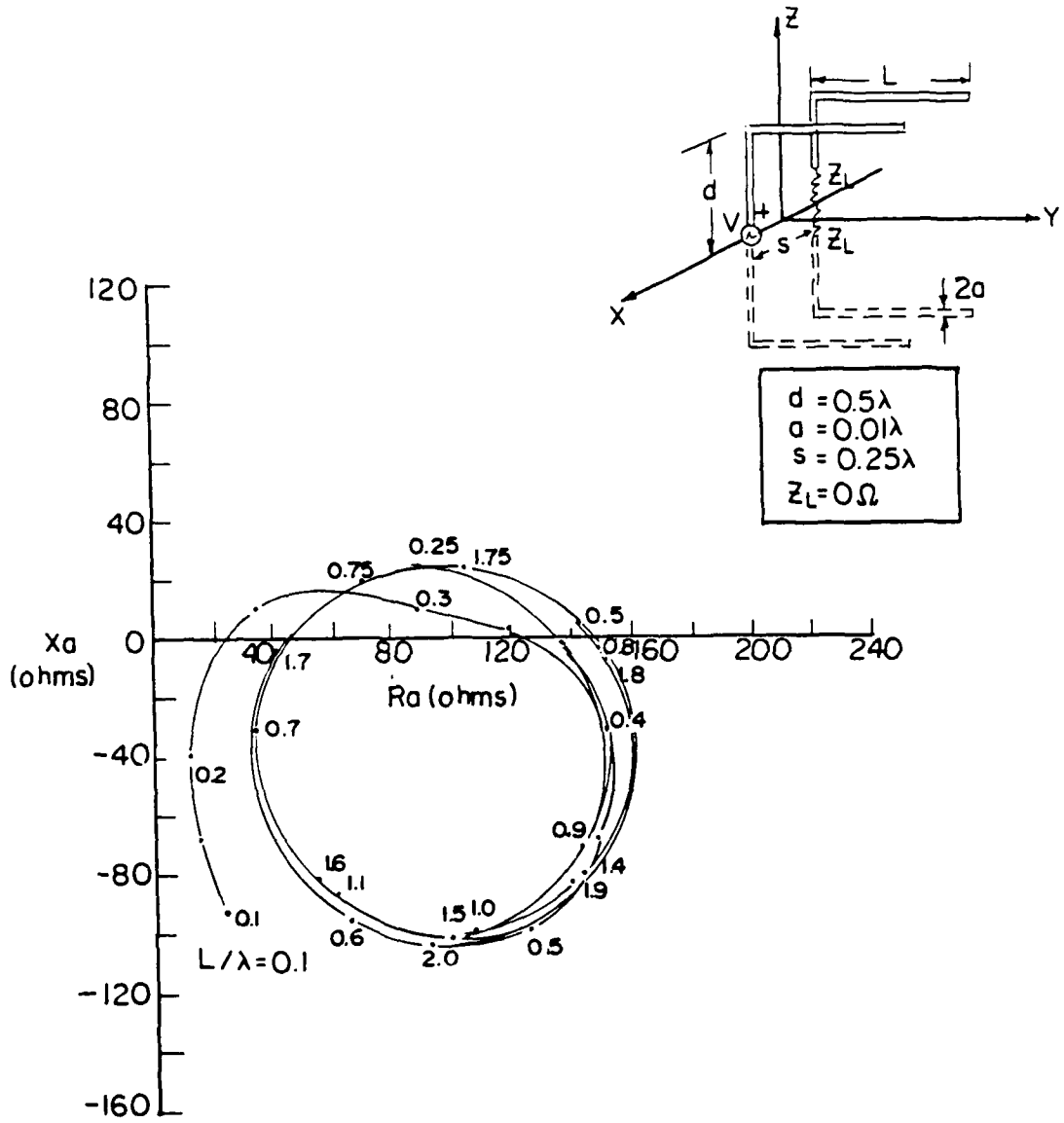

Fig. 4-4. Impedance of a two-conductor transmission line (S = 0.01λ, Z_L = 50Ω).

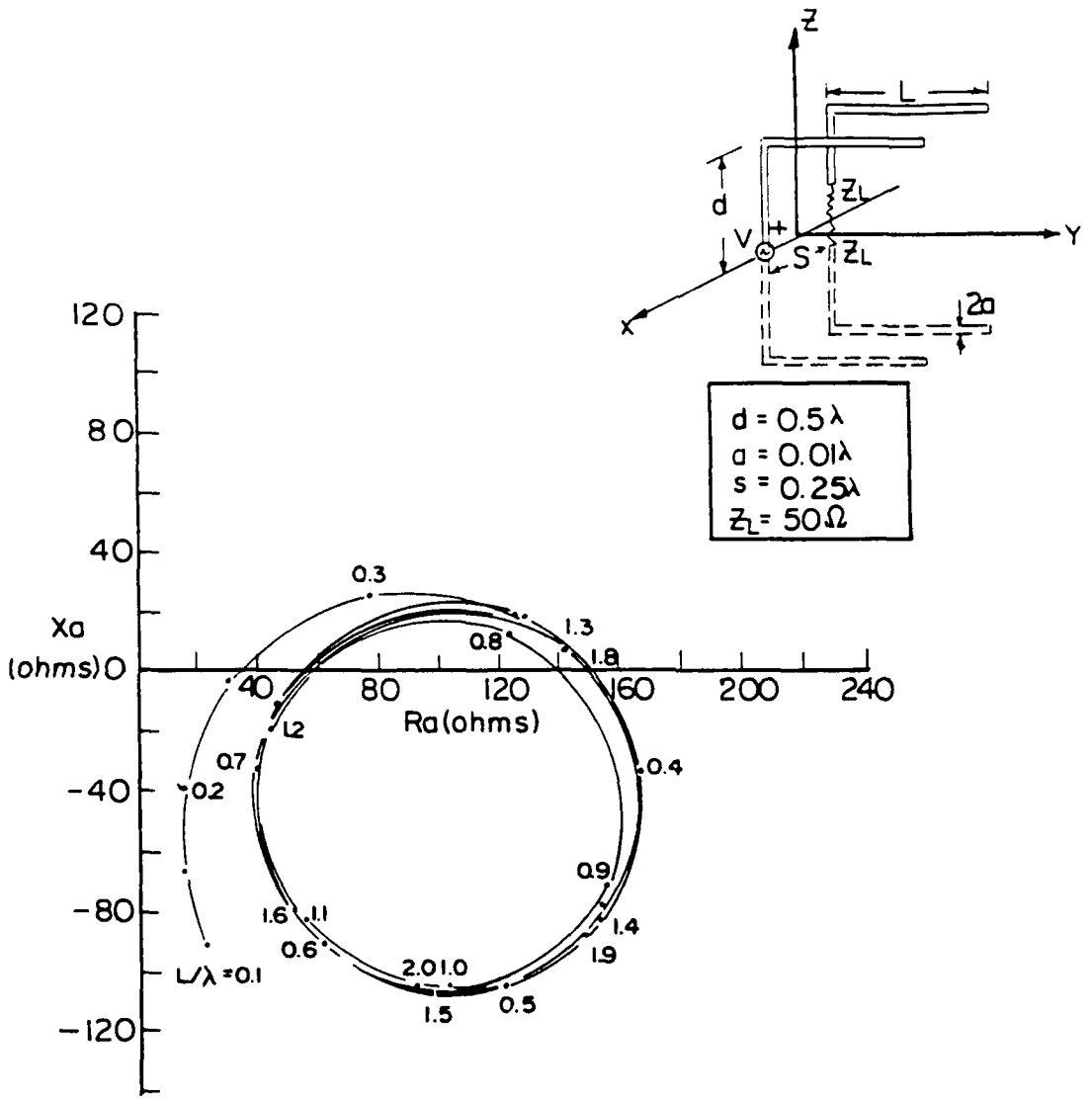

Fig. 4-5. Impedance of a two-conductor transmission line (S = 0.25λ, Z_L = 50Ω).

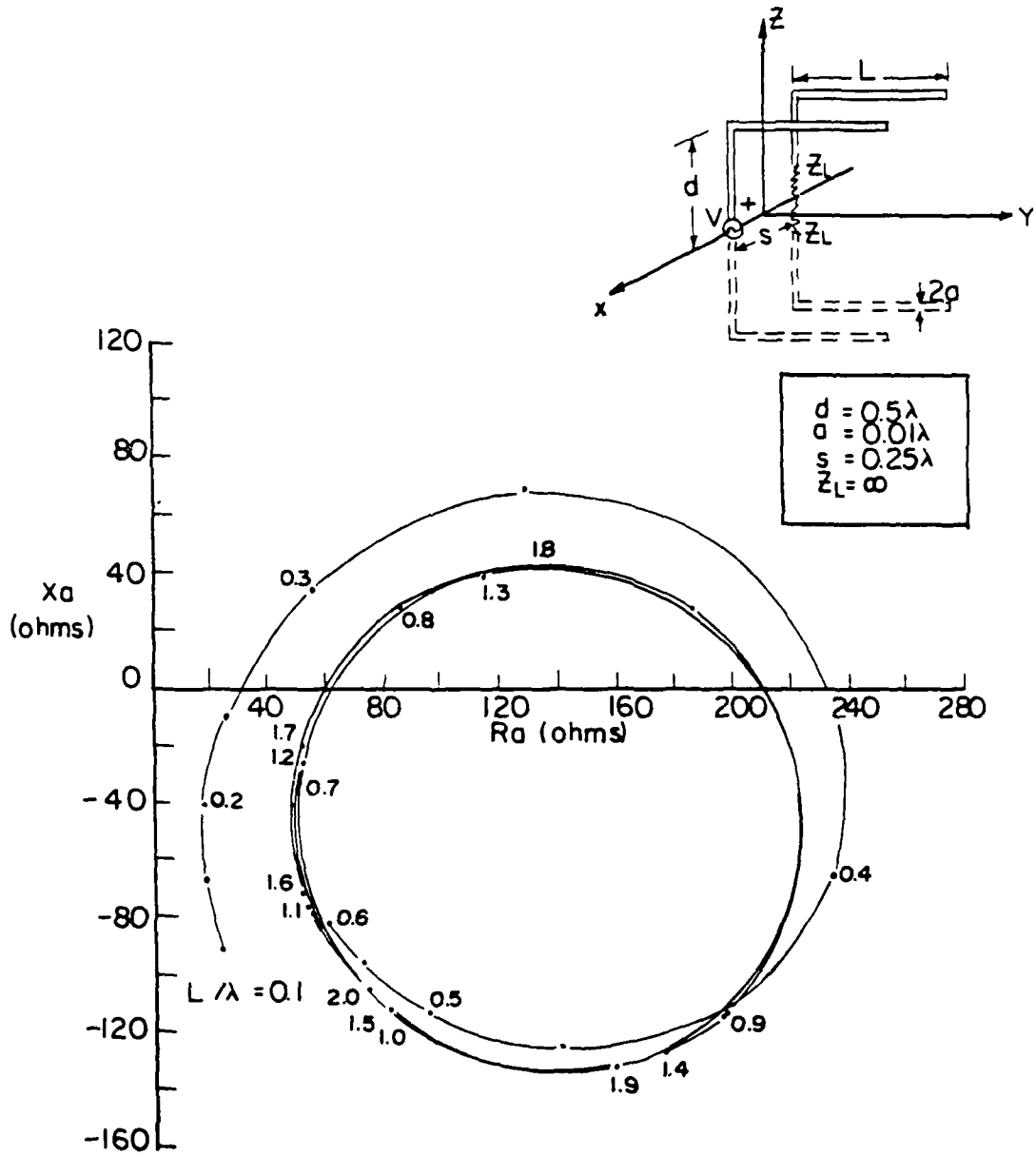

Fig. 4-6. Impedance of a two-conductor transmission line (S = 0.25λ, $Z_L = \infty$).

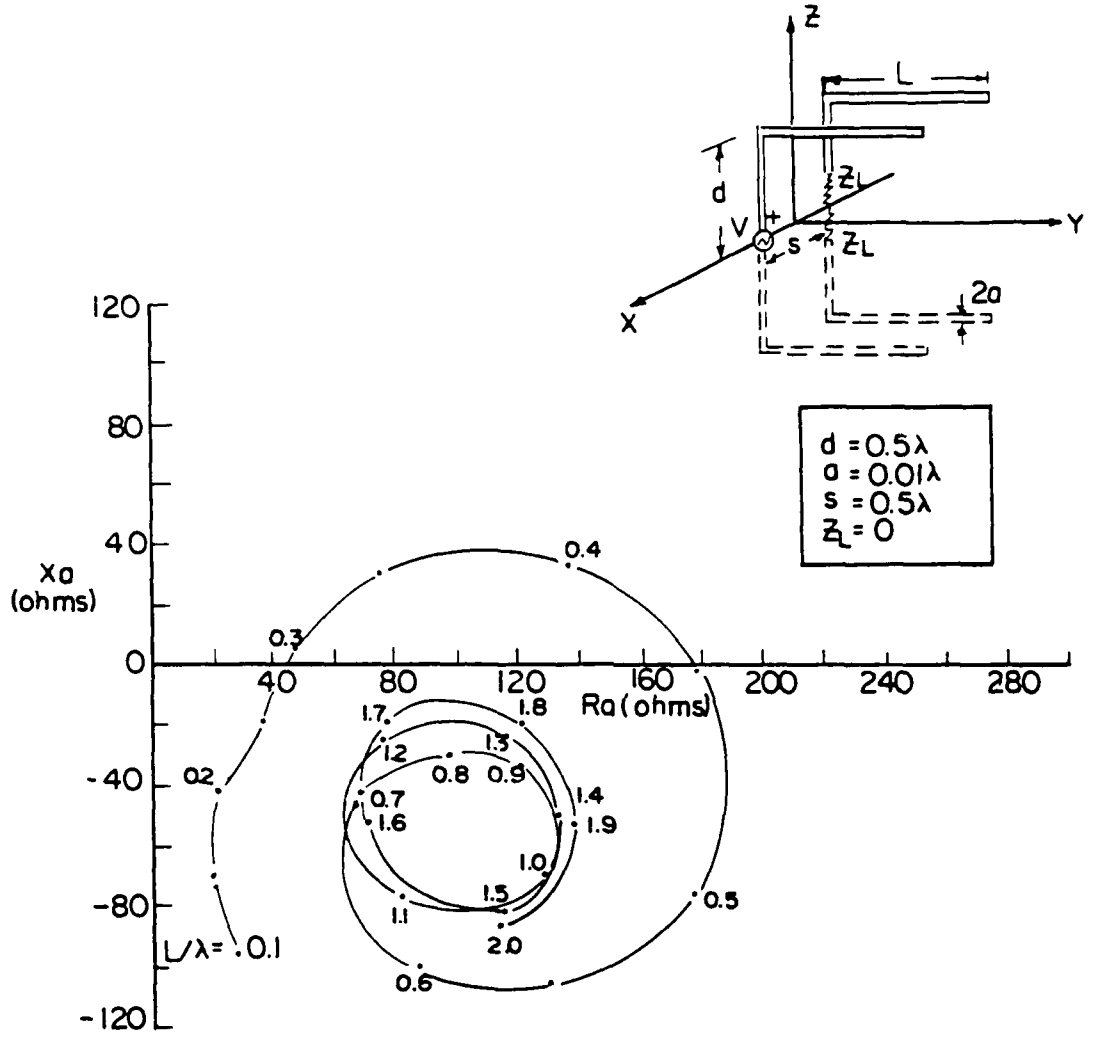

Fig. 4-7. Impedance of a two-conductor transmission line (S = 0.5λ, Z_L = 0).

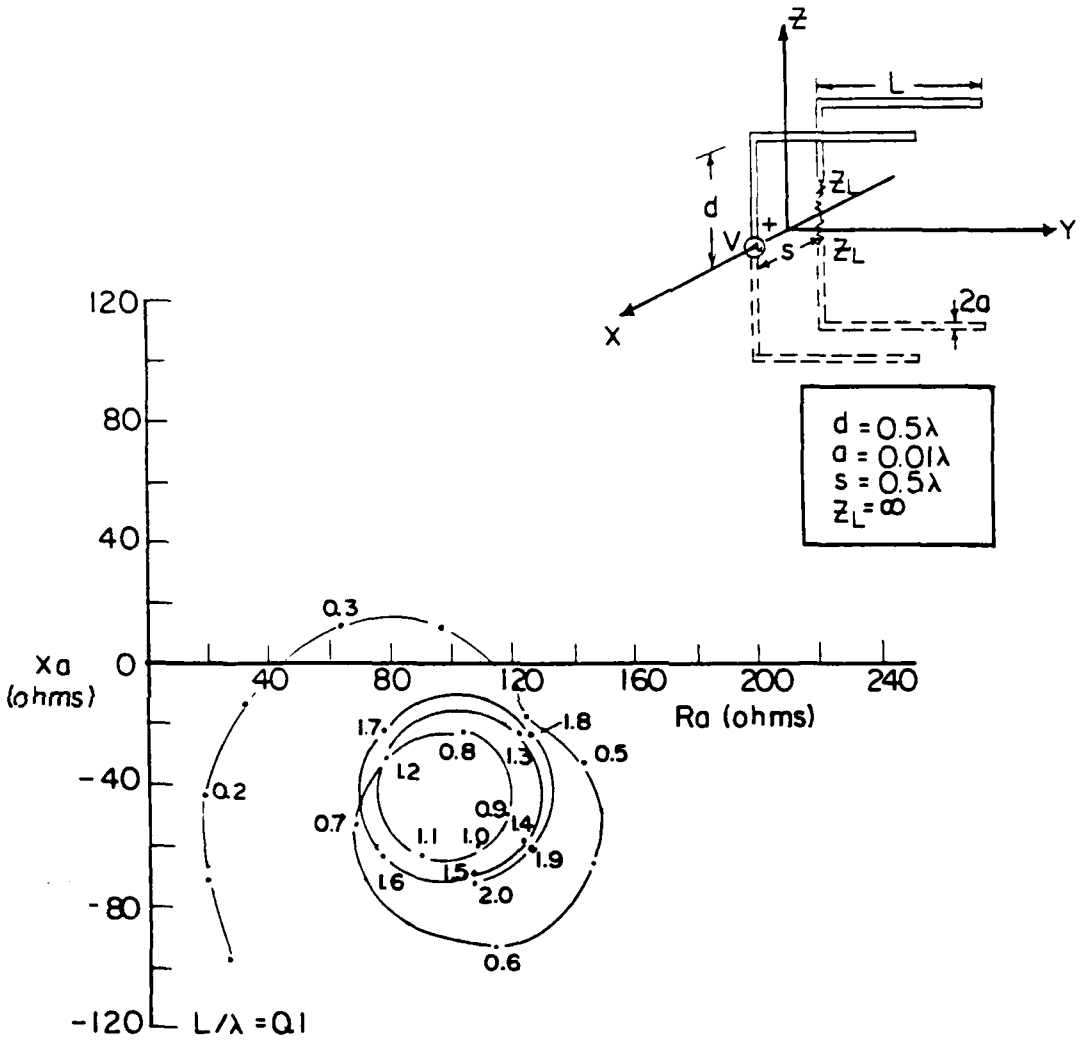

Fig. 4.8. Impedance of a two-conductor transmission line (S = 0.5λ, $Z_L = \infty$).

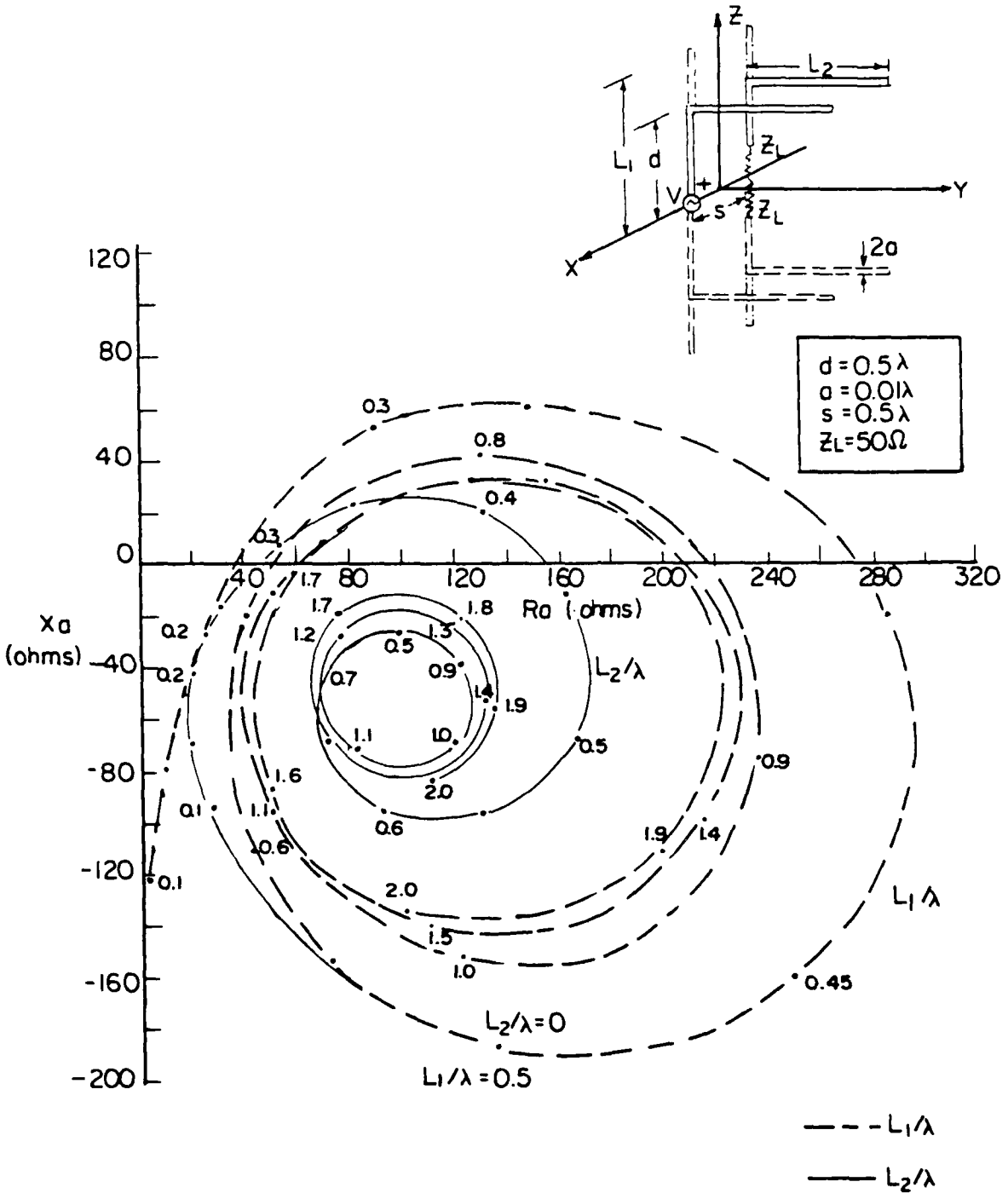

Fig. 4-9. Impedance of a two-conductor transmission line (S = 0.5λ, Z_L = 50Ω).

observed and bounds can be obtained. Figs. 4-4 to 4-6, with S = 0.25λ, show larger circles. Figs. 4-7 and 4-8 with S = 0.5λ, show very small circles, for both short and open circuit loads. Fig. 4-9 shows two dipoles and two transmission lines with trends similar to those noted before. Figs. 4-10 and 4-11 show similar trends for a pair of VEE antennas with quarter- and half-wavelength spacing S. Finally, Figs. 4-12 and 4-13 show similar trends for a combination of thin wires which represents the problem of Fig. 1-3.

In summary, all geometries tested exhibit the same general trends including (a) an absolute minimum value of impedance which occurs at low frequencies and can therefore be calculated using moment-method models (b) a nearly circular pattern for L > 2λ from which lower and upper bounds can be obtained.

4.3 COMPUTATION OF OPEN-CIRCUIT VOLTAGE V_{oc}

The open-circuit voltage V_{oc} may be computed by several different methods. For short transmission line lengths, where the minimum magnitude of impedance occurs, it is possible to computer V_{oc} directly. Since [2]

$$V_{oc} = \frac{1}{I} \iiint \underline{E}^{inc} \cdot \underline{J}_t \, dv, \tag{4-1}$$

the incident fields and the current when the antenna is excited as a transmitter are required. The antenna current $\underline{J}_t$ is obtained by moment methods. Then the beam pattern is computed. The absolute maximum of the beam pattern is found, and the incident field is then directed along the line of that maximum, in order to test for maximum susceptibility. Then Eq.(4-1) is evaluated numerically. The result is the maximum V_{oc} which can be obtained for the given structure at a given frequency. This computation

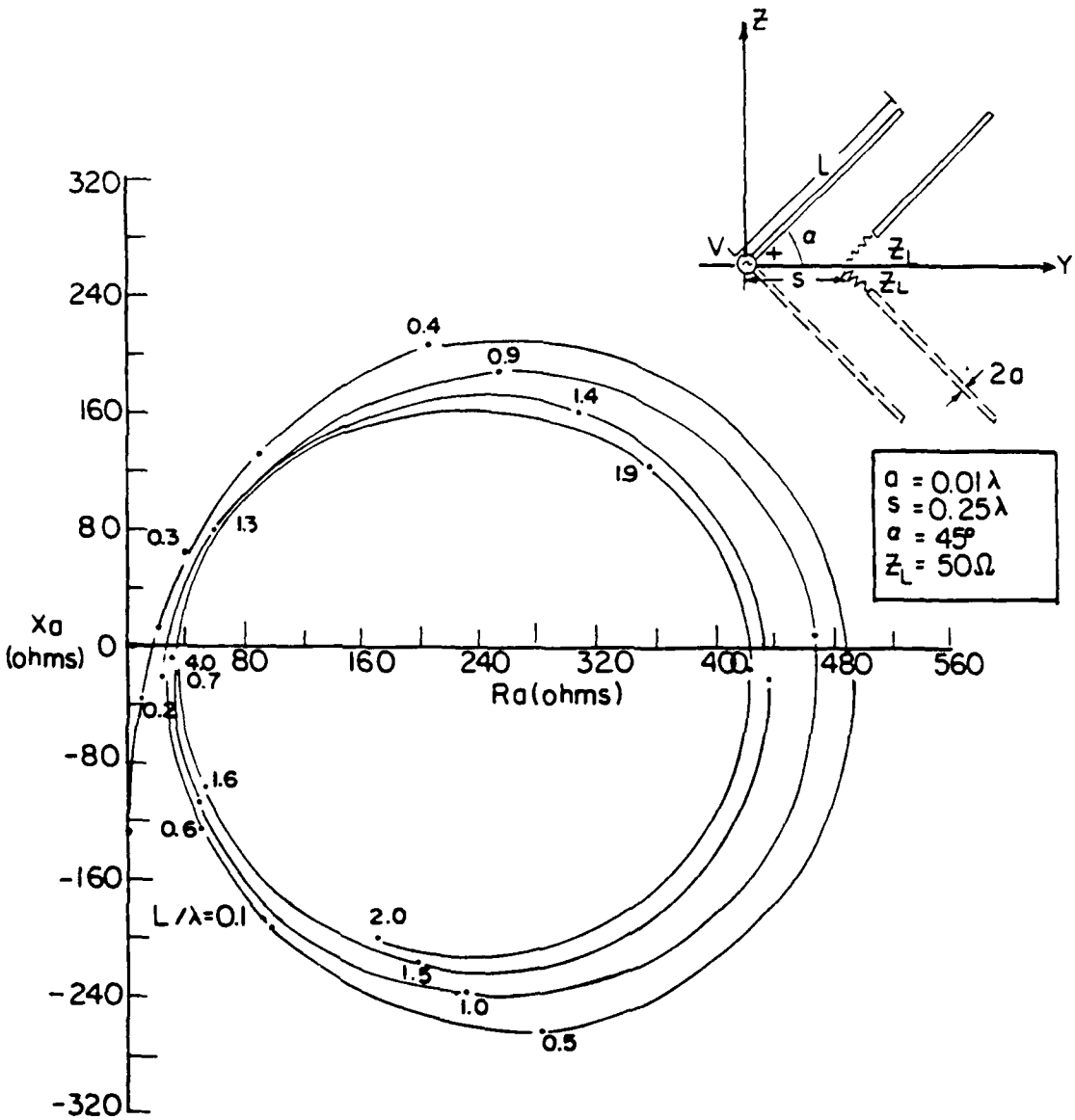

Fig. 4-10. Impedance of a two conductor VEE transmission line (S = 0.25λ).

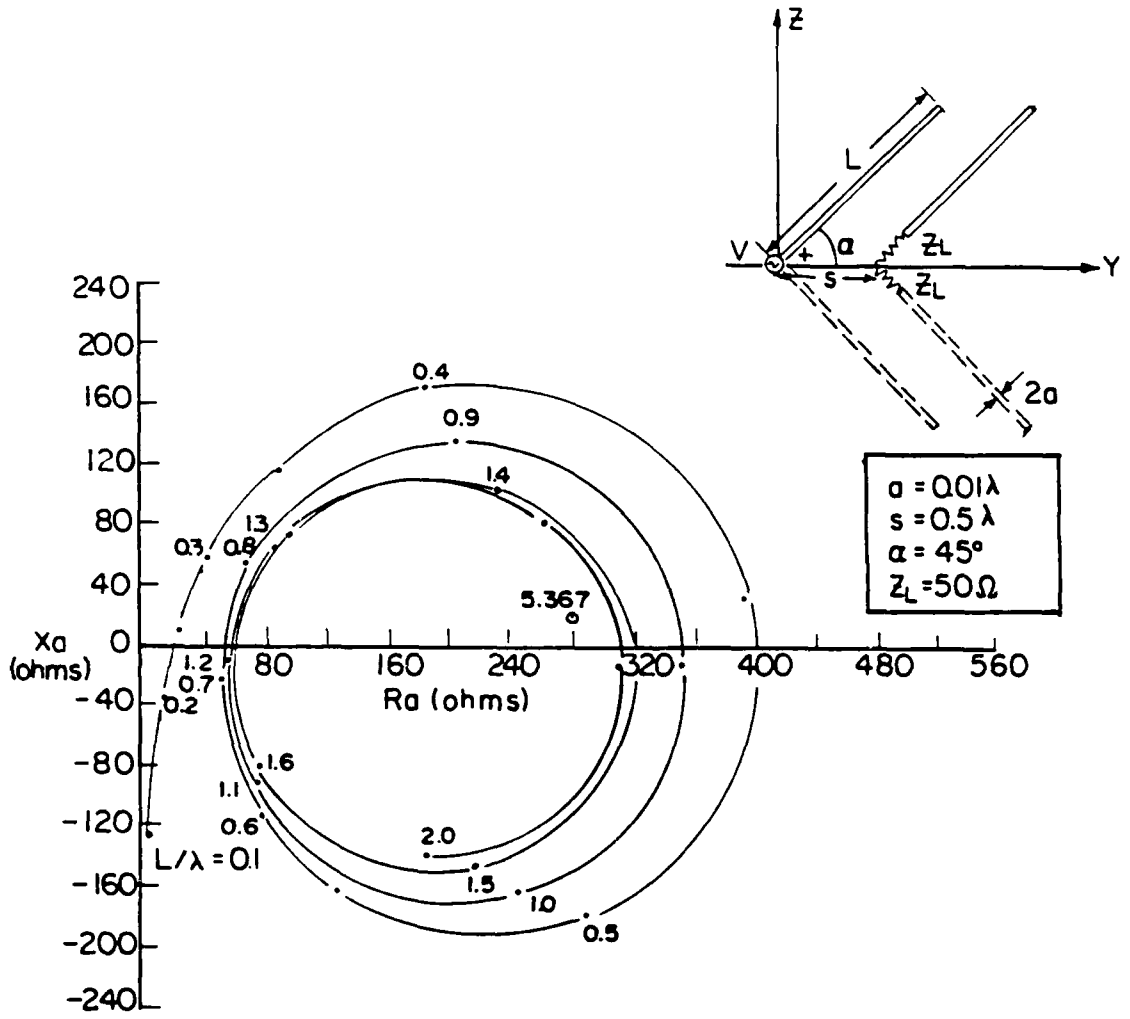

Fig. 4-11. Impedance of a two-conductor VEE transmission line (S = 0.5λ).

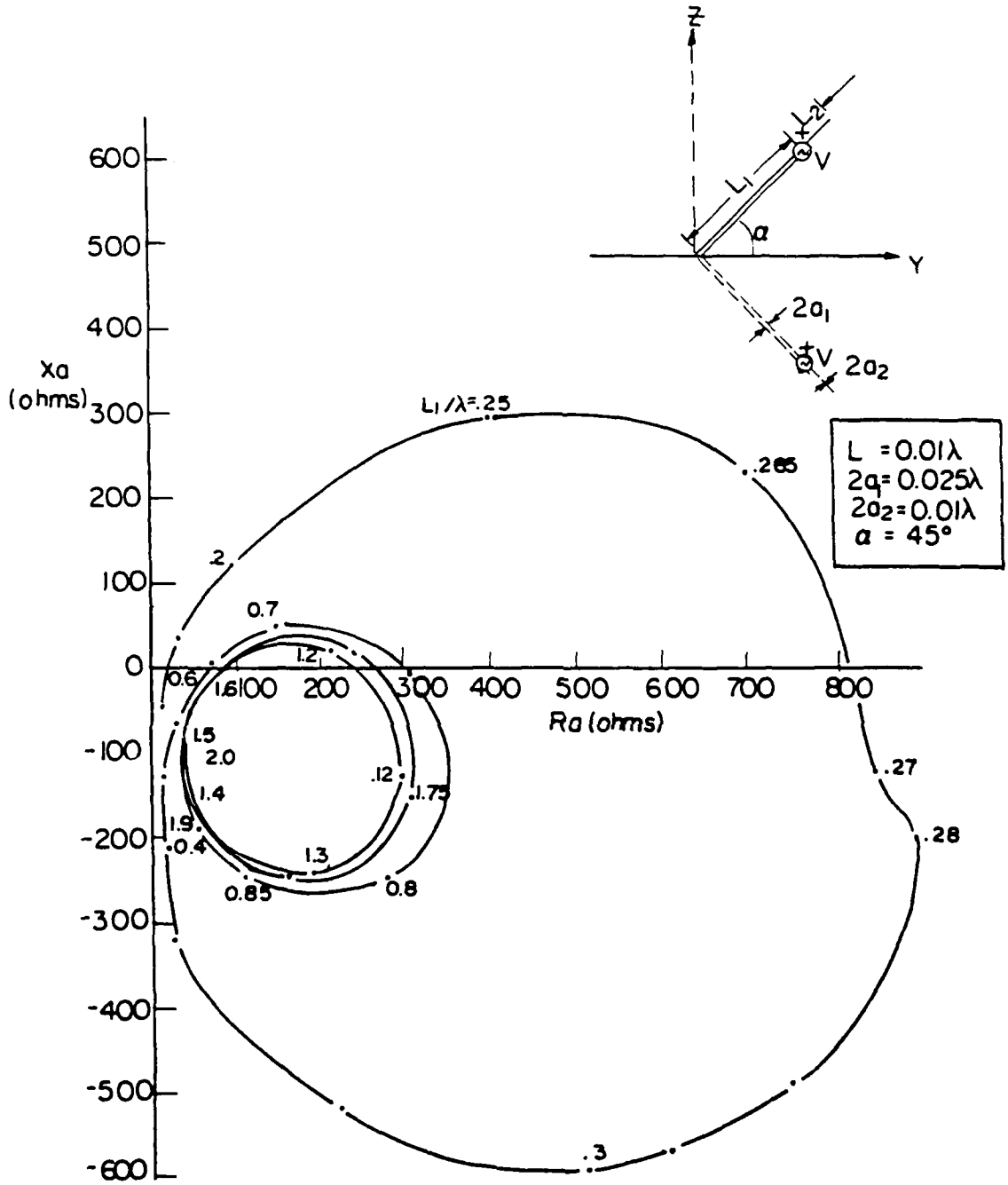

Fig. 4-12. Impedance of a coaxial VEE transmission line (L_2 = 0.01λ).

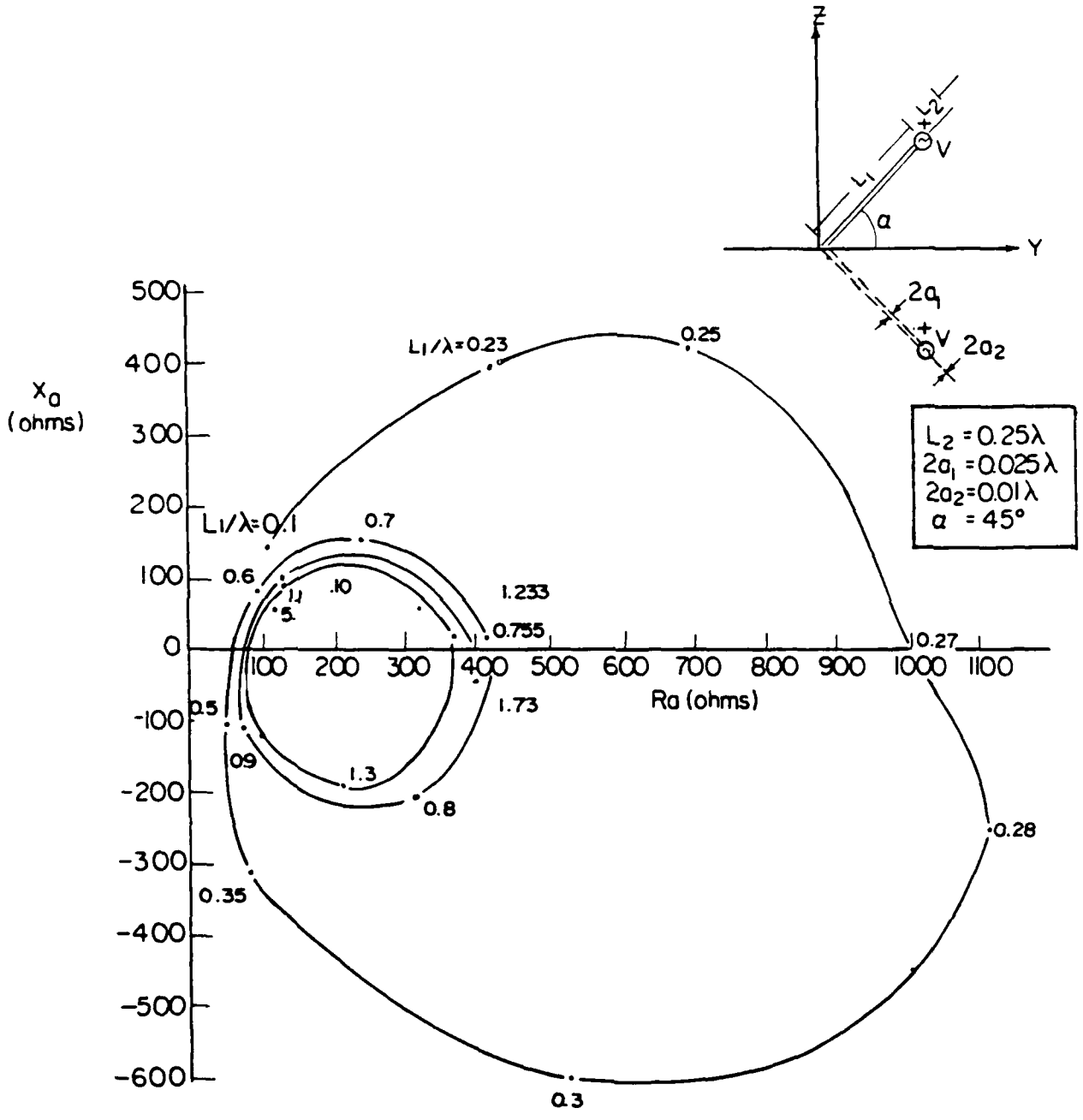

Fig. 4-13. Impedance of a coaxial VEE transmission line (L_2 = 0.25λ).

was done for a number of different cases and the results are presented in Tables 1 thru 8 which also include the induced current. Note that the induced current maximum does not vary significantly with distance. For example, in Table 1, the maximum current varies between .23mA and .18mA as length L_2 varies between 0.1λ and 10λ. The lengths L_2/λ chosen are those which correspond to maximum and minimum values of Z_a. The direction of the incident wave is chosen for maximum susceptibility, i.e., toward the maximum of the beam pattern. Table 2 shows similar results, the maximum current varies between 0.14 mA and 0.13mA. The remaining tables show similar results.

In all cases, the variation of maximum current is very small, on the order of ±10% for lengths between one and ten wavelengths. The reason for this small variation is that V_{oc}, Z_a have their maxima, minima at the same points and the ratio V_{oc}/Z_a does not vary at the minima. The minimum of I_{sc} has somewhat more variation. It would indeed be useful to determine if this small variation of the maximum of I_{sc} is maintained for larger and more widely separated transmission lines, i.e., for higher frequencies.

The open-circuit voltage can also be obtained by assuming a sinusoidal current distribution, or an attenuated sinusoidal distribution, computing the beam pattern, directing the incident beam pattern toward the maximum, and evaluating Eq.(4-1) directly.

4.4 REFERENCES FOR CHAPTER FOUR

[1] J. D. Kraus, Antennas, McGraw-Hill, 1950, p. 243.

[2] W. L. Weeks, Antenna Engineering, McGraw-Hill, NY, 1968, Section 8.1, pp. 292-296.

TABLE 1 TRANSMISSION LINE

(Fig. 4-1, d = 0.25λ, a = 0.01λ)

L_2/λ	V_{oc}(V)	Z_a(Ω)	I_{sc}(mA)
0.110	0.005	21.796	0.229
0.303	0.044	909.090	0.048
0.620	0.006	28.621	0.210
0.785	0.045	877.193	0.051
1.110	0.006	29.223	0.205
1.275	0.045	877.193	0.051
1.599	0.006	29.360	0.204
1.767	0.046	892.857	0.052
2.091	0.006	29.905	0.201
2.257	0.045	877.193	0.051
9.960	0.006	33.289	0.180
10.120	0.008	819.672	0.010

TABLE 2 TRANSMISSION LINE

(Fig. 4-2, $d = 0.5\lambda$, $a = 0.01\lambda$)

L_2/λ	V_{oc}(V)	$Z_a(\Omega)$	I_{sc}(mA)
0.150	0.022	454.546	0.048
0.500	0.011	91.075	0.121
0.650	0.018	352.113	0.051
1.000	0.012	99.602	0.120
1.140	0.021	333.334	0.063
1.500	0.013	106.157	0.122
1.640	0.023	328.945	0.070
2.000	0.014	110.375	0.127
2.120	0.023	306.749	0.075
9.850	0.014	107.296	0.130
9.980	0.019	259.068	0.073

TABLE 3 DOUBLE VEE ANTENNA

(Fig. 4-10, $\alpha = 45°$, $S = 0.25\lambda$, $Z_L = 50\Omega$)

L/λ	V_{oc}(V)	$Z_a(\Omega)$	I_{sc}(mA)
0.240	0.006	18.478	0.325
0.450	0.023	495.050	0.046
0.720	0.009	29.604	0.304
1.210	0.011	32.175	0.342
1.700	0.011	33.943	0.324
1.930	0.037	423.725	0.087

TABLE 4 DOUBLE VEE ANTENNA

(Fig.4-11, $\alpha = 45°$, $S = 0.5\lambda$, $Z_L = 50\Omega$)

L/λ	V_{oc}(V)	$Z_a(\Omega)$	I_{sc}(mA)
0.240	0.005	21.437	0.233
0.460	0.020	400.000	0.050
0.730	0.011	52.411	0.210
0.950	0.028	352.112	0.080
1.210	0.014	56.625	0.247
1.450	0.028	320.513	0.087
1.710	0.013	57.804	0.225
1.930	0.026	310.559	0.084
2.200	0.013	61.805	0.210

TABLE 5 COAXIAL LINE

(Fig. 4-13, $\alpha = 45°$, $L_2 = 0.25\lambda$, $2a_1 = 0.025\lambda$, $2a_2 = 0.01\lambda$)

L_1/λ	V_{oc}(V)	$Z_a(\Omega)$	I_{sc}(mA)
0.270	0.026	1010.000	0.026
0.500	0.009	49.780	0.181
0.755	0.012	423.730	0.028
0.983	0.009	70.270	0.128
1.233	0.016	371.750	0.043
1.483	0.008	67.600	0.118
1.733	0.014	403.230	0.035
4.930	0.006	83.890	0.072
5.160	0.004	328.950	0.122

TABLE 6 VEE ANTENNA

($\alpha = 30°$, $a = 0.02\lambda$, $Z_L = 0$)

L/λ	V_{oc}(V)	Z_a(Ω)	I_{sc}(mA)
0.260	0.004	12.950	0.309
0.480	0.023		
0.730	0.009	36.930	0.244
0.950	0.028	328.950	0.085
1.220	0.013		
1.446	0.026	333.330	0.078
1.716	0.017	49.430	0.344
1.942	0.043	295.860	0.145
2.212	0.019	47.620	0.399

TABLE 7 VEE ANTENNA

($\alpha = 45°$, $a = 0.02\lambda$, $Z_L = 0$)

L/λ	V_{oc}(V)	$Z_a(\Omega)$	I_{sc}(mA)
0.240	0.005	20.525	0.244
0.450	0.023	413.220	0.056
0.735	0.012	46.690	0.257
0.950	0.037	378.790	0.098
1.213	0.016	54.350	0.294
1.440	0.040	317.800	0.126
1.703	0.016	55.370	0.289
1.930	0.036	304.900	0.118
2.206	0.015	58.480	0.256
2.420	0.034	294.120	0.116
2.683	0.017	62.190	0.273

TABLE 8 VEE ANTENNA

($\alpha = 60°$, $a = 0.02\lambda$, $Z_L = 0$)

L/λ	V_{oc}(V)	Z_a (Ω)	I_{sc}(mA)
0.235	.006	28.970	0.207
0.450	.025	384.620	0.065
0.727	0.013	46.820	0.278
0.942	0.030	347.200	0.086
1.214	0.012	57.410	0.209
1.437	0.028	340.130	0.082
1.709	0.014	64.440	0.217
1.932	0.029	326.800	0.089
2.204	0.014	69.250	0.202

Chapter V

CONCLUSIONS AND RECOMMENDATIONS

5.1 CONCLUSIONS

A feasibility study has been conducted to examine methods of treating field-to-wire electromagnetic coupling in the SHF/EHF frequency range. At these frequencies, transmission line length L and wire separation d become large electrically ($L >> \lambda$, $d > \lambda$) and the field-to-wire coupling problems become intractable.

Four basic problems (Figs. 1-1 thru 1-4) have been considered, including both uniform and non-uniform transmission lines. For those cases investigated, current distributions are predominantly of a standing-wave and/or traveling-wave form. The higher-order modes do not seriously disturb the current distributions.

Bounds may be obtained for induced currents in the field-to-wire problems by considering the transmission line as an antenna and using the equivalent circuit of the receiving antenna, which has been extended to multiport receivers. Plots of antenna impedance Z_a show that bounds may be obtained for this quantity. Antenna open-circuit voltage V_c may be calculated using computed or estimated currents for the transmitting antenna. Resultant maximum induced currents I_{sc} under conditions of maximum susceptibility show a striking constancy as frequency is varied over wide ranges. A method has thus been outlined for treating transmission lines at SHF/EHF.

5.2 RECOMMENDATIONS FOR FURTHER WORK

An experimental program is recommended for verification and extension of the results noted here. A direct measurement of induced current should be carried out and compared with computed results. In particular the constancy of maximum current should be verified. Measurements should also be performed at frequencies higher than those treated here (longer line lengths and greater wire separation) to obtain frequency limits on the methods.

The theoretical study initiated here should be extended to higher frequencies. Additional methods should be considered, including iterative methods and special expansion functions appropriate to long transmission lines. Other basic geometries such as the twisted pair transmission line should be treated.

The study of V_{oc} should be extended to cover the direct evaluation of V_{oc}. The study of I_{sc} should be extended to determine the reason for the small variation of I_{sc}. What are the relationships between gain, V_{oc} and I_{sc} as the antenna becomes very long?

MISSION
of
Rome Air Development Center

RADC plans and executes research, development, test and selected acquisition programs in support of Command, Control, Communications and Intelligence (C^3I) activities. Technical and engineering support within areas of competence is provided to ESD Program Offices (POs) and other ESD elements to perform effective acquisition of C^3I systems. The areas of technical competence include communications, command and control, battle management, information processing, surveillance sensors, intelligence data collection and handling, solid state sciences, electromagnetics, and propagation, and electronic, maintainability, and compatibility.

END

DTIC

7-86